



**HAL**  
open science

# Improving Ergonomics Through Physical Human-Robot Collaboration

Waldez Gomes

► **To cite this version:**

Waldez Gomes. Improving Ergonomics Through Physical Human-Robot Collaboration. Engineering Sciences [physics]. Université de lorraine, 2021. English. NNT : 2021LORR0208 . tel-03500477

**HAL Id: tel-03500477**

**<https://hal.science/tel-03500477>**

Submitted on 22 Dec 2021

**HAL** is a multi-disciplinary open access archive for the deposit and dissemination of scientific research documents, whether they are published or not. The documents may come from teaching and research institutions in France or abroad, or from public or private research centers.

L'archive ouverte pluridisciplinaire **HAL**, est destinée au dépôt et à la diffusion de documents scientifiques de niveau recherche, publiés ou non, émanant des établissements d'enseignement et de recherche français ou étrangers, des laboratoires publics ou privés.

# Improving Ergonomics Through Physical Human-Robot Collaboration

## THÈSE

présentée et soutenue publiquement le 13 decembre 2021

pour l'obtention du

**Doctorat de l'Université de Lorraine**  
(mention informatique)

par

Waldez Azevedo Gomes Junior

### Composition du jury

<i>Rapporteurs :</i>	Christine Chevallereau Bastien Berret	Directrice de Recherche, CNRS, Nantes Professeur, Université Paris-Saclay
<i>Examineurs :</i>	Alexis Aubry Vincent Padois	Maître de Conférences, Université de Lorraine, Nancy Directeur de Recherche, Inria Bordeaux Sud-Ouest
<i>Invitée :</i>	Pauline Maurice	Chargée de Recherche, CNRS, Loria, Nancy
<i>Encadrants :</i>	Jean-Baptiste Mouret Serena Ivaldi	Directeur de Recherche, Inria Nancy Grand-Est Chargée de Recherche, Inria Nancy Grand-Est



## Acknowledgments

The work in this thesis represents one of the greatest challenges of my entire life. Such a grand one that I could not have faced it entirely alone. For this reason, I have many people to acknowledge in this space.

First, I would like to thank my parents, Waldez and Valdiros, who have always been the greatest supporters of my academic endeavors. Especially to my father, who has faced, and overcame, so many hurdles this last year.

I would like to thank my sisters, Crisane, Carolina and Cristiane, for their constant support. As well as all of my family, that even though far, still sent messages of encouragement through social networks.

During my time in Nancy, I have met some of the most amazing people I know outside of the laboratory and who made a positive change in my life. Just to name a few: Alexis, Mariana, Melissa, Sebastien, Johann, Amalia, Daryna, Joanna, Claudia and many others. In particular, Lidia, who have always encouraged me throughout the Ph.D. in the best way possible.

I will also mention the group that does not allow me to forget how amazing it is to have brazilian friends around me: Guilherme, Gabriel, Talita, Jéssica, Mia, Barbara, Christian, Thais, Ozaíne and still many others.

I have also been fortunate to have had some of the most amazing colleagues to work with at the LARSEN team in INRIA Nancy. I would like to thank the entire team as a whole, and just to name a few: Debaleena, Eloïse, Jessica, Lucien (a.k.a. c.b.), Yassine, Rituraj, Oriane, Lorenzo, Yohann, Ivan, Edoardo, and many others that were in the lab over the years. I will not forget, in particular, of Luigi, for being such a good friend throughout all of these years.

Naturally, I would like to thank Dr. Pauline Maurice, Dr. Serena Ivaldi, and Dr. Jean-Baptiste Mouret for believing in my potential, and guiding me in this journey towards a Ph.D. title. It was a true honor to have you as my advisors. Then, I would also like to kindly thank all of the most respected researchers that accepted the invitation to be part of the jury in my Ph.D. defense: Dr. Christine Chevallereau, Dr. Bastien Berret, Dr. Vincent Padois and Dr. Alexis Aubry.

Finally, I would like to thank Université de Lorraine, Loria, and Inria Nancy, as well as the Horizon 2020 European project AnDy who financed and supported this thesis.



*Aos meus pais,  
às minhas irmãs,  
à minha madrinha Miriam,  
e ao meu padrinho Roberto (in memoriam).*



# Contents

<b>Summary in French</b>	<b>1</b>
<b>Introduction</b>	
1 From Human to Robot Collaboration . . . . .	12
2 Contributions and Thesis Organization . . . . .	14
3 Publications . . . . .	17
<b>Chapter 1</b>	
<b>Human Ergonomics Evaluation</b>	
1.1 Musculoskeletal Disorders and Ergonomics Evaluations . . . . .	19
1.2 Digital Human Model . . . . .	20
1.3 Ergonomics Scores Evaluation . . . . .	22
1.4 Real case study on Ergonomics Evaluation: Exoturn Project . . . . .	24
1.4.1 Preliminary Prone Positioning Kinematic Analysis . . . . .	26
1.4.2 Ergonomics Evaluation of Exoskeleton Usage . . . . .	28
1.4.3 Ergonomics Analysis Results . . . . .	31
1.5 Discussion . . . . .	32
<b>Chapter 2</b>	
<b>Whole-Body Motion Optimization</b>	
2.1 Whole-body Trajectory Generation and Optimization . . . . .	35
2.2 Multi-Objective Trajectory Optimization . . . . .	37
2.3 Whole-body Trajectory Parameterization . . . . .	38
2.4 Constrained Trajectory Optimization . . . . .	40
2.4.1 Optimization Algorithms . . . . .	41
2.4.2 Single- and Multi-Objective Trajectory Optimization . . . . .	41
2.5 Humanoid Whole-body Motion Optimization from Retargeted Human Motions . . . . .	42
2.5.1 Experiments . . . . .	45
2.5.2 Results and Discussion . . . . .	47

2.6	Multi-objective Trajectory Optimization to Improve Ergonomics in Human Motion . . .	49
2.6.1	Experiments . . . . .	49
2.6.2	Results and Discussion . . . . .	51
2.7	Discussion . . . . .	58

<b>Chapter 3</b> <b>Human-Human Co-Manipulation</b>
--

3.1	Human Dyad Interactive behaviors . . . . .	59
3.2	Methods . . . . .	60
3.2.1	Participants . . . . .	60
3.2.2	Task Description . . . . .	61
3.2.3	Apparatus . . . . .	61
3.2.4	Experiment Description . . . . .	61
3.2.5	Data Collection . . . . .	64
3.2.6	Data Analysis . . . . .	66
3.2.7	Methods for Statistical Analysis . . . . .	68
3.3	Results . . . . .	70
3.3.1	Collaboration leads to muscle co-contraction as high as in leaders . . . . .	70
3.3.2	Trajectories are deviated towards the dyad’s leader . . . . .	70
3.3.3	Fewer errors during collaboration than during cooperation conditions . . . . .	71
3.4	Discussion . . . . .	73

<b>Chapter 4</b> <b>Human-Robot Co-Manipulation</b>
--

4.1	Introduction . . . . .	77
4.2	Impedance Control and Role Definition . . . . .	78
4.3	Human-Robot Experiment . . . . .	80
4.3.1	Participants . . . . .	80
4.3.2	Task Description . . . . .	80
4.3.3	Duration . . . . .	82
4.3.4	Apparatus . . . . .	82
4.3.5	Experiment Description . . . . .	82
4.3.6	Data Collection . . . . .	83
4.3.7	Desired Robot Trajectory and Stiffness . . . . .	84
4.3.8	Statistical Analysis . . . . .	84
4.4	Results . . . . .	85
4.5	Discussion . . . . .	88

---

**Chapter 5****Conclusions**

5.1	Discussion . . . . .	91
5.2	Perspective . . . . .	95
5.2.1	Whole-Body Trajectory Optimization w.r.t Ergonomics . . . . .	95
5.2.2	Human-Robot Interaction with Shared Task Autonomy . . . . .	96

**Appendix****Appendix A****Exoturn Exoskeletons****Appendix B****Human Co-Manipulation Data**

B.1	Timing Measurements . . . . .	101
B.2	Index of Co-Contraction . . . . .	102
B.3	Pipe Trajectory . . . . .	105

**Appendix C****Human-Robot Co-Manipulation Data**

C.1	Index of Co-Contraction . . . . .	107
C.2	Pipe Trajectory . . . . .	108
C.3	Interaction Torque . . . . .	109

**Bibliography****111**



# List of Figures

1	Distribution of costs due to work-related injuries and diseases . . . . .	9
2	Overhead drilling task example . . . . .	10
3	Humans and robots in close proximity in and out of the industrial environment . . . . .	11
4	Worldwide market for service robotics . . . . .	11
5	Increasing complexity of human-robot interactions . . . . .	12
6	Thesis Organization . . . . .	15
1.1	Illustration of ergonomics visual feedback for a human holding an object above the head.	19
1.2	Digital Human Model Example: Xsens. . . . .	21
1.3	Digital Human Model (DHM) joints description . . . . .	21
1.4	Latent Ergonomics Maps . . . . .	23
1.5	Whole-body Posture in a Latent Ergonomics Map . . . . .	24
1.6	Prone-Positioning maneuver executed on a manikin . . . . .	25
1.7	ExoTurn preliminary analysis . . . . .	27
1.8	The four commercial exoskeletons used in the ExoTurn exploratory study . . . . .	28
1.9	Motion analysis during prone-positioning . . . . .	29
1.10	Lumbar spine flexion with different exoskeletons . . . . .	30
1.11	Boxplots of lumbar spine flexion angles . . . . .	30
1.12	Boxplots of estimated human torque profiles . . . . .	32
1.13	Estimation of assistive torque from Laevo exoskeleton, and human effort. . . . .	32
1.14	Hysteresis effect on assistive torque estimation . . . . .	33
2.1	Whole-body motion optimization . . . . .	35
2.2	Ergonomics human motion optimization . . . . .	37
2.3	Process of extracting trajectories from demonstrations . . . . .	40
2.4	Modified whole-body motion optimization framework for the iCub robot . . . . .	43
2.5	Process of extracting trajectories from demonstrations for the iCub Robot . . . . .	43
2.6	iCub task description . . . . .	44
2.7	COBYLA and CCMA-ES converge to a solution much faster than AGS . . . . .	47
2.8	Optimal cost function from unfeasible starting sets $(s_1, s_2, s_3, s_4, s_5, s_{all})$ . . . . .	47
2.9	Optimal cost function, and improvement from feasible starting sets $(r_1, r_2, r_3, r_4, r_{all}, all)$ . . . . .	47
2.10	Reference trajectories . . . . .	48
2.11	Torque values at the most critical joints in $\epsilon_{icub}$ . . . . .	48
2.12	Demonstrations for work activities A and B captured with the motion capture suit . . . . .	50
2.13	Optimized hand trajectories w.r.t. torques shoulder and RULA-C scores. . . . .	52
2.14	Median of the ergonomics scores during the execution of the initial and optimal motions . . . . .	54
2.15	Time evolution of selected angles of the initial movement and the optimized motions . . . . .	54

2.16	Experiment 3 - Activity A - Pareto front . . . . .	56
2.17	Experiment 3 - Activity B - Pareto front . . . . .	56
3.1	Human-human physical interaction study . . . . .	59
3.2	Main Experiment: Human Dyads. . . . .	62
3.3	Complementary Experiment: Solo Human Agent . . . . .	63
3.4	Dimensions of the pipe and tubes. . . . .	63
3.5	Positions of the Qualisys reflective markers . . . . .	64
3.6	Equipment used for data collection . . . . .	66
3.7	Enveloped EMG Signal . . . . .	67
3.8	Angle of trajectory deviation, $\alpha$ . . . . .	68
3.9	Index of Co-Contraction (ICC) for the muscle pair Extensor/Flexor Carpi Ulnaris . . . . .	69
3.10	Both agents increase their muscle co-contraction in the collaboration condition . . . . .	70
3.11	Pipe trajectory analysis . . . . .	71
3.12	Solo Manipulation Experiment: Deviation Angle . . . . .	72
3.13	Dyad Manipulation Experiment: Touches in the wall base w.r.t. relative tube position. . . . .	72
3.14	Solo Manipulation Experiment: Number of touches in the wall . . . . .	73
4.1	Human-Robot physical interaction study . . . . .	77
4.2	Human-robot object co-manipulation setup . . . . .	81
4.3	Trajectory designed for the robot . . . . .	84
4.4	Index of co-contraction, and robot stiffness modulation in human-robot co-manipulation . . . . .	86
4.5	RMS values of the index of co-contraction during human-robot co-manipulation . . . . .	86
4.6	Modulation on the perceived external torque during human-robot co-manipulation . . . . .	86
4.7	RMS values of $\tau_{ext}$ during human-robot co-manipulation . . . . .	87
4.8	Planar Trajectory for a Subject's Hand during the Human-Robot Object Co-Manipulation . . . . .	87
4.9	Deviation Angle during Human-Robot Co-manipulation . . . . .	87
4.10	Precision Task Error During Human-Robot Co-manipulation . . . . .	88
5.1	Perspective Future Work . . . . .	96
B.1	Sequence of key instants during the manipulation . . . . .	101
B.2	Average Index of Co-Contraction for dyads 1, 2, 3 . . . . .	102
B.3	Average Index of Co-Contraction for dyads 4, 5, 6 . . . . .	103
B.4	Average Index of Co-Contraction for dyads 7, 8, 9 . . . . .	104
B.5	Average Index of Co-Contraction for dyad 10 . . . . .	104
B.6	Trajectory of the barycentre of the agents' hands. Dyads 1 to 6 . . . . .	105
B.7	Trajectory of the barycentre of the agents' hands. Dyads 7 to 10 . . . . .	106
C.1	Average Index of Co-Contraction during Human-Robot Co-Manipulation Experiment . . . . .	107
C.2	Trajectory of the barycentre of the agents' hands for HR Co-Manipulation . . . . .	108
C.3	Interaction torque during human-robot co-manipulation . . . . .	109

# List of Tables

1.1	Ergonomics Evaluation Scores. $\varepsilon_{obj}(t)$ is the instantaneous score . . . . .	22
1.2	RMS errors between DART Simulation and Xsens reference trajectories . . . . .	29
2.1	Description of initial sets of human motion demonstration used on the benchmark. . . . .	45
2.2	Final $\mathcal{J}$ scores after optimization . . . . .	46
2.3	Improvement of the ergonomics score after single-objective optimization . . . . .	52
2.4	Ergonomics score improvement after SOTO and MOTO . . . . .	57
4.1	Robot's role definition . . . . .	80



# Summary in French

Le corps humain est un système extrêmement complexe composé d'un grand nombre de sous-systèmes intrinsèquement connectés, qui façonnent ses fonctions de base et ses capacités individuelles. L'une de ses caractéristiques les plus uniques est peut-être sa capacité à apprendre et de s'adapter à son environnement. De la petite enfance à l'âge adulte, les gens apprennent à utiliser leur corps de manière de plus en plus complexe: de la marche à la course, des pleurs à la parole, de la saisie d'objets à l'écriture. L'apprentissage et l'adaptation des comportements et des compétences motrices constituent en soi une demande élaborée qui repose non seulement sur la génération de forces et de couples, d'un point de vue biomécanique, mais aussi sur des fonctions psychologiques essentielles telles que la cognition et la perception [2]. Pourtant, les humains excellent largement dans ce domaine.

Dans le contexte du travail, les humains s'adaptent couramment aux conditions de leur environnement. Cependant, certaines situations nécessitent des adaptations qui pourraient être préjudiciables au corps humain. Par exemple, une personne peut être capable d'exécuter une certaine activité même en présence de sources de chaleur excessive, de bruit, de charge physique ou même de stress mental. À court ou à long terme, tous ces facteurs peuvent nuire au corps humain. Il peut être très difficile, voire impossible, de trouver les conditions exactes dans lesquelles l'exécution d'une tâche sera adéquate pour une personne donnée, car chaque individu a un corps unique et complexe, mais l'essentiel est de trouver une gamme de conditions dans lesquelles l'activité ne risque pas de nuire au corps à court ou à long terme. C'est exactement l'un des principaux objectifs de l'ergonomie [83].

L'ergonomie examine en tandem l'environnement de travail et les capacités des travailleurs qui s'y trouvent. L'environnement doit permettre au travailleur d'effectuer l'activité dans les limites de ses capacités physiques et mentales. Comme tous les corps ne sont pas faits de la même manière, les environnements de travail le sont aussi, et l'analyse ergonomique doit s'y adapter. Par exemple, un ingénieur industriel doit tenir compte d'un large éventail de capacités de force dans un échantillon d'ouvriers d'usine travaillant sur une chaîne de montage. Inversement, lors de la conception d'une voiture de course, on s'attend à ce que le pilote soit une personne athlétique. Dans les deux cas, l'analyse est toujours centrée sur l'humain qui exécute la tâche. À juste titre, l'ergonomie a été définie comme "la science de la conception du travail en fonction du travailleur, plutôt que du corps du travailleur en fonction du travail" [152].

De nos jours, les industries choisissent de poursuivre des taux de production de plus en plus élevés tout en améliorant la qualité de leurs produits, simplement pour rester compétitives. Indirectement, cela peut entraîner des activités professionnelles nuisibles à long terme : soulever des objets lourds ou encombrants ; spécialisation des tâches nécessitant une répétition excessive des mouvements ; travail plus de 8 heures par jour ; rythme de travail plus élevé que celui recommandé [71, 152]. Ce sont tous des facteurs qui peuvent nuire à la santé d'un travailleur, tant sur le plan cognitif que physique [160, 169, 189]. Un stress cognitif excessif au cours d'une tâche qui repose fortement sur le traitement de l'information peut détériorer le bien-être du travailleur et la performance de la tâche. Les exemples de stress cognitif comprennent les interruptions multiples au travail, le multitâche, ou même la perturbation par le bruit [71]. Le stress physique, quant à lui, est souvent corrélé au développement de troubles

musculo-squelettiques liés au travail (TMSLT).

Les TMSLT sont parmi les premières causes de maladies professionnelles dans le monde, représentant un problème de santé majeur, avec des coûts pour les entreprises et pour la société [160]. Selon l'Organisation internationale du travail, les TMSLT constituent la principale cause de pertes économiques liées aux maladies [115, 179]. Il n'est pas surprenant que les environnements de travail présentant de tels facteurs puissent présenter une incidence de TMSLT jusqu'à 3 ou 4 fois plus élevée que dans la population générale [139]. Elles se développent lorsque les exigences biomécaniques dépassent de façon répétée les capacités physiques des travailleurs et, avec l'effort, les postures contraignantes représentent l'un de leurs principaux facteurs de risque [139].

Les progrès technologiques peuvent créer des outils qui améliorent les conditions ergonomiques d'une activité professionnelle en étendant les capacités humaines et en minimisant la probabilité de TMSLT à l'avenir. Par exemple, un travailleur qui doit assembler un meuble avec un tournevis manuel mettra généralement plus de temps à assembler le meuble qu'un autre travailleur qui possède un tournevis électrique. Même si des postures contraignantes sont maintenues pendant l'opération, comme le temps est beaucoup plus limité, le travailleur équipé de l'outil électrique ne sera pas autant exposé à des conditions non ergonomiques et aura donc moins de chances de développer des TMSLT dues à l'activité d'assemblage à long terme.

Chaque génération de la révolution industrielle apporte avec elle de nouveaux outils pour le travailleur humain, et l'un d'entre eux a été particulièrement important pour l'avènement de l'automatisation moderne: les robots. Les robots peuvent être programmés pour détecter leur environnement et agir en conséquence pour obtenir un résultat attendu dans l'environnement en utilisant une certaine forme d'actionnement physique. Dans de nombreuses applications, ils effectuent des manœuvres puissantes et précises qui surpassent les capacités physiques humaines. En fait, dans bon nombre de ces cas, si les humains tentent même d'obtenir des performances similaires, ils courent un risque très sérieux de développer immédiatement une TMSLT. Dans un sens, on peut dire que les robots ont déjà amélioré les conditions d'ergonomie dans les industries depuis des décennies, car ils effectuent de nombreuses activités lourdes qui seraient certainement non ergonomiques pour les humains. Contrairement à l'exemple du tournevis, au siècle dernier, les robots étaient principalement utilisés dans des scénarios industriels, situés loin ou dans des espaces clôturés pour éviter tout contact humain avec eux. Toutefois, à bien des égards, cette distance devient rapidement de plus en plus courte de nos jours.

La dernière décennie a vu le développement de robots ayant une capacité de plus en plus grande à comprendre leur environnement et leurs éventuels partenaires humains. Les robots petits et légers dotés d'un haut niveau de perception peuvent potentiellement être utilisés en toute sécurité pour améliorer la vie quotidienne et l'ergonomie, non seulement dans les environnements industriels, mais aussi au bureau ou à la maison, et même en tant que robot portable. L'industrie de la robotique de service, les robots de nettoyage et de livraison par exemple, n'a cessé de croître ces dernières années, et rien n'indique que cette tendance va s'arrêter bientôt. Les robots de service capables d'assister physiquement les humains, pour la réadaptation ou les soins aux personnes âgées, ont même été identifiés comme des priorités de recherche par de nombreux pays développés, y compris des organisations européennes [1]. De plus, pendant la crise sanitaire actuelle causée par COVID-19, l'industrie de la robotique de service pourrait même avoir bénéficié du besoin croissant d'automatisation et de la distanciation sociale [187].

Dans le cas de l'industrie manufacturière, la position de la Fédération internationale de robotique (IFR en anglais) est que la demande des clients pour une grande variété de produits pousse les usines vers une fabrication à faible volume et à forte mixité [118]. Les usines doivent disposer de machines interconnectées numériquement, y compris des robots qui doivent être flexibles pour répondre à cette demande. Au premier plan de tout cela, les humains devraient être ceux qui fournissent le degré de flexibilité et les capacités de prise de décision nécessaires pour faire face à ces demandes [118]. Par conséquent, les humains sont la clé du succès des stratégies d'automatisation actuelles et futures, et les

---

robots devraient y être préparés.

Dans ce contexte, cette thèse a été financée dans le cadre du projet européen AnDy [61], qui prévoit de fournir aux robots des capacités de prédiction et d'anticipation de plus en plus importantes pour agir et réagir correctement lors d'une interaction homme-robot. Pour cette raison, il devient essentiel de développer des capacités de détection avancées sous forme de matériel et de logiciel pour que le système robotique soit capable d'atteindre la *conscience humaine*. Pour qu'un robot soit conscient d'un humain, il doit non seulement être capable d'estimer partiellement le mouvement de l'humain, mais aussi d'estimer la dynamique du mouvement du corps complet, ainsi que son statut ergonomique. Des mesures humaines complètes et efficaces fournissent des données plus précises pour l'estimation de l'ergonomie et des données plus pertinentes pour les modèles prédictifs. A la limite, ces modèles prédictifs plus efficaces confèrent au robot la capacité de s'adapter, de raisonner, non pas avec un protocole prédéfini, ou avec un autre robot, mais avec un être sensible rationnel qui adapte lui aussi en permanence son comportement: un être humain. Cette approche centrée sur l'humain est donc de la plus haute importance au sein du projet AnDy et également pour cette thèse.

Les travaux de cette thèse sont issus d'une approche pluridisciplinaire qui aboutit à un ensemble d'outils permettant d'améliorer l'ergonomie du mouvement du corps complet. **Le comportement moteur humain est évalué du point de vue de la robotique, mais pas exclusivement, des concepts issus des domaines de l'ergonomie et de la biomécanique sont également essentiels à notre approche.** Cette approche centrée sur l'humain est justifiée pour proposer des méthodes dans lesquelles un robot peut collaborer avec un partenaire humain de manière ergonomique tout en étant capable d'interagir physiquement et efficacement avec lui.

Les deux premiers chapitres de cette thèse traitent du problème de l'analyse du mouvement du corps complet d'un humain pendant une activité de travail spécifique selon un ensemble donné de scores ergonomiques. Le mouvement du corps complet est paramétré, rejoué, évalué et finalement optimisé pour l'ergonomie. Ce mouvement ergonomique, ou cet ensemble de mouvements ergonomiques, peut être exploité de différentes manières ; dans ce travail, une interaction homme-robot est proposée. Cependant, avant de conduire l'homme vers des trajectoires ergonomiques optimales connues, un contrôleur de robot doit être capable de coordonner ses actions avec le partenaire humain d'une manière efficace et engageante. Les deux derniers chapitres suivent cette voie centrée sur l'humain en étudiant le comportement moteur de l'homme pendant une tâche de co-manipulation d'objets. Le comportement moteur humain est analysé à la fois dans une dyade homme-homme et dans une dyade homme-robot où le robot essaie d'émuler le comportement humain de la dyade homme-homme.

**Simulation et optimisation de modèles humains numériques :** dans le chapitre 1, nous nous sommes inspirés de travaux récents sur la simulation de modèles humains numériques, ou DHMs en anglais [98, 156]. Nous avons proposé notre propre DHM dont le contrôle du corps complet est défini par un contrôleur QP basé sur la vitesse. La simulation du DHM dans un moteur physique léger permet d'évaluer rapidement et simultanément plusieurs trajectoires de mouvement du corps complet selon des scores ergonomiques qui évaluent non seulement la cinématique du mouvement mais aussi sa dynamique. L'optimisation du mouvement du corps complet est réalisable à condition d'obtenir une paramétrisation initiale adéquate du mouvement, tant au niveau du nombre de paramètres que de la qualité de la reproduction du mouvement. Le paramétrage et l'optimisation du mouvement du corps complet sont réalisés dans le chapitre 2.

Notre DHM imite les cadres anatomiques du corps humain, et contient donc 43 articulations rotatives. Si la paramétrisation du mouvement du corps complet est prise pour ce nombre élevé d'articulations, on peut s'attendre à un nombre très élevé de paramètres. Pour éviter ce problème, la formulation QP est utilisée ici à notre avantage. Le contrôleur QP peut essentiellement suivre plusieurs positions cartésiennes

tout en respectant toutes les contraintes des articulations du DHM. Par conséquent, au lieu de paramétrer directement toutes les trajectoires des articulations, une poignée de trajectoires cartésiennes est suffisante pour représenter le mouvement du corps complet. La paramétrisation elle-même est réalisée à l'aide de ProMPs (Primitives Probabilistiques de Mouvement), qui sont particulièrement intéressantes pour la paramétrisation des mouvements humains car elles encodent à la fois les mouvements humains et leur variance, étant donné qu'elles sont formées à partir de différentes démonstrations de trajectoires avec différentes durées. En fait, un ProMP peut être représenté de manière compacte par un seul vecteur de poids, et ce vecteur peut être utilisé pour générer la trajectoire moyenne codée. La trajectoire du corps complet est alors représentée par une pile de ProMPs individuels. Cette représentation du corps complet à l'aide d'un empilement de poids cartésiens ProMP tout en tirant parti des propriétés du contrôleur QP pour maintenir les contraintes au niveau des articulations fait partie des contributions de cette thèse, car elle permet une représentation très compacte, mais facile à saisir, du mouvement du corps complet. Après avoir proposé une solution au problème de paramétrage du corps complet, nous revenons à l'optimisation des mouvements du corps complet humain en fonction des scores d'ergonomie.

**Personnalisation et optimisation multi-objectif du mouvement:** Le corps humain est capable d'exécuter des mouvements de nombreuses façons différentes en raison du nombre élevé de DoF du corps et de l'efficacité du système musculo-squelettique. En outre, la population humaine présente une très grande variété de morphologies corporelles avec des capacités de puissance encore plus diverses. Par conséquent, si deux personnes ayant des morphologies corporelles très différentes tentent d'exécuter un ensemble identique de trajectoires cartésiennes, une évaluation ergonomique, comme celles du chapitre 1, pourrait donner des résultats très différents. En outre, chaque personne peut également avoir des contraintes particulières, comme une limitation de la flexibilité, ou un handicap par exemple. Ces facteurs individuels, ou contraintes particulières, ne sont pas pris en compte par les scores ergonomiques classiques. En un mot, un mouvement qui est ergonomique pour un individu peut être différent pour un autre, et de nombreuses exigences individuelles peuvent être difficiles à appréhender avec les évaluations ergonomiques classiques. Même si certaines stratégies ou certains modèles peuvent être conçus, nous montrons dans le chapitre 2 que les mouvements ergonomiques optimaux sont individuels.

Outre le caractère unique de chaque morphologie corporelle, l'optimisation d'une trajectoire du corps complet en fonction des scores d'ergonomie doit être traitée avec soin. Les TMSLT sont multifactoriels et peuvent se développer dans différents segments du corps. C'est pourquoi il existe de nombreuses façons de quantifier le risque de développer une TMSLT. Certains de ces scores d'ergonomie sont exposés dans le chapitre 1, et cela peut toujours se produire dans différentes parties du corps humain. Par conséquent, si l'objectif de l'optimisation de la trajectoire est de réduire le risque global de développer une TMSLT, l'optimisation d'un seul score ergonomique peut ne pas être suffisante ni optimale d'un point de vue ergonomique. Nos résultats de simulation avec l'optimisation de trajectoire à objectif unique montrent clairement que l'optimisation pour un seul score ergonomique n'est pas suffisante pour obtenir un mouvement ergonomique global à partir de l'optimisation. Pour résoudre ce problème, au lieu d'une optimisation à objectif unique, nous proposons une optimisation multi-objectifs. Dans l'expérience d'optimisation multi-objectifs, les conditions de simulation restent les mêmes, et deux ou plusieurs scores d'ergonomie sont choisis pour l'optimisation. Le résultat de toute approche d'optimisation multi-objectif est un ensemble de solutions non dominées, un front de Pareto, qui met généralement en évidence les compromis potentiels entre les fonctions objectives choisies. Il s'avère que c'était également le cas pour notre expérience. L'optimisation multi-objectif de la trajectoire a mis en évidence les compromis entre les différents scores d'ergonomie. De plus, à partir d'un front de Pareto, il est possible de choisir des mouvements du corps complet qui améliorent simultanément plusieurs scores d'ergonomie. Cette approche multi-objectif contraste avec les solutions de pointe pour l'optimisation des trajectoires ergonomiques

---

qui ne prennent en compte que l'optimisation mono-objectif.

**Comportement moteur humain pendant la coopération et la collaboration:** pour conduire une personne vers une posture ergonomique optimale de l'ensemble du corps à l'aide d'une interaction physique homme-robot, la trajectoire de référence elle-même n'est qu'une partie de la solution : le robot doit coordonner ses actions avec l'humain de manière efficace et finalement le conduire vers la trajectoire ergonomique. Dans le chapitre 3, l'approche consiste à étudier la façon dont les humains coordonnent leurs actions dans une tâche de co-manipulation sous différentes conditions de coordination du leadership : coopération leader/suiveur, ou pas de leader (collaboration). Dans la tâche proposée, la dyade humaine doit effectuer une manipulation difficile qui nécessite des mouvements précis. La configuration de l'expérience ne permet que la communication haptique entre les agents humains, sinon les résultats de l'expérience auraient pu être faussés par d'autres formes de communication qui ne sont pas suivies par la configuration, comme la parole ou le regard. Le comportement moteur des agents est suivi à l'aide de marqueurs de capture de mouvement et de signaux d'activation musculaire, ainsi que d'une mesure de l'efficacité d'exécution de la tâche. Les résultats de l'expérience confirment que lorsqu'un humain dirige la tâche, la co-contraction des muscles de son bras est significativement plus élevée que lorsque les agents sont des suiveurs, c'est-à-dire que les dirigeants augmentent la rigidité de leur bras par rapport aux suiveurs. Nous avons constaté que lorsqu'aucun leadership n'est assigné, dans une coordination s'apparentant à une collaboration telle que définie par Jarrassé *et al.* [66], les deux agents ont des niveaux de co-contraction du bras similaires à leur condition de leadership. La dyade humain-humain est plus efficace dans l'exécution de la tâche difficile de co-manipulation que lorsque l'un des agents est désigné comme leader.

Le mouvement des mains de la dyade suggère également que lorsque chaque agent humain dirige la tâche, leurs trajectoires souhaitées pour atteindre l'objectif de la tâche sont significativement différentes, ce qui signifie que dans ce cas, ils pourraient également favoriser des objectifs biomécaniques individuels tels que la manipulabilité du bras [150] par exemple. Cependant, d'autres expériences sont nécessaires pour confirmer cette hypothèse. En attendant, lorsqu'aucun leader n'est assigné, la trajectoire résultante semble être un arbitrage entre les trajectoires des deux autres conditions. Parallèlement aux résultats de modulation de la rigidité et d'efficacité de la tâche, cela pourrait signifier que pendant la collaboration, les agents communiquent haptiquement leurs intentions de mouvement en modulant la rigidité de leur bras [109], tout en estimant éventuellement les objectifs des autres pour arbitrer leur trajectoire souhaitée et améliorer l'exécution de la tâche [176]. Ce type de comportement moteur humain dans des conditions de coopération et de collaboration entre leader et suiveur s'inscrit dans la classification unifiée de contrôle partagé/autonomie partagée définie par Selvaggio *et al.* [163].

**Collaboration homme-robot :** Dans le chapitre 4, une dyade homme-robot exécute la même tâche que son homologue homme-homme. L'objectif de cette expérience est double : étudier le comportement moteur humain pour la même tâche, mais avec un robot, et essayer d'émuler ce comportement du côté du contrôle du robot. Compte tenu des résultats de l'expérience homme-homme, chaque fois que le robot se voit attribuer un leadership, on considère qu'il dispose d'une autonomie complète sur la tâche, tandis que le robot et l'humain partagent cette même autonomie lors d'une collaboration. Les deux comportements sont exprimés en modifiant la rigidité cartésienne souhaitée de l'effecteur du robot : le robot leader a une rigidité élevée, le robot suiveur une rigidité faible. De plus, dans cette expérience, l'autonomie de la tâche est arbitrée par la co-contraction du bras humain, en utilisant deux profils de contrôle d'impédance variable différents : réciproque et miroir.

Le profil réciproque fait passer le comportement du robot du statut de leader à celui de suiveur, tandis que l'humain cocontracte son bras, et par conséquent, passe du statut de suiveur à celui de leader. Par

conséquent, dans ce cas, l'autonomie est prise du robot dans les mains de l'humain, pour ainsi dire. Ce profil est similaire à celui mis en œuvre dans le [131] de Peternel, qui était arbitré par la somme des signaux d'activation musculaire d'une paire de muscles antagonistes, alors que dans le 4, un indice de co-contraction a été utilisé. Il s'agit d'une différence importante car la co-contraction musculaire est un phénomène associé à une stabilité et à une précision accrues du mouvement [14, 51] alors que la somme des efforts des muscles antagonistes n'a pas été associée à un tel résultat. Le profil miroir considère que le robot et l'humain doivent toujours partager la tâche à parts égales, il n'y a jamais de leader total ni de suiveur total. Dans ce profil, la rigidité cartésienne souhaitée du robot est directement proportionnelle à la co-contraction du bras humain. Il s'agit d'un comportement similaire à celui observé pour les comportements de collaboration homme-homme où les deux agents ont des valeurs élevées de co-contraction du bras. En outre, ce profil est également similaire à celui de Grafakos *et al.* [50], à la différence que dans ce travail connexe, le robot était toujours un suiveur, et la co-contraction du bras augmentait seulement l'amortissement cartésien souhaité du robot, qui était destiné à simplement intensifier la stabilisation du mouvement cartésien et non à partager l'autonomie de la tâche comme cela a été fait dans le chapitre 4. D'une part, le profil réciproque utilise une approche d'interpolation lisse leader/suiveur pour le partage de l'autonomie, similaire à d'autres travaux dans la littérature [3, 88, 110], et d'autre part, le profil miroir est plus proche en ressemblance avec ce qui a été observé pendant l'expérience humaine-humaine proposée pour la même tâche. Les deux profils de commande à impédance variable sont testés.

L'expérience homme-robot a été exécutée par un petit nombre de sujets, par conséquent, nous ne pouvons pas tirer de conclusions précises des résultats préliminaires, cependant, une tendance importante semble apparaître. Dans les conditions de collaboration, profils réciproque et miroir, la dyade homme-robot a exécuté la tâche avec plus de précision que lorsque l'homme ou le robot était en totale autonomie. De plus, il semble que la co-contraction du bras pendant les conditions de collaboration diminue par rapport aux conditions de leader/suiveur, ce qui pourrait être lié au fait que l'humain ne s'engage dans la tâche qu'à des moments spécifiques, comme s'il percevait qu'une trajectoire du robot ne serait pas suffisante pour accomplir l'objectif de la tâche par exemple. Le comportement leader-suiveur correspond à ce qui était attendu, avec une efficacité sous-optimale de la tâche, et l'humain présentant une faible co-contraction du bras lorsqu'il agit en tant que suiveur, et une co-contraction élevée lorsqu'il agit en tant que leader. Cependant, il n'est pas encore clair lequel des profils d'impédance variable est le plus adéquat pour la tâche. Il est néanmoins possible qu'en ayant une autonomie partagée, l'humain maintienne son engagement dans la tâche et sa conscience de la situation à un niveau élevé. Cela peut ne pas être le cas lorsque le robot dispose d'une autonomie complète pour la tâche [47] et cela pourrait entraîner une inefficacité de la tâche si l'exécution du robot n'est pas fiable ou si le robot a un potentiel de conscience situationnelle plus faible que le partenaire humain.

Globalement, au cours de cette thèse, il a été possible de développer des outils qui peuvent servir de base à une interaction physique homme-robot visant à améliorer l'ergonomie humaine. Dans notre approche, la prochaine étape au-delà de cette thèse est de rassembler ces pièces dans une seule application, où le mouvement humain optimisé est utilisé comme référence pour les profils d'impédance variable proposés dans le chapitre 4. Tout d'abord, le DHM doit être couplé avec un robot en simulation afin que les efforts du DHM reflètent mieux la réalité. Cela sera également facilité par le fait que le DHM est simulé sur un moteur généralement utilisé pour les simulations de robots [85]. Deuxièmement, davantage de données doivent être collectées pour l'expérience homme-robot afin de vérifier si les tendances observées présentent effectivement des effets significatifs. Enfin, la tâche conçue pour les expériences homme-homme et homme-robot est déjà très difficile du point de vue de la précision, mais les mouvements réussis sont déjà très contraints, de sorte qu'il n'y a pas beaucoup de marge pour l'optimisation ergonomique de la trajectoire. Par conséquent, une autre tâche de co-manipulation devrait être conçue,

---

dont l'exécution exigerait de la précision à certaines périodes de temps, tandis qu'à d'autres périodes de temps, le mouvement serait suffisamment libre pour permettre à l'optimisation ergonomique de produire des résultats significatifs. En d'autres termes, la tâche doit être suffisamment difficile pour que l'assistance du robot soit nécessaire pour obtenir à la fois la précision et l'ergonomie du mouvement.

Le développement des méthodes d'optimisation des mouvements et des profils d'impédance variable a été rendu possible par l'adoption d'une approche centrée sur l'homme, mettant l'accent sur la mesure et la compréhension de l'état humain. En outre, l'optimisation des mouvements et la coordination des dyades par l'interaction physique peuvent également être améliorées. Les perspectives de travaux futurs dans ces domaines sont ensuite discutées dans la section suivante.



# Introduction

The human body is an extremely complex system with a large amount of intrinsically connected sub-systems, shaping its basic functions and individual capabilities. Perhaps one of its most unique characteristics is the ability to learn and adapt to its environment. From infancy to adulthood, people learn how to use their bodies in progressively more complex ways: from walking to running, from crying to speaking, from grasping objects to writing. Learning and adapting motor behaviors and skills is in itself an elaborate demand that relies not only on generating forces and torques, from a biomechanical point of view, but also on core psychological functions such as cognition and perception [2]. Yet, humans largely excel at it.

In the context of labor, humans routinely adapt to their environment conditions. However, some situations require adaptations that could be detrimental to the human body. For instance, people may still be able to execute a certain activity even in the presence of sources of excessive heat, noise, physical load, or even mental stress. In the short or in the long term, all of these could harm the human body. It may be very hard, or impossible, to find the exact conditions in which the execution of a task will be adequate for any given person, as each individual has a unique and complex body, but the key point is to find a range of conditions for which the activity is not likely to harm the body in the short or in the long term. This is exactly one of the main goals of *Ergonomics* [83].

Ergonomics examine the work environment and the capabilities of the workers within it in tandem. The environment has to allow the worker to perform the activity under the worker's physical and mental limits. As not all bodies are made the same, so are work environments, and the ergonomics analysis has to adapt to it. For instance, an industrial engineer should consider a large range of strength capabilities in a sample of factory workers in an assembly line. Conversely, when a racing car is designed, the pilot is expected to be an athletic person [83]. In either case, the analysis is always centered around the human executing the task. Rightfully so, **ergonomics has been defined as “the science of designing the job to fit the worker, rather than the worker's body to fit the job” [152].**

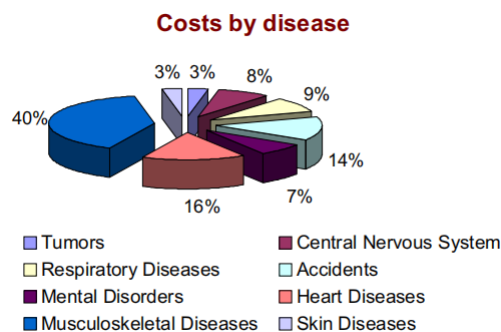


Figure 1: Distribution of costs due to work-related injuries and diseases (Image taken from an International Labor Organization report [179]).

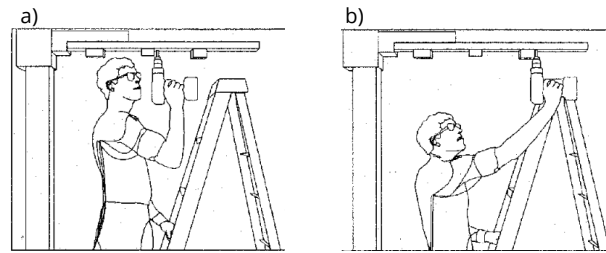


Figure 2: Different body postures for an overhead drilling task (Image taken from Anton *et al.* [7]): a) Ergonomically adequate posture. b) Ergonomically non-adequate posture.

Nowadays, industries choose to pursue higher and higher production rates along with their product quality just to remain competitive. Indirectly, this may incur in job activities that are harmful in the long term: lifting heavy or awkward items; task specialization that requires excessive motion repetition; working more than 8 hours a day; higher than recommended pace of work [71, 152]. Those are all factors that may hinder a worker's health both cognitively and physically [160, 169, 189]. Excessive cognitive stress during a task that heavily relies on information processing may deteriorate the worker's well-being and task performance. Physical stress, on the other hand, is often correlated to the development of Work-related Musculoskeletal Disorders (WMSDs).

WMSDs are among the first causes of occupational diseases worldwide, representing a major health issue, with costs for companies and society [160]. The International Labor Organization reported that the biggest single reason for economic losses regarding diseases are WMSDs [115, 179] (Fig. 1). Not surprisingly, work environments with such factors may present an incidence of WMSDs of up to 3 or 4 times higher than in the overall population [139]. They develop when biomechanical demands repeatedly exceed the workers' physical capacities, and, along with force exertion, awkward postures represent one of their major risk factors [139] (Fig. 2).

Technology advancements can create tools that improve the ergonomic conditions of a work activity by extending the human capabilities and minimizing the likelihood of WMSDs in the future. For instance, a worker that has to assemble a piece of furniture with a manual screwdriver will generally take longer to assemble the piece than another worker that possesses an electrical screwdriver. Even if awkward postures are sustained while doing so, because the time is much more limited, the worker with the powered tool will not be exposed to non-ergonomic conditions as much, and therefore will have a lesser chance of developing WMSDs due to the assembly activity in the long-term.

Each generation of the industrial revolution brings with it new tools for the human worker, and one of them has been specially important to the advent of modern automation: *robots*. Robots can be programmed to sense their environment and act accordingly to obtain an expected outcome in the environment by using some form of physical actuation. In many applications, they display powerful and precise maneuvers that outperform human physical capabilities. As a matter of fact, in many of those cases if humans even attempt to have similar performance this would incur in a very serious risk of developing a WMSD immediately. In a sense, it can be argued that robots have already been improving ergonomics conditions at industries for decades as they have been doing many heavy activities that would be certainly non-ergonomic to humans. Contrarily to the screwdriver example though, in the past century, robots were mainly used in industrial scenarios, located far away or in fenced spaces to avoid any human contact with them. However, in many ways, this distance is rapidly becoming shorter and shorter nowadays.

The past decade has seen the development of robots with increasingly more capacity of understanding its environment and its possible human partners. Small and light robots with a high-level of perception can potentially be used in a safe manner to improve daily life, and ergonomics, not only in industrial



Figure 3: Humans and robots in close proximity in and out of the industrial environment [119]. a) Active exoskeleton that supports lumbar motion at the sagittal plane (German Bionic); b) Active exoskeleton that transforms itself into a stool (Noonee); c) Robotic arm attached to a wheelchair (Kinova); d) Telepresence robot supports independent living for the elder (Giraff Telepresence Robot) .

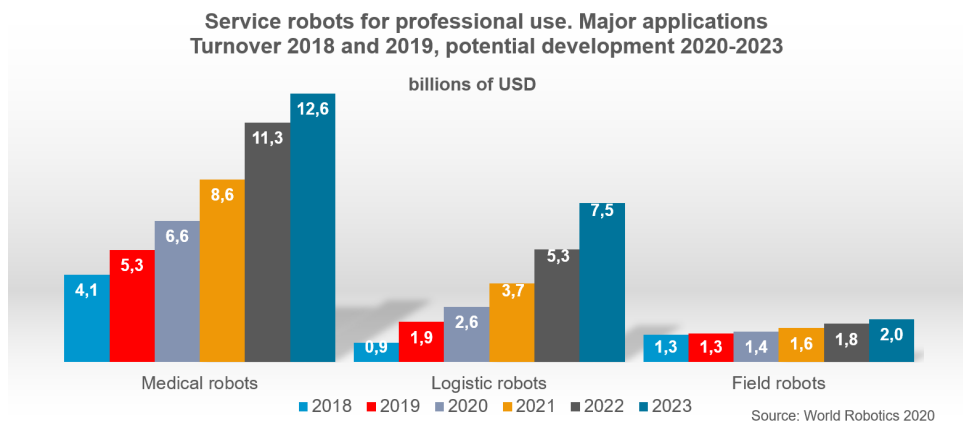


Figure 4: Yearly increasing in sales projections for the worldwide market in service robotics [117].

environments but also in the office, or at home, and even as a wearable robot (Fig. 3). The industry of service robotics, cleaning and delivery robots for instance, has been steadily growing over the recent years, and there is no indication that this trend will stop soon (Fig. 4). Service robots that are capable of physically assisting humans, for rehabilitation, or elderly care have been identified as research priorities by many developed countries, including European organizations [1]. Moreso, during the current sanitary crisis caused by COVID-19, the service robotics industry may even have been benefitted from a growing need for automation and for enabling social distancing [187].

In the case of the manufacturing industry, the International Federation of Robotics (IFR) position is that customer demand for a high variety of products drives the factories towards low-volume and high-mix manufacturing [118]. Factories should have digitally interconnected machines, including robots that need to be flexible to attend that demand. At the forefront of it all, humans should be the ones to provide the degree of flexibility and decision-making capabilities required to deal with those demands [118]. Therefore, humans are key for the success of current and future automation strategies, and robots should be prepared for it.

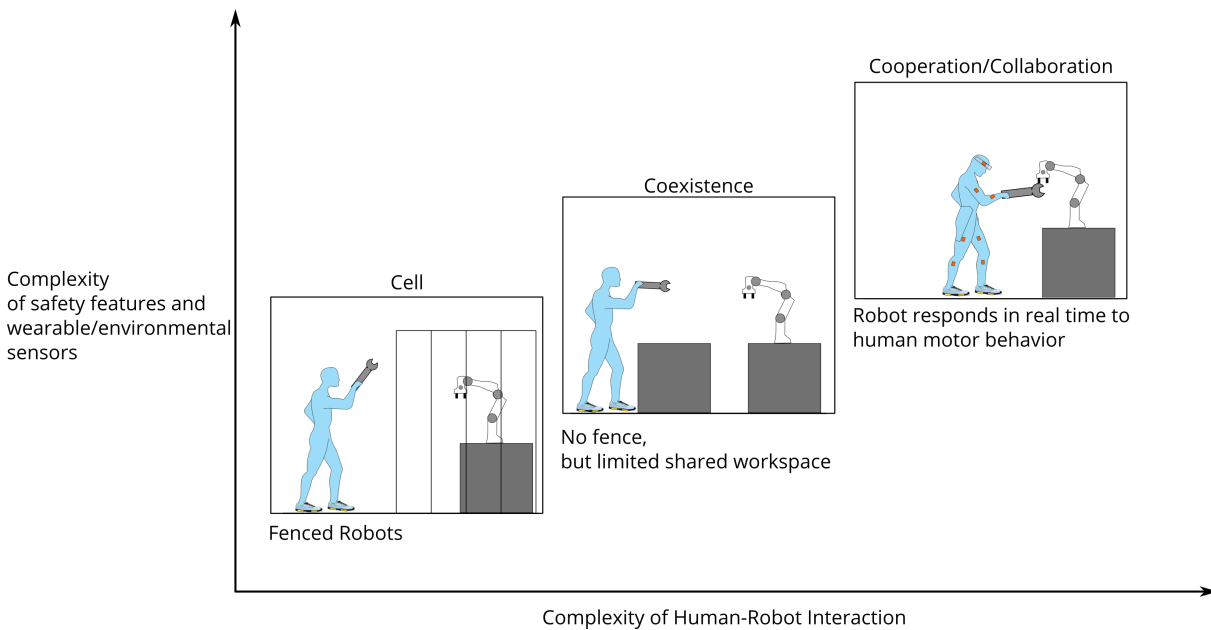


Figure 5: The more complex the human-robot interaction is, the more complex are the required safety features and sensors external to the robot in an industrial environment. Robots enclosed by cages or fences without any interactions with human; Robots coexisting without a shared workspace with humans, or at most working in the same workspace but at different periods of time; Robots working with human at the same workspace at the same time in a cooperative/collaborative interaction.

In this context, this thesis was funded under the European project AnDy<sup>1</sup> [61], that foresees robots being supplied with increasingly more prediction and anticipation capabilities to act and react properly during a human-robot interaction. For this matter, it becomes key to develop advanced sensing capabilities in the form of both hardware, and software for the robot system to be able to achieve *human awareness*. For a robot to be aware of a human,



it should not only be able to estimate the human motion partially, but also to be able to estimate the dynamics of the whole-body motion, as well as its ergonomics status. Comprehensive and efficient human measurements provides more accurate data for ergonomics estimation and more relevant data for predictive models. At the limit, these more efficient predictive models endow the robot with the capability to adapt, to reason, with not just a predefined protocol, or with another robot, but with a rational sentient being that is also constantly adapting its behavior: a human being. This human-centered approach is, therefore, of the utmost importance within the AnDy project and equally for this thesis.

## 1 From Human to Robot Collaboration

In the past, industrial robots were relegated to special areas of the factory floor, where they were guaranteed not to enter in contact with the human workforce. But the need for human-centric approaches in automation has been changing that. Leveraging the superior capabilities of humans and robots, applications where the two are not only able to, but need to interact with each other are becoming more and more common in industry, especially with the advent of cobots. Cobots, as defined by Colgate *et al.* [25],

<sup>1</sup>Advancing anticipatory behaviors in Dynamic human-robot collaboration.

are robotic devices that can provide assistance to a human operator and guide the motion along the task execution. The constant evolution of cobot's safety standards, and hardware actuation [11, 105, 114] make it possible for modern cobots to be designed to be in close proximity to a human worker, even around the worker's peripersonal space<sup>2</sup>. The requirements of human awareness for the robot increase as the human gets closer to the robot (Fig. 5). Safety is of course one of the main reasons, however, not the only one. The human is a partner that is constantly adapting and reacting to its environment. If the robot has autonomy over a different task or sub-task than the human partner (cooperation), then it is possible to overlook the human actions in the given task or sub-task. To achieve true human-robot collaboration, where the robot and the human share the same task, with the same goals, we point out that the robot should exhibit the same social sensorimotor control mechanisms that humans have during a human-human collaboration.

The main sensorimotor control mechanisms that drive human-human interaction are: shared representation, prediction, and signaling [18]. The mere presence of another human agent in the execution of a task changes the perception and motor behavior of a human agent [39, 101], even if the other's actions do not influence on the task directly [161]. Recent studies have reported that in a dyadic interaction, humans may see themselves as a dyadic unit, rather than the sum of its parts [36, 198]. Interacting humans also seem to utilize sensorimotor forward models to predict their partner motor behaviors [201]. Moreover, humans also expect other humans to make accurate predictions over their own goals and the environment [18, 80]. In addition, to improve their own predictability, humans signal their intentions to their partners in many different ways, such as gaze [193], haptic sensory cues [109], or their kinematic behavior [154]. As a matter of fact, changing motor behavior may incur in extra energy expenditure, but as long as the benefit of signaling balances this cost, humans are willing to do it [20].

Given the many possible ways a human can interact, and be represented, human-robot interaction applications have also used a varied set of sensors, for modeling, estimation and prediction of the human state. State-of-the-art motion capture techniques remain widely used to provide high-fidelity and high-frequency measurements of human kinematics [194]. While human kinematics can serve to inform about human's intent, the on-line estimation of human dynamics is receiving a lot of attention since it enables the robot to consider aspects such as balancing, or humans' internal force distribution [82]. Dynamics estimation requires a measure of external forces, either via generic force/torque (F/T) sensors that can be embedded in the robot, or via specific sensors such as force plates for human/ground reaction force. Wearable force sensors such as sensorized insoles are also of interest due to their portability [168].

Measurements of physiological quantities are also common in human-robot cooperation. Physiological quantities can be used as such, for instance, electromyography (EMG) signals have been used to estimate human muscle fatigue [132]. But physiological quantities can also serve to estimate the human cognitive state: electrocardiography (ECG) and galvanic skin response (GSR) signals have been linked to stress and anxiety levels [27], while eye gazing was correlated with engagement and proactivity levels during social human robot interactions without physical contact [9].

In more recent works, there are indications that individual factors such as personality, can affect the human posture and motion while interacting with a humanoid robot [192] (motor contagion), or even the level of trust towards the robot [58]. These emotional, and perception factors should also be monitored by the robot in order to provide mental safety during interactions [72].

Control approaches that consider the task autonomy to be shared between the robot and the human (collaboration as defined by Jarrassé *et al.* [66]) are becoming more and more frequent. These shared autonomy approaches arbitrate the robot's level of autonomy towards the task based exactly on the human representation [163]. However, not all of them attempt to represent the human, constantly predict their behavior, and signal to the human the robot's intent at the same time. Therefore, we argue that in those

---

<sup>2</sup>Some of which are depicted in Fig. 3.

cases the human may not perceive this collaboration attempt as a natural interaction, however this is a hypotheses that still needs to be tested. Meanwhile, a study on young children suggested that humans have a tendency to act in a collaboratively manner, even if the task does not require collaboration [200]. Bütepage and Kragic [18] suggest that to achieve a similar behavior, robot action should be rewarded not only for the task execution but also by the quality of the collaboration. In a human-robot collaboration of good quality the robot would be able to accurately predict human's actions while the human would also respond properly to the robot's actions, in sum, the agents would constantly co-adapt to each others motor behaviors. This collaborative behavior can be potentially used to induce trajectories during a physical human-robot interaction, including ergonomic trajectories.

## Ergonomics Intervention Through Human-Robot Collaboration

The classic approach to assess the risk of WMSDs in industrial environments is to observe the work activity, and manually compute ergonomics scores, typically, using paper-based spreadsheets. These spreadsheets are meant to be filled by the evaluator, an ergonomics expert, *in loco* or by video observations. This approach has been widely successful in assessing the risk of WMSDs in industrial environments, but it has important limitations due to its mostly paper-based methods [41]. The first problem with this approach is that if there is any significant change to the work environment, such as a new machine for instance, the expert needs to redo the evaluation, and the evaluation is of course subject to their availability. This alone would be a bottleneck for any given factory that needs to be flexible. In addition, even if the assessment evaluation is highly standardized, there will always be a level of subjectivity, and imprecision related to the manual scoring of a task. Different ergonomics experts could diverge when choosing the postures in which they will evaluate the task for example. Therefore, automatic risk-assessment evaluations aim to conserve the success of the classic evaluation tools, while still being flexible. However automatic evaluation is only part of the solution, if it is not followed by an automatic ergonomic intervention, then the factory bottleneck may still be present.

A human-aware robot can be used to improve the human ergonomics status during some tasks [16, 141, 166]. In physical interactions, moving a box or table with the robot's assistance for instance, recent works have been able to change the robot motion in order to decrease human joint efforts [74], muscle activation [43], fatigue [129], or other indexes based on classic evaluation tools [190, 205]. In many of those cases, even though the robot is only assisting the human to achieve a more ergonomic body posture, and assisting on the task *per se*, the robot needs to actively engage in the task. We argue that physical interaction could be more effective, and perceived as more natural to the human partner during robot ergonomics interventions if sensorimotor control mechanisms present in human-human interactions are also taken into account [18]

## 2 Contributions and Thesis Organization

**The main objective of this thesis is, to provide tools to improve the ergonomics of the human body postures during an object co-manipulation task.** Our approach is summarized as follows (Fig. 6):

1. Automatically reproduce and ergonomically evaluate a whole-body motion for a task execution using a Digital Human Model simulation
2. Generate “optimal” ergonomic motions for the human body posture
3. Study the human motor behavior executing a task that requires coordination of the human actions
4. Evaluate different robot control laws to emulate the human motor behavior for task collaboration

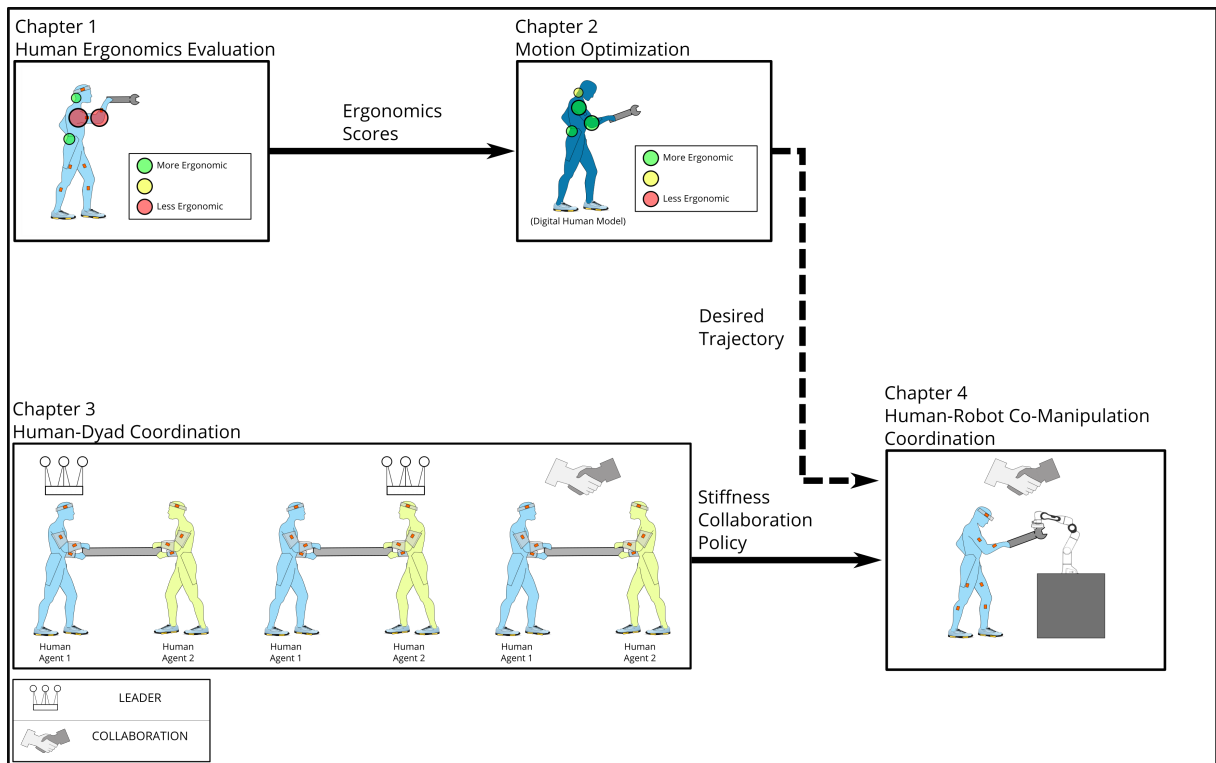


Figure 6: Thesis organization. In chapter 1, we discuss how to evaluate movements with respect to ergonomics. Then, in chapter 2, an initial motion is optimized for several ergonomics scores using multi-objective optimization. In chapter 3, we present a human-dyad study where we investigate different coordination configurations, and compare their efficiency in a precision task. Finally, in chapter 4, we present a physical human-robot interaction where the robot tries to emulate the human-human coordination using haptic signals. The desired ergonomics trajectory input to the human-robot coordination is represented with a dashed line since this scenario was not experimented in this thesis, but it is in the future work perspective.

This approach includes both whole-body posture ergonomics evaluation, and dyadic interaction analysis, from which a human-robot application can leverage a better physical interaction. Given the multi-disciplinary nature of the topics, for clarity of presentation, each chapter presents a state-of-the-art review of its relevant topics.

Chapter 1 reviews some classic ergonomics criteria and their scoring system. We took inspiration on recent works on the simulation of DHMs [98, 156] to propose methods for automatic ergonomics evaluation using a custom Digital Human Model (DHM) controlled by a Quadratic Programming (QP) controller within a physics simulator. Furthermore, **in the end of this chapter, a real-world case study of ergonomics evaluation in a work environment is presented.**

Chapter 2 proposes methods to optimize whole-body motion trajectories for a DHM and humanoid robot under single- and multiple-objective optimization experiments. The motions are parameterized using stacks of Probabilistic Movement Primitives, ProMPs [125]. **The whole-body representation using a stack of Cartesian ProMPs while leveraging the QP controller properties to maintain the joint-level constraints is one of the novel contributions in this thesis, as it allows for a very compact, yet easy to grasp, representation of the whole-body motion.** Moreover, if two people with very different body morphologies attempt to execute an identical set of Cartesian trajectories, then an ergonomics evaluation could yield widely different results. Each person can also have special constraints, such as a limitation on flexibility, or a handicap for instance. These individualities, or special constraints are not taken into account by classic ergonomics scores. **Even though some strategies or patterns could be devised, we verify using single-objective trajectory optimization that optimal ergonomic motions are individual.**

The causes for WMSDs are multi-factorial and may be developed at different body segments. Therefore, if the goal of the trajectory optimization is to decrease the overall risk of developing any WMSD, then optimizing for a single ergonomics score may not be sufficient. **Our experiment results with single-objective trajectory optimization make it clear that optimizing for a single ergonomics score is not sufficient to obtain an overall ergonomics motion from the optimization.** The resulting trajectories in the multi-objective optimization experiment highlighted trade-offs between different ergonomics scores. In addition, **we show that from a Pareto front of optimal motions regarding different ergonomics scores, it is possible to pick whole-body motions that simultaneously improve many ergonomics scores.**

Chapter 3 presents a study on the human-dyad motor behavior during an object co-manipulation. The motor behavior is analyzed through the agents' kinematics, muscle activation signals, and the dyad efficiency at executing the proposed task. The human-human dyad has to perform a challenging manipulation that requires precise movements from the dyad. **During the human collaboration, the human-human dyad seems to be more effective at executing the challenging co-manipulation task than when one of the agents is assigned as a leader, in cooperation. We also observed different patterns in arm co-contraction and trajectory modulation according to cooperation and collaboration conditions.**

Chapter 4 presents a human-robot object co-manipulation using an industrial cobot under different control strategies whose aim is to emulate the cooperation and collaboration capabilities presented in the human-human study. It presents two different variable impedance control profiles to emulate the human motor behavior seen on the human-human experiment during the collaboration condition.

The human-robot experiment was executed by a small number of subjects, so statistical tests are

not conclusive, however, an important trend could be identified: **during the collaboration conditions, reciprocal and mirrored profiles, the human-robot dyad executed the task more accurately than when the human or the robot were given full autonomy to the task.**

### 3 Publications

The body of work of this Ph.D. has produced several contributions in the form of academic articles, software, and videos. All of which are described below.

#### Accepted / Published Articles

- **Exoturn Project:** this project aimed to select exoskeletons to alleviate efforts from healthcare workers during the execution of a strenuous and non-ergonomic task.

**Contribution:** Our Digital Human Model simulation was used to make ergonomic evaluations of the human motion with and without the exoskeleton of choice. The study is presented within chapter 1.

Serena Ivaldi, Pauline Maurice, **Gomes, Waldez**, Jean Theurel, Lien Wioland, Jean-Jacques Atain-Kouadio, Laurent Claudon, Hind Hani, Antoine Kimmoun, Jean-Marc Sellal, Bruno Levy, Jean Paysant, Serguei Malikov, Bruno Chenuel, and Nicla Settembre. Using exoskeletons to assist medical staff during prone positioning of mechanically ventilated covid-19 patients: A pilot study. In Jay Kalra, Nancy J. Lightner, and Redha Taiar, editors, *Advances in Human Factors and Ergonomics in Healthcare and Medical Devices*, pages 88–100, Cham, 2021. Springer International Publishing

- **Optimization of Retargeted Whole-Body Motion:** this study proposes optimizing motions that have been previously retargeted from a human to a humanoid robot with respect to the robot’s capabilities.

**Contribution:** We showed how to use movement primitives to parameterize and optimize whole-body motion. The study is presented within chapter 2.

**W. Gomes**, V. Radhakrishnan, L. Penco, V. Modugno, J. Mouret, and S. Ivaldi. Humanoid whole-body movement optimization from retargeted human motions. In *2019 IEEE-RAS 19th International Conference on Humanoid Robots (Humanoids)*, pages 178–185, 2019

**Video** is available at: [youtu.be/rJZVrVAVLMs](https://youtu.be/rJZVrVAVLMs).

- **Review on Human-Humanoid interaction:** it reviews different aspects of human-humanoid interaction, such as social factors, robot interaction control, human perception and human behavior modelling. Additionally it also reviews relevant applications on the field.

**Contribution:** Our role on the review was related to the state-of-the-art on sensing and measuring the human status which is also partially present in this introduction chapter.

Lorenzo Vianello, Luigi Penco, **Gomes, Waldez**, Yang You, Salvatore Anzalone, Pauline Maurice, Vincent Thomas, and Serena Ivaldi. Human-humanoid interaction and cooperation: a review. *Current Robotics Reports*, 2021

- **Multi-Objective Whole-Body Optimization w.r.t. Ergonomics:** this study proposes optimizing the ergonomics of a human whole-body motion using several ergonomics scores simultaneously.

**Contribution:** This work pushed forward the current work on whole-body motion generation by making the case for taking into account several ergonomics score simultaneously. The proposed methods are presented in chapter 2.

**Gomes, Waldez**, Pauline Maurice, Eloïse Dalin, Jean-Baptiste Mouret, and Serena Ivaldi. Multi-objective trajectory optimization to improve ergonomics in human motion. *IEEE Robotics and Automation Letters*, 2021, Accepted for publication

Video is available at: [youtu.be/vgQ0Ybs9TTo](https://youtu.be/vgQ0Ybs9TTo).

## In Preparation

- **Motor Behavior of a Human-Human Dyad in an Object Co-manipulation:** the dyad was analyzed according to their motion, muscle activation signals and efficiency executing the task.

**Contribution:** We found important differences on the motor behavior of a human-human dyad between different forms of coordination. This study is presented in chapter 3.

**Gomes, Waldez**, Pauline Maurice, Jan Babic, Jean-Baptiste Mouret, and Serena Ivaldi. In a collaborative co-manipulation, humans have a motor behaviour similar to a leader. *Nature Human Behaviour*, In Preparation

The raw **dataset** is available at the DOI: 10.5281/zenodo.3989616 [183].

**Custom code** developed for the experiment is available at: <http://github.com/inria-larsen/emg-processing>

- **Latent Ergonomics Maps:** demonstration of real-time activity recognition and ergonomics visualization tools on a human-robot object co-manipulation task.

**Contribution:** We participated on the development of the Digital Human Model, and on the data collection for the experiments. Even though it was not an integral part of this Ph.D thesis body of work, we believe Latent Ergonomics Maps to be an important tool for ergonomics visualization going forward. For this reason, they are also briefly presented in chapter 1.

Lorenzo Vianello, **Gomes, Waldez**, Francis Colas, Pauline Maurice, Freek Stulp, and Serena Ivaldi. Latent ergonomics maps: Real-time visualization of estimated ergonomics maps. *Sensors*, In Preparation

Video is available at: [youtu.be/bPJ5HfE3wAw](https://youtu.be/bPJ5HfE3wAw).

# 1

## Human Ergonomics Evaluation

In this chapter, we briefly review the main procedures and criteria for evaluating ergonomics at work with the aim to reduce the risk of musculoskeletal disorders. Then, we follow-up by showing some of the advantages of leveraging Digital Human Models to automate ergonomics evaluations tools. We show our proposed Digital Human Model, and how we control its whole-body under a lightweight physics engine in simulation. Some ergonomics scores are presented in more detail as they are used throughout this thesis.

At the end of this chapter, we present a real-world case study in which we evaluate the ergonomics of a specific healthcare maneuver in a hospital intensive care unit under stress from the COVID-19 outbreak.

### 1.1 Musculoskeletal Disorders and Ergonomics Evaluations

Work-related musculoskeletal disorders (WMSDs) represent a major health issue with important costs for companies and society [160]. For instance, the incidence of some WMSDs in certain industries and occupations can be up to 3 or 4 times higher than the overall frequency of the same disorders on the general population [139]. They include a wide-range of syndromes and conditions on muscles, tendons, joints and peripheral nerves, usually developing when a work activity repeatedly exceeds the workers' physical capacities, as in with excessive force, or maintaining awkward body postures [139]. The risk of developing those disorders may also vary according to age, gender, muscle strength, smoking, and other personal factors. Nonetheless, ergonomics processes of evaluation and intervention that reduce or eliminate physical stressors are still a great help in preventing WMSDs.

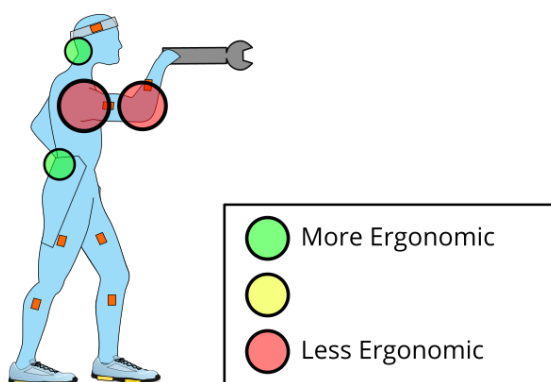


Figure 1.1: Illustration of ergonomics visual feedback for a human holding an object above the head.

Before changing a setup, or modifying a certain work-activity towards a more ergonomic environment, one needs to choose and define ergonomics methods and/or scores to assess the risk of developing WMSDs associated with the activity in question [29]. A proper choice of the ergonomics evaluation is key to avoiding potentially harmful misclassifications. For instance, if a work activity generates major stress on the worker's shoulders, it may not be appropriate to evaluate the ergonomics of the lower limbs. Even if an ergonomics score related to the shoulder is chosen, if the evaluation is based on an observation made over a brief period of time that is not representative of the entire work-day, then misclassifications may still occur.

In industry, most ergonomics evaluations are based on observations made by ergonomists that report their findings on worksheets [147]. These worksheets were designed as field tools, that could be easily calculated with pen and paper by a practitioner. Generally speaking, most evaluation tools output bad scores for activities that maintain human joints out of known ergonomic neutral positions, and that require several motion repetitions, or transportation of heavy loads. To facilitate, and standardize policies for intervention they also classify the activity according to overall scores. Some of the most used scores are: RULA (Rapid Upper Limb Assessment), a standard sheet that evaluates some upper body joint angles [100]; REBA (Rapid Entire Body Assessment), an extension of RULA that additionally takes into consideration some joint angles from the lower body [55], OWAS (Owako Working Posture Analysis System) [26], OCRA (Occupational Repetitive Actions) [116], EAWS (European Assessment Worksheet) [158].

Even though they may be commonly regarded as classic and standard tools, the aforementioned observational scores have important limitations. They require a reliable assessment of the body posture [6, 41] which is not always achievable from the naked eye, or from video observations [86, 191]. Furthermore, the overall scores can also vary greatly for joint angles that are close to the score boundaries, e.g., a 60.5 degrees of elbow flexion could be disproportionately worse for a RULA score than 59.5 degrees would. Therefore, the overall score is subject to high intra- and inter-observer variability [135]. In addition, those methods may need to be run several times, if there is any major change to the setup, or if workers with very different body morphologies are hired after the initial evaluation, a new evaluation will have to be done to take those changes into account. In order to automate those evaluations, many studies have started using Digital Human Models as digital twins for the workers in simulated work environments [156].

## 1.2 Digital Human Model

Digital Human Models (DHMs) are articulated human body representations that can be used to study the human motion. As the industry starts to focus on manufacturing solutions that are more and more human-centric [91], DHMs are used to capture information of the human state. For instance, state-of-the-art motion capture systems such as the Xsens MVN suit [146] use Inertial Measurement Unit (IMU) sensors to capture the joint angles of the human body and retarget them to a proprietary DHM (Fig. 1.2).

The level of complexity of a DHM varies on the level of detail needed by a given application. In the biomechanics community, one is often interested on studying complex interactions between a given motion and the actuation and interaction between the involved muscles and tendons [28, 33]. Although potentially more precise, those types of musculoskeletal models [28] are very computationally expensive, often, taking many hours to analyze brief motions. For this reason, many applications that require quick ergonomics evaluations such as optimization [190], or real-time ergonomics assessment [76] prefer using less complicated DHMs where the human is modelled as a set of rigid bodies connected by ideal rotational joints.

Similarly to other recent works [76, 186], the DHM used here is modelled with basic shapes, and

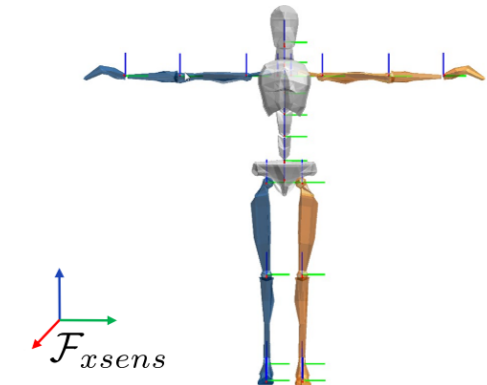


Figure 1.2: Digital Human Model Example: Xsens MVN system [146]. The origin of the Xsens frame is defined by the system's initial calibration.

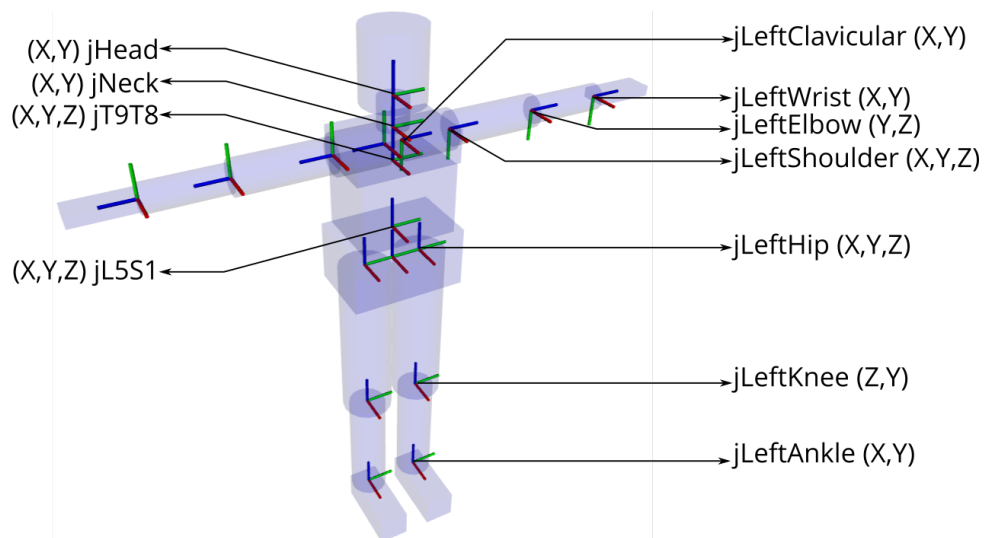


Figure 1.3: .  
Digital Human Model (DHM) joints description. The axes are X=Red, Y=Green, Z=Blue.

Table 1.1: The ergonomics evaluation scores used in this thesis.  $\varepsilon_{obj}(t)$  is an instantaneous score.

Description	Score	$\varepsilon_{obj}(t)$
RULA-C	Regression of RULA [99]	$\varepsilon_{rc}$
Normalized whole-body effort	$\frac{1}{n_{joints}} \sum_{i \in joints} \left( \frac{\tau_t^i}{\tau_{max}^i} \right)^2$	$\varepsilon_{nwe}$
Torques Shoulder	$\ \boldsymbol{\tau}_{shoulder}\ $	$\varepsilon_{tsh}$
Torques Lumbar	$\ \boldsymbol{\tau}_{lumbar}\ $	$\varepsilon_{tlb}$
Back Flexion	$\ \theta_{L5S1}^Y\ $	$\varepsilon_{back}$

inertia properties. The DHM (Fig. 1.3) consists of 19 rigid bodies linked together by 18 compound joints, for a total of 43 DoFs,  $\mathbf{q} \in \mathbb{R}^{43}$ , (11 for the back and neck, 9 for each arm including the sternoclavicular joint, and 7 for each leg), plus 6 DoFs for the free-floating base. Each DoF is a revolute joint controlled by a single actuator. Different human morphologies are easily generated from a desired body mass and height, by scaling the geometric and inertial parameters of the human model according to average anthropometric coefficients [22, 120].

Our DHM's simple shapes are particularly useful to simulate the whole-body motion in a physics engine (DART [85]). This allows us to evaluate the DHM not only w.r.t. kinematical ergonomics scores, related to the body's joint and Cartesian positions, but also w.r.t. scores that consider the dynamics of the motions, such as the efforts exerted by or on the body. Additionally, the DHM is controlled using multi-task Quadratic Programming (QP) controller [106]. The QP controller generates whole-body motions that respect whole-body motion constraints, such as the DHM's joint limits. The QP controller takes reference Cartesian trajectories that define the activity, and outputs desired joint velocities for the DHM. The QP is set to minimize the tracking error of these references while handling task priorities defined by the user. The priorities are defined by hierarchical levels, and tasks within the same level are further prioritized by their task weights. The control of  $n$  tasks  $\mathcal{T}$  is formulated as a QP problem:

$$\dot{\mathbf{q}}^* = \arg \min_{\dot{\mathbf{q}}} \|\mathbf{A}_n \dot{\mathbf{q}} - \mathbf{b}_n\|_{\mathbf{W}} \quad (1.1)$$

$$\text{s.t.} \quad \mathbf{C}_{1,n} \dot{\mathbf{q}} \leq \mathbf{b}_{1,n} \quad (1.2)$$

$$\mathbf{C}_{2,n} \dot{\mathbf{q}} \leq \mathbf{b}_{2,n} \quad (1.3)$$

where  $\dot{\mathbf{q}}^*$  is the desired velocity sent to low-level controllers (solution for the QP problem),  $\mathbf{A}_n \in \mathbb{R}^{(n_j+6) \times (n_j+6)}$  is the Jacobian matrix for the task,  $\mathbf{b}_n \in \mathbb{R}^{(n_j+6)}$  is a reference value for the task,  $\mathbf{W}$  is a positive definite weight matrix,  $\mathbf{C}_{c,n} \in \mathbb{R}^{(n_j+6) \times (n_j+6)}$  and  $\mathbf{b}_{c,n} \in \mathbb{R}^{(n_j+6)}$  encode lower, upper bounds, equalities and inequalities from the  $c$ -th constraint for  $\dot{\mathbf{q}}$ .

If a task  $\mathcal{T}_1$  has a hard priority over  $\mathcal{T}_2$ , this means that  $\mathcal{T}_2$  is solved within the null space of  $\mathcal{T}_1$ .

### 1.3 Ergonomics Scores Evaluation

Typically, each ergonomics score represent a different physiological phenomena that could increase the risk of developing WMSDs [29]. In particular, we want to define an ergonomics score as an objective function to our formulation, both for simplicity in the evaluation, and later to use it in optimization processes. However, neither for evaluation, nor for optimization there is a strict consensus on a single score to use. Moreover, different ergonomics scores might be antagonistic among themselves, *e.g.* the same movement could produce ergonomically suitable results for a score, and unsuitable results for another.

For this reason, instead of using an aggregated score, that is often task-specific, we consider several scores,  $\varepsilon_{obj}$ , separately (Tab. 1.1). In order to obtain an evaluation of the entire trajectory execution, we can use a cost proportional to the squared RMS value of  $\varepsilon_{obj}$  for each score, for the entire activity duration:

$$\mathcal{J}_{obj} = \sum_{t \in [0 \dots T]} \varepsilon_{obj}^2(t) \quad (1.4)$$

where  $T \in \mathbb{R}$  is the final simulation instant. Below, we describe each of the selected scores  $\varepsilon_{obj}$ .

**RULA-C or RULA Continuous:** The Rapid Upper Limb Assessment (RULA) tool [99] is often used by ergonomists to evaluate work activities involving upper-body motion. It consists of a score ranging from 1 to 7, calculated based on the joint positions (posture), the force/load applied at the worker's arm, and the number of times the activity is repeated. Since RULA is a discontinuous function calculated over a continuous domain, RULA time evolution during an activity is likely to have discontinuities and plateaus that make its domain exploration less efficient for many optimizers. To alleviate this problem, we propose a continuous version of RULA instead: RULA-C,  $\varepsilon_{rc} \in \mathbb{R}^+$ . To compute RULA-C, we fit second-degree polynomial functions to calculate intermediate scores for the RULA joints. The joint scores for each limb are combined with weighted sums whose weights are computed from linear regressions of the standard RULA tables. Moreover, differently from RULA, RULA-C only takes into account the body posture.

**Normalized whole-body effort:** the torques at every joint are summed to quantify the whole-body effort (Tab. 1.1), where all joint torques are normalized w.r.t. average maximum human capacity for each joint [22] in order to handle the joint torque capabilities.

**Local measurements:** WMSDs at the shoulder and lumbar areas are among the most common in the population [139], therefore, we choose scores that target them. For the shoulder joint, we monitor its absolute torque values,  $\varepsilon_{tsh}$ , and for the lumbar joint, we monitor its absolute torque values,  $\varepsilon_{tlb}$ , and the lumbar back flexion angle,  $\varepsilon_{back}$ .

## Latent Ergonomics Maps

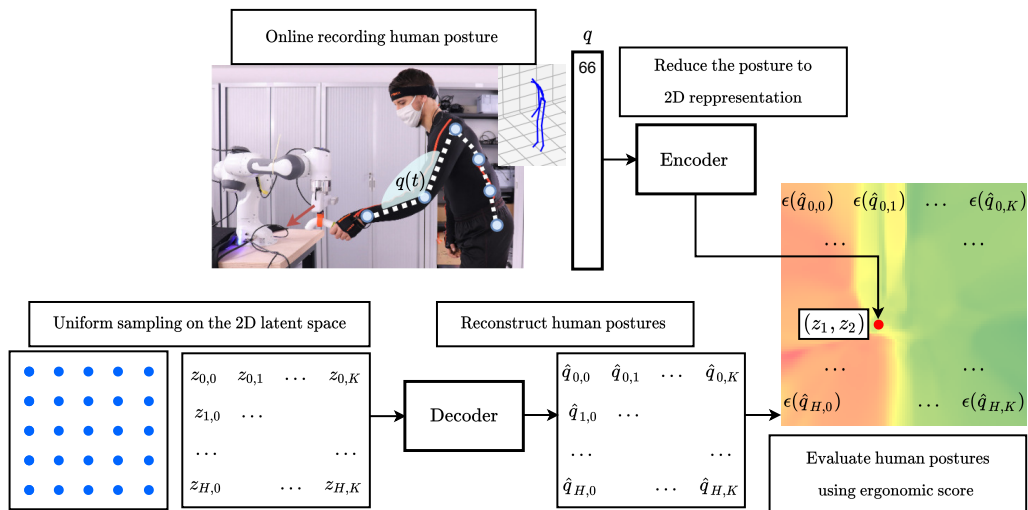


Figure 1.4: Latent Ergonomic Maps (LEM): The VAE is used both to reduce the dimension of the current human posture (*encoder*), and to create the LEM (*decoder*).

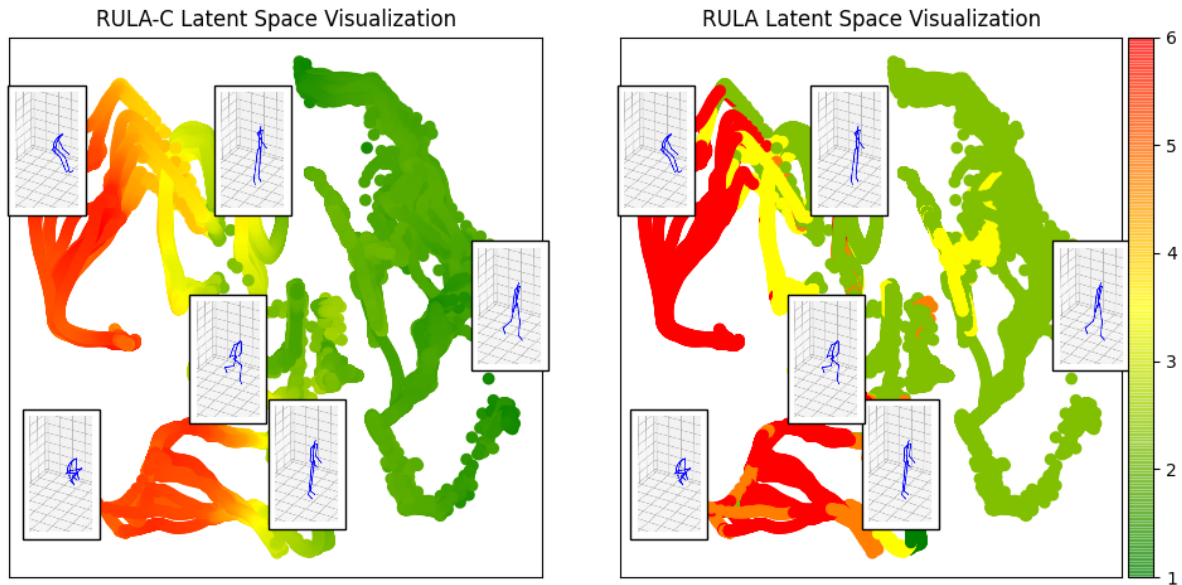


Figure 1.5: Whole-body Posture in a Latent Ergonomics Map. Each point in the map represents a whole-body posture. Each point’s color represents the corresponding ergonomic score for the point. Some points are illustrated as their reconstructed whole-body posture.

In the context of this thesis, we have also collaborated in the development of a tool for real-time visualization of the human ergonomics status using the RULA, and the RULA-C implementation from this chapter [195]. The method consists of learning Variational Auto-encoders (VAEs) [77] to encode a high-dimensional body posture configuration into a low-dimensional latent space, and posteriorly use the same VAE to map the low-dimensional space w.r.t. to the RULA or the RULA-C scores (Fig. 1.4, Fig. 1.5). This latent space is then called a Latent Ergonomic Map (LEM), and it can be used to intuitively indicate if given whole-body postures are ergonomic or not. Furthermore, by associating ergonomics scores with a low-dimensional (2D space) and smooth (in the case of RULA-C) LEM, many efficient approaches with very low computational time could be used to find ergonomic whole-body motion paths. For instance, finding a path in an LEM is akin to finding a path using classic path planning techniques such as the RRT family of algorithms [84].

In the next section, we showcase how some of those ergonomics scores alongside our DHM simulation can help to evaluate the ergonomics of a real-world work activity, even in the presence of external assistive devices such as exoskeletons.

## 1.4 Real case study on Ergonomics Evaluation: Exoturn Project

*Exoturn* was a short-term project developed jointly by the Larsen team of Inria Nancy and the Hospital University of Nancy during the first waves of the COVID-19 pandemic in the city of Nancy in France. The project aimed to improve the ergonomics of healthcare professionals at the Hospital University of Nancy for a physically stressing and nonergonomic maneuver. In the context of this thesis, it was a good opportunity to apply our DHM simulation and ergonomics evaluation methods within a real-world scenario beyond the laboratory.

Since the initial outbreak, the COVID-19 pandemic has stressed healthcare systems worldwide as never before, with significant consequences for clinical management, including rationing of care, and

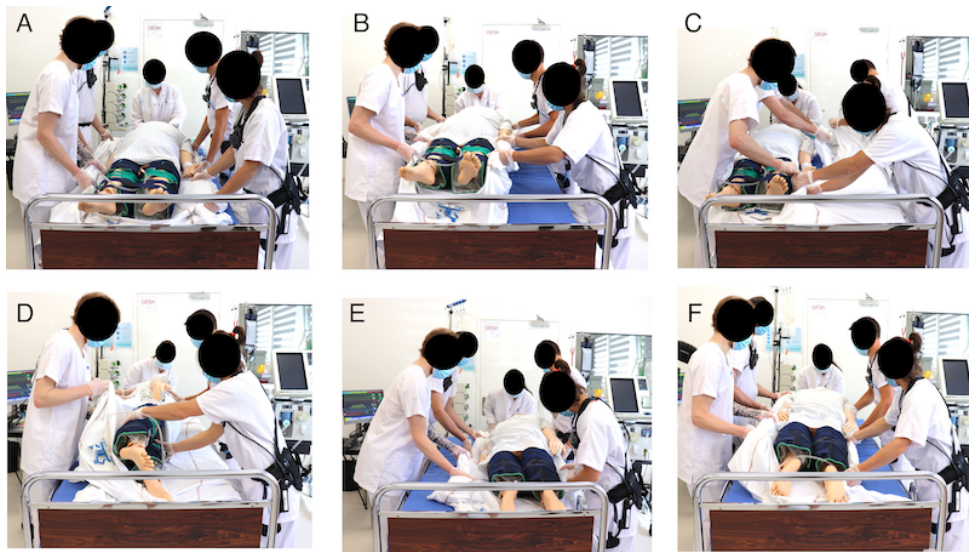


Figure 1.6: Although small differences in the practice of PP can happen from one hospital to another, the maneuver is substantially standardized (video tutorial: <https://www.youtube.com/watch?v=X-qyeN3e8iU>). A: A doctor positioned behind the head of the patient secures the head to avoid extubation and coordinates the whole procedure. Four teammates are distributed on both sides of the patient to reposition and turn the patient. B: The 4 teammates lift the patient and position him/her on one side of the bed. C: The 2 teammates on the right place a clean bed linen. D: The 2 teammates on the left pivot the patient temporarily on the side using the old linen. E: The patient is rotated toward vent until in prone position, lying on his/her abdomen. F: The 4 teammates lift the patient to position him/her at the center of the bed and add a pillow underneath him/her.

facing a limitation of capacity and resources of Intensive Care Units (ICU) to safely maintain a high number of patients on mechanical ventilation during the surge. Prone positioning (PP) (Fig. 1.6), when a patient is repositioned from a supine position (i.e., lying on his/her back) to lie on a prone position (i.e., on his/her front side), is known to improve oxygenation and ventilatory mechanics in Acute Respiratory Distress Syndrome (ARDS) patients who require mechanical ventilatory support [53]. Therefore, PP has been largely used during the COVID-19 pandemic.

In the University Hospital of Nancy, the ICU performed 116 PP maneuvers in the first 10 days of the outbreak, which is equivalent to the number of maneuvers usually performed during an entire year. Although turning a patient into the prone position is not an invasive procedure, it is an exhausting, time-consuming, complex maneuver with many potential complications that require adequate and well-trained healthcare staff. Notably, a PP procedure requires the medical staff to remain with their torso bent forward for several minutes, thus, increasing the potential for lower back injuries [57]. In addition, obesity-related complications have been identified as risk factors for severe COVID-19 cases [21]. As a matter of fact, patients weighting up to 150 kg are common in COVID-19 ICUs, making the PP maneuver ever more daunting for the caregivers.

As we discussed before, musculoskeletal injuries and back pain generated by the repetition of strenuous tasks are well-known in industrial scenarios [57], and many back-support systems have been proposed to alleviate the problem. Given the similarity of the postures, robotics assistance used in industry might also be useful to assist caregivers. In the specific case of a PP maneuver, collaborative robots or mobile manipulators are not suitable, mainly due to limited robot payload and lack of available space in the ICU. Alternatively, motorized beds that can help with manual repositioning of patients (e.g., the commercial products Hospidex toto with inflatable air cells and Vendlet V5S with motorized bars) do exist, but they cannot fully replace the work of the caregivers and require substantial time and financial resources to be put in place. Conversely, occupational exoskeletons [30] appear to be less invasive for the daily practice, as they are easy to set up, cheap, and compatible with the caregivers' work in the ICU.

Given the task-specific efficiency and functionality of exoskeletons, a multidisciplinary team within the Exoturn project conducted a pilot study to evaluate the potential and feasibility of using occupational back-support exoskeletons to help caregivers in the ICU during PP maneuvers. In the remaining of the chapter, we report on the pilot study that defined a suitable exoskeleton for daily usage at the ICU of the University Hospital of Nancy. Additionally, we showcase how we used our DHM simulation to complement the ergonomics analysis of the PP maneuver with and without the exoskeleton.

#### 1.4.1 Preliminary Prone Positioning Kinematic Analysis

In a preliminary test, video analysis of PP maneuvers revealed that the medical staff can assume postures with forward trunk bending up to 45 degrees with arms raised straight forward, exert traction to the trunk bending up to 20-30 degrees, and hold prolonged static postures with the trunk bent forward up to 60 degrees. Then, to confirm the visual observation, we recorded the whole-body kinematics of one physician (M, 35 years old, 175cm) performing a PP maneuver, using the Xsens MVN inertial motion capture system (Xsens, Enschede, Netherlands, capture rate: 240Hz).

Postural analysis with the Anybody biomechanical simulation software (AnyBody Technology, Aalborg, Denmark) revealed that when operating at the side of the patient, the physician spends approximately 40% of the maneuver time with the torso bent more than 20 degrees forward (Fig. 1.7). Additionally, when operating behind the head of the patient to secure the head and avoid extubation, the physician maintains a static posture with important flexion of the trunk for several minutes. The precise angle of flexion, in this case, depends on the height of the patient's bed, his/her location relative to the bed, and the physician's height. Even when not associated with load manipulation, such postures cause mechanical load in the lower back [57]. Exoskeletons for lumbar support can help, but to be used in the

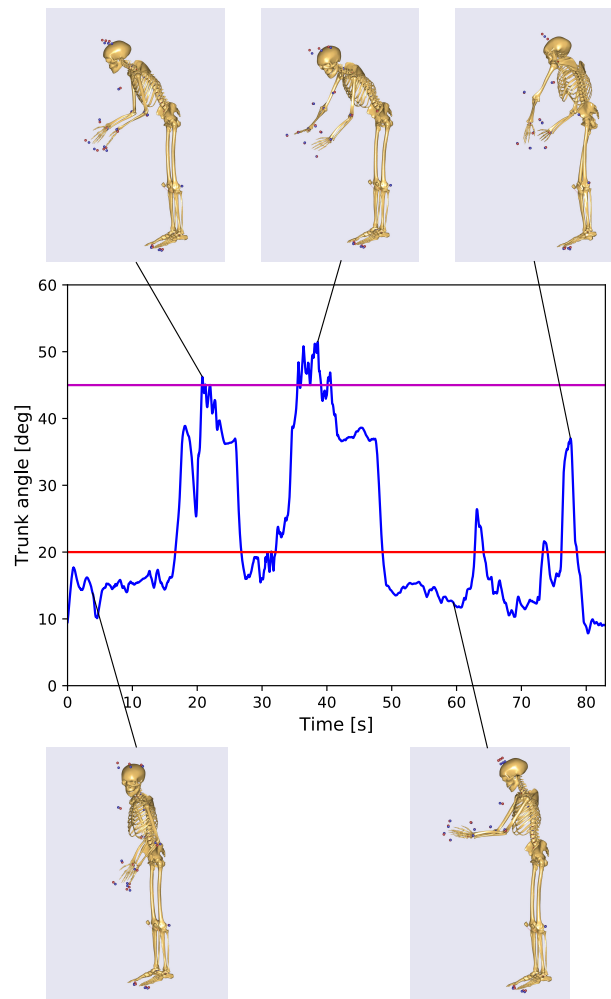


Figure 1.7: Preliminary analysis of the trunk flexion angles of a subject performing a prone-positioning maneuver. Angles above 20 degrees (red line on the graph) are considered risky for ergonomics when maintained or repeated; values greater than 45 degrees (magenta line) indicate postures with severe risk to the worker's health [165].

ICU they have to match many usability constraints, such as being lightweight and unburdensome for the users.



Figure 1.8: The four commercial exoskeletons used in the ExoTurn exploratory study: Corfor, LAEVO, BackX, CrayX.

Based on the previous analysis, we identified four commercial exoskeletons (Fig. 1.8) that could meet the requirements and aid the medical staff: Corfor (Corfor, France), Laevo v1 (Laevo, Netherlands), BackX (SuitX, USA), and CrayX (German Bionics, Germany). Corfor is a passive soft exoskeleton (also known as exosuit), Laevo and BackX are passive rigid exoskeletons based on springs, while CrayX is an active exoskeleton, employing electrical actuators. To verify their feasibility for a PP maneuver, an exploratory study was designed where 5 volunteers from the Hospital of Nancy performed 11 PP maneuvers with a 100kg manikin, and one of the volunteers (M, 30) executed the maneuver while wearing each one of the aforementioned exoskeletons at a time.

### 1.4.2 Ergonomics Evaluation of Exoskeleton Usage

The whole-body motion of the participant that wore the exoskeletons is replayed using our DHM. His motion was captured using the Xsens suit, and was used as a reference to the DHM simulation in a DART physics engine (Fig. 1.9). The length of each segment of the DHM was scaled to match the participant's body segment length, while the DHM inertial parameters were scaled based on the participant's height and mass using average anthropometric coefficients.

Here, to control the DHM, we add Cartesian tasks at different priority levels of the DHM's QP controller:

- Level 1 (Top priority tasks): Center of Mass (balance) position task; feet position task (fixed);
- Level 2: Pelvis and thoracic spine body segments (position and orientation); Shoulder, elbow and wrists (position only); Head (orientation);

where, in the first level, the center of mass position task handles the balance of the DHM, and the feet task keeps the DHM in double support during the motion replay. In the second level, the tasks track the reference trajectories coming from the poses of the Xsens avatar's body segments.

The Xsens system exports position and orientations (poses) for every segment of their model. However, since the human subjects move from their initial position along the PP maneuver, the DHM would also need to replay walking and lateral movements of the human subject. In order to simplify the replay in the physics engine, we replay the movements on the DHM always in double support, by taking the

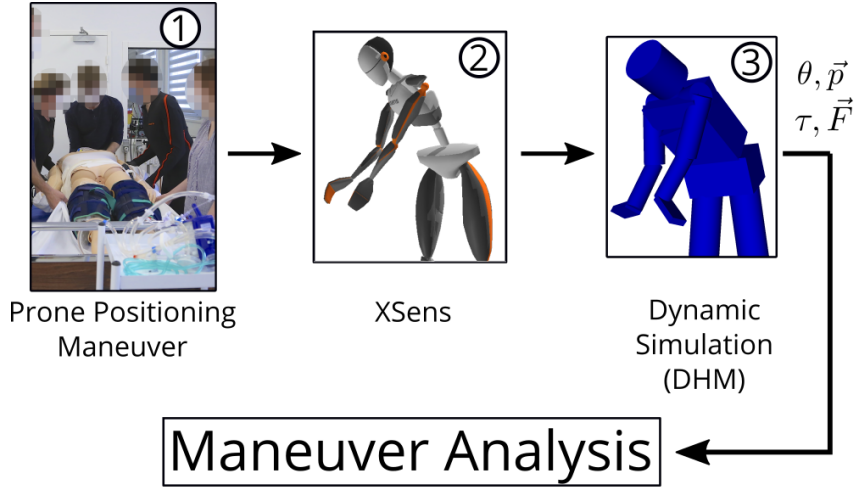


Figure 1.9: In the study conducted at the Hospital Simulation Center, the motion of one physician executing the PP maneuver was captured with the Xsens MVN suit (Step 1). We used the whole-body kinematic estimation of the Xsens MVN software (Step 2) as an input to our dynamic simulation with a Digital Human Model (Step 3). The analysis of motion and estimation of human lumbar effort are based on this dynamic simulation.

Assistance	L Shoulder	R Shoulder	L Elbow	R Elbow	L wrist	R wrist
No Exo	3.6 cm	3.0 cm	5.5 cm	6.1 cm	5.7 cm	5.4 cm
Corfor	3.5 cm	3.0 cm	5.5 cm	5.1 cm	5.7 cm	5.5 cm
LAEVO	3.4 cm	3.3 cm	5.5 cm	5.4 cm	5.3 cm	5.4 cm
BackX	3.1 cm	3.4 cm	5.4 cm	6.2 cm	4.7 cm	4.8 cm
CrayX	3.8 cm	3.9 cm	5.8 cm	5.7 cm	5.3 cm	5.8 cm

Table 1.2: RMS errors between DART Simulation and Xsens reference trajectories for all experiments.

Xsens body segments poses w.r.t. the Pelvis frame:

$$\mathcal{F}_{pelvis}^{bSeg_i} = (\mathcal{F}_{xsens}^{pelvis})^{-1} \mathcal{F}_{xsens}^{bSeg_i} \quad (1.5)$$

where the Cartesian pose for a body segment  $i \in \mathbf{Segments}$  w.r.t to  $\mathcal{F}_{xsens}$  is given by  $\mathcal{F}_{xsens}^{bSeg(i)}$ , and then posteriorly the same coordinates are taken w.r.t. the DART frame before sending it as reference to the QP controller:

$$\mathcal{F}_{DART}^{bSeg_i} = (\mathcal{F}_{DART}^{pelvis}) \mathcal{F}_{pelvis}^{bSeg_i} \quad (1.6)$$

where the DART frame,  $\mathcal{F}_{DART}$  is the projection of the initial pelvis position on the ground.

To guarantee that our controller is able to reproduce the captured movements in the DHM we need to compare the trajectories between the Xsens and the resulting simulation. Due to the nature of the movement, it is particularly necessary that the shoulder, elbow and wrist positions to be as close to the captured reference as possible. Therefore, we verify the root mean square error (RMSe) for those body segments for each experiment. In Tab. 1.2 it is possible to verify that the replay was able to track the shoulder trajectories closely, which assures a good approximation for the thoracic spine angle.

Given the nature of the PP maneuver, and where the exoskeleton most affect the movement, the lower back, we chose to evaluate both the lumbar flexion angle (sagittal plane of the human),  $\varepsilon_{back}$ , and the lumbar torques at the same axis for the 2 most demanding phases of the maneuver, Prone to Supine

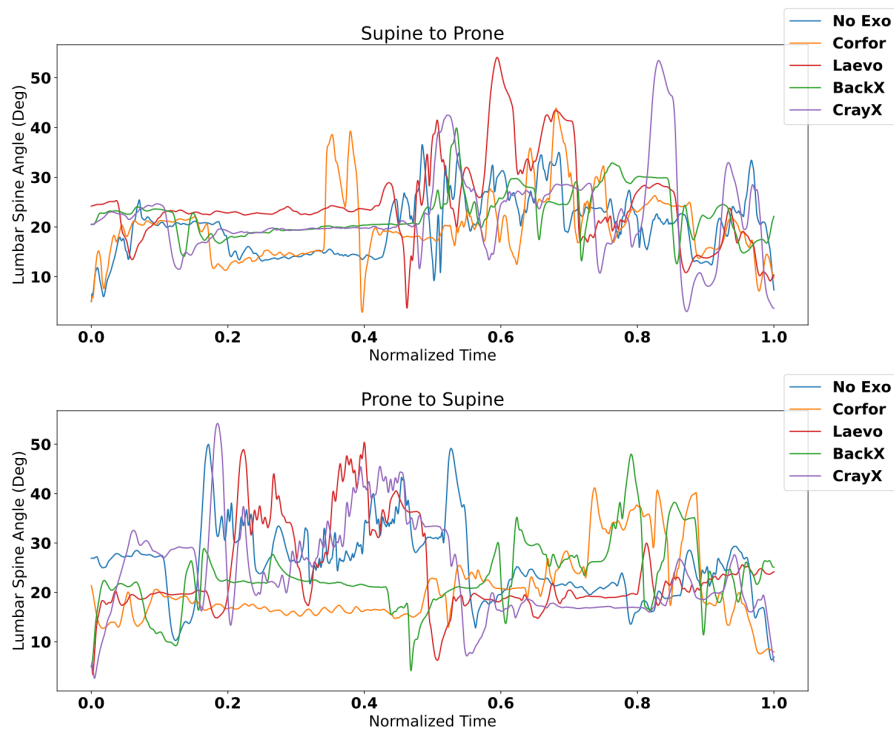


Figure 1.10: Lumbar spine flexion angle of one participant performing prone-positioning maneuvers with different exoskeletons.

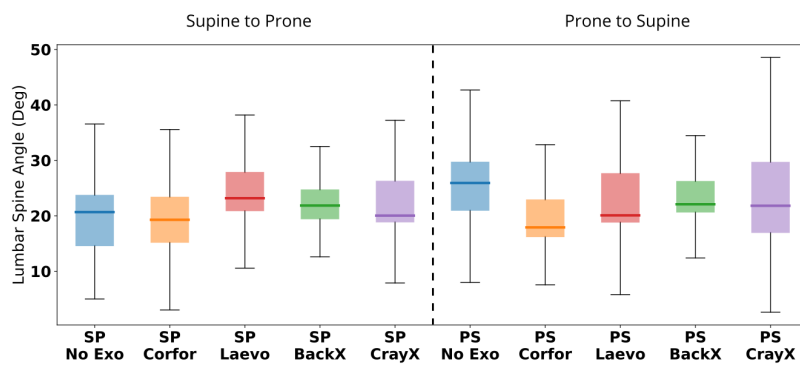


Figure 1.11: Boxplots represent the distribution of Lumbar spine flexion angle across time for all tested exoskeletons, both for the prone to supine (PS), and supine to prone (SP) maneuvers.

(PS), and Supine to Prone (SP). In the absence of physiological measures, DHM computed joint torques are used as a surrogate measure of the efforts performed by the participants during the experiment to investigate the effect of the exoskeleton.

The DHM L5/S1 flexion/extension joint torques estimated with the dynamic simulation are used to compare the lumbar effort exerted by the participant with and without the exoskeleton. When no exoskeleton is worn, the joint torque exerted by the human is directly retrieved from the simulation. However, when the participant is equipped with the exoskeleton, the net torque exerted at the L5/S1 joint to counter the dynamics and gravity effects on the upper-body is a sum of the human-generated torque and of the exoskeleton assistive torque:  $\tau_{L5S1} = \tau_{human} + \tau_{exo}$ . In order to estimate the human torque, the assistive torque  $\tau_{exo}$  provided by each exoskeleton is needed, however in order to compute it one needs details about the exoskeleton's mechatronics design.

The following torque estimation is used only with the Laevo exoskeleton, since it was the exoskeleton unanimously perceived by the participants as the most suitable candidate for use during PP maneuvers (Appendix A). Based on the Laevo empirical calibration curve published by Koopman *et al.* [78] and on the Laevo user manual which specifies that its set of springs provides a maximum torque of 40 *N.m*, we estimated the exoskeleton torque contribution,  $\tau_{exo}$ , as follows:

$$\tau_{exo}(\theta) = \begin{cases} k_0 + k_1\theta, & \dot{\theta} > 0 \\ k_0 + k_1\theta - k_{loss}, & \dot{\theta} < 0 \end{cases} \quad (1.7)$$

where  $\theta$  is the back flexion angle,  $k_0$  and  $k_1$  are constants that encode the spring linearity in its range of operation from 20 to 50 degrees (with the maximum assistance of 40 Nm at 50 degrees), and  $k_{loss}$  represents frictional losses which introduce hysteresis in the system (numerical values of the model's coefficients were set so that the model matches the calibration curve in [78] as closely as possible).

In addition, given the estimated,  $\tau_{exo}$ , the torque generated by the human,  $\tau_{human}$  is also estimated (Fig. 1.13):

$$\tau_{L5S1}(\theta) = \begin{cases} \tau_{exo} + \tau_{human}, & \text{with exoskeleton} \\ \tau_{human}, & \text{without exoskeleton} \end{cases} \quad (1.8)$$

### 1.4.3 Ergonomics Analysis Results

The profiles for the lower back flexion angles of one human subject are overall similar for different conditions (Fig. 1.10): prone-to-supine, supine-to-prone; and all four exoskeletons. The median value of the back-flexion angle of the participant across one trial does not vary significantly from one condition to another (Fig. 1.11), and can be explained by small differences in the manikin's position on the bed and/or intrinsic variability in the entire maneuver performed by the team. These results suggest that **the range of motion of the L5/S1 flexion/extension joint during the PP maneuver was not affected by the use of any of the exoskeletons.**

When using Laevo for the SP and PS maneuvers, the lower back torque medians were reduced by 11.3% and 13.0% respectively (Fig. 1.12). Those results, though limited to one participant, suggest that **wearing the Laevo may reduce the human lumbar torque during PP maneuvers.** This result also agrees with the 15% reduction of the L5/S1 moment observed in [78] for a similar static forward bending task.

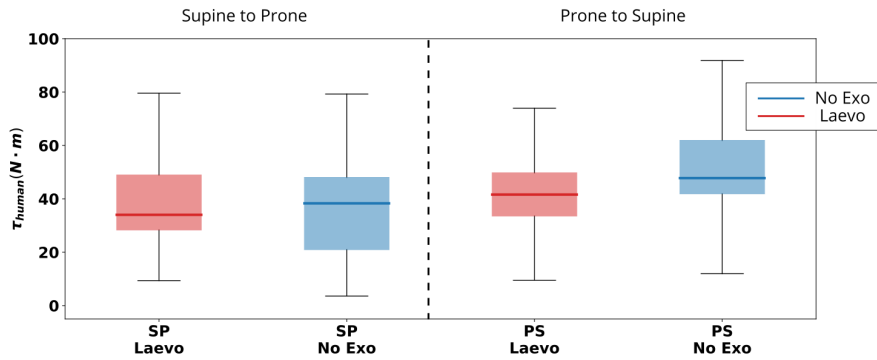


Figure 1.12: Boxplots represent the distribution of estimated human torque profile with and without the Laevo Exoskeleton.

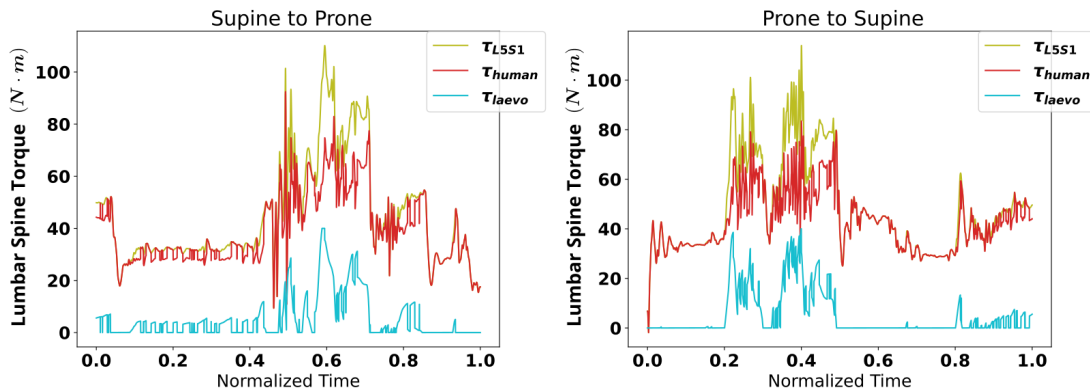


Figure 1.13: Estimation of assistive torque from Laevo exoskeleton, and human effort.

## 1.5 Discussion

In this section, we proposed to use a DHM simulation in a physics engine to perform ergonomics evaluations of human motions. Particularly, we demonstrated its usage to complement the evaluation of a strenuous work activity for health professionals: prone-positioning (PP). In the exploratory study [62], using the motion capture suit was key to obtain precise measures of the lumbar flexion angles of the physician or nurse not only for selected moments as is the case with classic observational methods, but for the entire maneuver execution. Furthermore, since the PP maneuver was assisted by an exoskeleton, then observational methods may not be advisable for precise ergonomics evaluation [149]. These classic methods do not take into consideration exoskeletons, robots, or any external devices attached to the human body, therefore, they are likely to misclassify the risk of WMSDs if an exoskeleton is worn by the human. With the physics engine simulation, and the estimation of the assistive torque curve for the Laevo exoskeleton (Fig. 1.13, Fig. 1.14), it was possible to obtain an estimation of the effort realized by the human subject at the lumbar back during the maneuver. However, there were still simplifications to the PP simulation: the effects of the Laevo weight (2.5 kg) and of the manikin were ignored during the torque estimation. This simplification matters only at the lateral position, since the external load at the head position was only associated with maintaining the endotracheal tube.

The torque estimation is particularly important, as our DHM can be scaled both in weight and height to the human's measurements. Different people, with different body morphologies may require vastly different efforts for the same PP maneuver, and this is a subtlety that would be otherwise impossible to

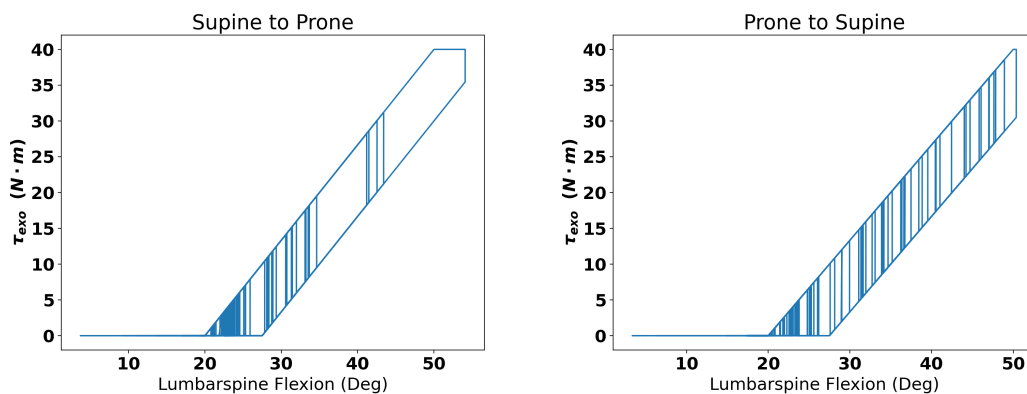


Figure 1.14: Laevo exoskeleton assistive torque for the lower back flexion angle of one participant, including the hysteresis effect due to frictional losses, under supine-to-prone and prone-to-supine conditions.

measure with classic observational methods. In the next chapter, we investigate if it is possible to find motions that are optimal for a given body morphology, and activity according to one or more ergonomics scores.



# Whole-Body Motion Optimization

In this chapter, we propose a set of methods that leverage the control and ergonomics evaluation tools from the previous chapter to generate ergonomic whole-body motions (Fig. 2.1). First, we discuss whole-body trajectory optimization for both humans, and humanoid robots with kinematic chains similar to a human. Then, we detail how we are able to encode whole-body motions with few parameters and use them as optimization variables for a given activity’s trajectory. Both single-objective and multi-objective optimization algorithms are considered and their use is discussed.

At the end of the chapter, two different studies are presented: Optimization of retargeted motions for a humanoid robot; and Multi-objective trajectory optimization to generate ergonomic human motion. The former is a real-world application that was used to showcase the framework under a model with simpler kinematic chains than the ones of a DHM, as well as to benchmark some of the proposed single-objective optimizers. The latter optimized human motion for different body morphologies and activities, ultimately, verifying that the ergonomics evaluation should include multiple ergonomics scores. Additionally, it showed that optimal ergonomic motions are sensitive to user-specific requirements and capabilities, and therefore, should be taken on a case-by-case approach.

## 2.1 Whole-body Trajectory Generation and Optimization

Humanoid robots are able to execute a given activity in many different ways (motion redundancy), although not with the same dexterity as humans in many cases. As it was the case for the DHM on Chapter 1, a well-established approach to control both DHMs and humanoid robots is to use quadratic programming (QP) formulations. They implement strict [40, 137] or soft [13, 153] priorities among many tasks while dealing with low-level constraints (e.g. joint or torque limits). However, even though those QP

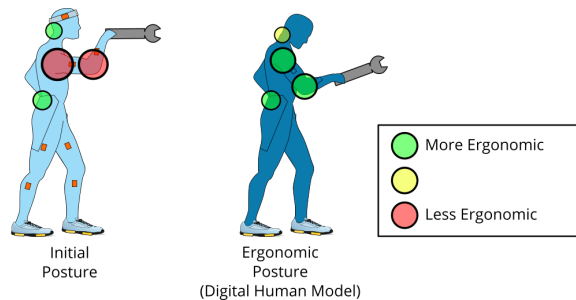


Figure 2.1: Motion optimization with respect to ergonomics scores using a Digital Human Model (DHM)

controllers have shown satisfactory results, they still demand good input trajectories. Otherwise, the high number of degrees of freedom and constraints in humanoid robots may hinder the generation of motions that do not violate the robot constraints.

One solution for whole-body trajectory generation for both DHMs and humanoid robots is to learn the movements from human demonstrations [134, 157]. In [127], the authors retarget human motion onto a humanoid robot using a QP controller while taking into consideration higher-level constraints such as balance. Other works have achieved motion retargeting in different challenging scenarios, with multiple contacts [37], or heavy object manipulation [123]. Furthermore, demonstrations may be used to learn useful robot control policies. For instance, Lin *et al.* [89] learn movement constraints from demonstrations, and Ortenzi *et al.* [121] estimate contact constraints.

The trajectories executed by humans are likely optimal according to one or more criteria related to human motor behavior [63]. However, even after motion retargeting, there is no guarantee that retargeted trajectories are adequate for the robot. In order to execute robot movements optimally, some studies set or define multiple reference trajectories for the robot, and optimize controller parameters. In [107, 167, 206] for instance, the authors parameterize hard or soft priorities for multiple trajectories in a QP controller and posteriorly optimize them w.r.t. to different cost functions related to the humanoid kinematics or dynamics. In this work, we take the approach of keeping the QP controller parameters fixed, and optimizing the reference trajectories directly. Furthermore, before trajectory optimization, those trajectories need to be compactly parameterized so that the optimization only deals with a small set of parameters, as it is typically done in motion planning and reinforcement learning [79, 138].

In [90], the authors used reinforcement learning (RL) to modify waypoints in a reference trajectory for the robot's hand. The waypoints were used as parameters for a Bayesian Optimization (BO) framework. It included cost function evaluations directly from robot demonstrations to have only a few roll-outs in comparison to optimizations in simulations.

In [108], the authors parameterized a reference trajectory for the robot Center of Mass (CoM). A compact representation of the entire trajectory is provided through a radial basis function (RBF) network. Furthermore, the trajectory optimization was done in 2 steps: Unconstrained optimization; and black-box constrained optimization, where the solution of the first step was used as an initial point for the second step. The main issue of this study was exactly the fact that its main optimization step required a prior bootstrapping step from a successful unconstrained optimization to guarantee a trajectory that does not violate any constraints. In contrast, here we leverage human demonstrations for bootstrapping the optimization.

In [172], the authors used dynamic movement primitives (DMPs) to parameterize humanoid joint trajectories, and posteriorly optimize them in a RL framework. Similarly, Stulp *et al.* [173] use DMPs in a hierarchical RL framework that optimizes for sequences of movement, which was further extended in a later work [174] to learn the trajectory's end goal and to improve robustness in pick and place applications. The DMPs in all those approaches were trained after task demonstrations by humans.

## Ergonomic Motion Generation

Techniques that optimize whole-body motion for humanoid robots can also be used to generate optimal motion in DHMs according to given ergonomics criteria. Prior works utilize human models to automate human whole-body motion analysis for a given activity [98, 156]. There is even a recent trend in the human-robot interaction community to use DHMs to improve the human posture with respect to ergonomics scores during physical interactions. For instance, Marin *et al.* optimized a shared object's position in order to minimize the maximum muscle activation signal taken from a fast-to-compute musculoskeletal surrogate model [96]. Van der Spaa *et al.* optimizes a discrete sequential plan of poses for a shared object during its transportation by both human and robot, with respect to the Rapid Entire Body

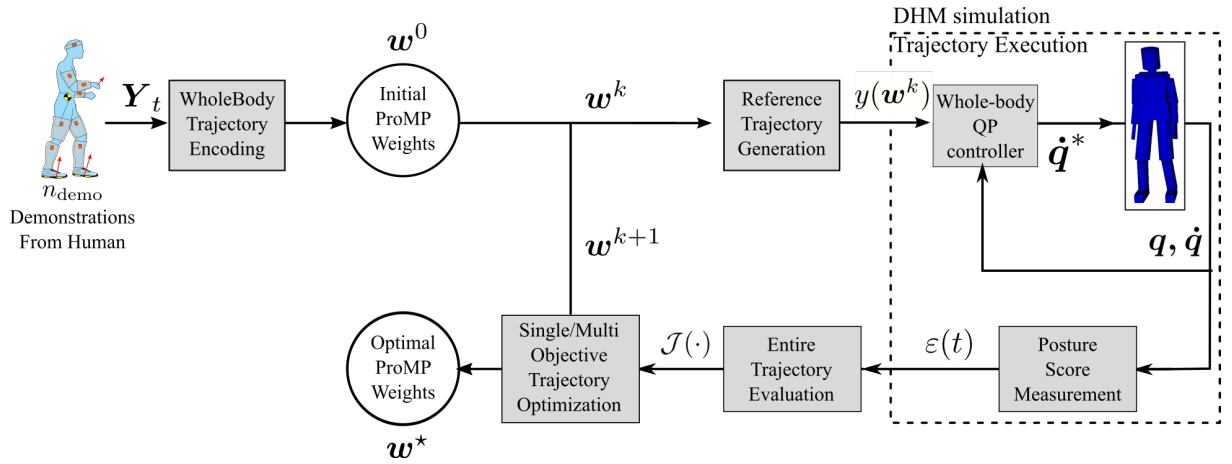


Figure 2.2: Ergonomics human motion optimization. The entire motion is encoded into motion primitives that can be readily optimized with respect to a single, or multiple, ergonomics scores using a user-specific Digital Human Model (DHM) Simulation for motion evaluation.

Assessment (REBA) score, a standard whole-body ergonomics score [190].

Other works continuously evaluate the human kinematics/kinetics to try to influence the human posture with different robot actions. Shafti. *et al.* use wearable sensors to compute the Rapid Upper-Limb Assessment (RULA) score and adapt the robot’s end-effector accordingly until the ergonomics evaluation is considered satisfactory [166]. Kim *et al.* minimized the human joint torque due to an external load [75]. Similar optimization techniques were used to improve human operator ergonomics during teleoperation [141, 204].

The examples above consider single ergonomics scores, however, given the multi-factorial causes of WMSDs, optimizing the movement for one ergonomics score could deteriorate other possible antagonistic scores. For this matter, there are some examples of multi-objective ergonomics optimization in the literature. For instance, Xiang *et al.* optimized a human’s posture w.r.t. ergonomics and stability scores [203], and Iriondo *et al.* optimized a workstation setup parameter w.r.t RULA, and the human’s upper-arm elevation angle [59]. In a physical human-robot application, Maurice *et al.* optimized a robot’s design parameters to simultaneously improve several ergonomics scores [97]. Figueredo *et al.* combined muscle activation predictions and the REBA score to calculate a comfortability index that can be used in a physical human-robot interaction to guide the human partner towards postures that minimize both types of scores [43].

In the next sections, we propose a set of methods to optimize human- and activity-specific whole-body motions w.r.t. several ergonomics scores. We also show that the resulting optimal motions are sensitive to different body morphologies, and ergonomics scores.

## 2.2 Multi-Objective Trajectory Optimization

We propose to generate optimal whole-body motions with respect to one or more objective functions, or scores (Fig. 2.2). Given the high redundancy of motion in humanoid rigid body models, it may be difficult to find a first feasible motion otherwise. Therefore, this step guarantees that the optimization process is aware of at least one feasible point in the search space. Human motion demonstrations are captured from a given subject executing a given activity. This initial movement is used to bootstrap the optimization procedure, as the initial motion corresponds to a feasible initial point in the optimization

process.

Then, we manually select and encode the Cartesian trajectories from human body segments that are able to represent the whole-body motion. For instance, if the human lifts a box from the ground, both the pelvis and the hand trajectories can be used to represent the whole-body motion. Those selected trajectories are encoded into a single vector using Probabilistic Movement Primitives (ProMPs) [126], which can capture motion variability computing a Gaussian trajectory distribution from a set of demonstrations.

The whole-body trajectory references are generated from the ProMPs and executed by a hierarchical multi-task whole-body controller [56] that controls the DHM we proposed in chapter 1. During the execution, the encoded motion is evaluated according to one or more of the ergonomics scores in Tab. 1.1 that can be used to evaluate the entire trajectory execution using Eq. (1.4).

Finally, an optimization algorithm, single or multi-objective, is used to find and select feasible, and optimal wholebody trajectories for the given activity, and DHM morphology according to the chosen score. We use non-linear constrained optimization algorithms to ensure that the solutions are always safe, not violating any constraints for the DHM or the activity [23, 108].

In the next sections, we detail the methods of our framework, and then we show its effectiveness under 2 different applications. In the first application, the whole-body motion of a humanoid robot is optimized with respect to a single objective, the robot's joint efforts. The robot's initial motion comes from retargeted whole-body human demonstration motions even though the robot and the human have very different dimensions. Additionally, the method's viability was also tested for different non-linear constrained optimization algorithms. In the second application, we move our focus back into DHMs, and optimize the whole-body motion of DHMs in several different scenarios: varied body morphologies, ergonomics scores and two different activities. In this case, we also show that multi-objective optimization potentially generates motion that is more ergonomic than with single-objective optimization.

In summary, this chapter provides a framework that generates ergonomic motions for DHMs by optimizing encoded whole-body motions from human demonstrations. Several experiments explore the framework capabilities under different optimization algorithms, additionally, providing practical knowledge for its usage in future experiments, including the human-robot experiments of chapter 4.

## 2.3 Whole-body Trajectory Parameterization

In order to represent a whole-body motion in a DHM or in a robot, one could use different tools for motion parameterization such as dynamic movement primitives (DMPs) [155] or probabilistic movement primitives (ProMPs) [125]. ProMPs can even account for multi-dimensional trajectories accounting for all joints degrees of freedom [35]. However, given the high number of joints in DHMs and humanoid robots, this would mean that a great number of parameters would have to be used to encode even simple motions. Instead, we propose to select Cartesian trajectories of the human motion that are few but representative of the motion we want to encode.

Given the set of body segments of a DHM or a humanoid robot,  $Segments$ , there is a Cartesian trajectory  $Y_t^{seg}, \forall seg \in Segments$ . Then, given the activity we want to encode we select a subset  $Selected \subset Segments$ , that is representative of the motion, i.e., in a lifting task we could select the Pelvis and Hands segments,  $Selected = \{Pelvis, Right Hand, Left Hand\}$ , and then we learn a ProMP for each trajectory  $Y_t^{seg}$  within  $Selected$ .

### Probabilistic Movement Primitives

ProMPs are Bayesian parametric models that associate a mean and a standard deviation to a set of trajectory demonstrations [125]. From its formulation, a ProMP can compactly represent trajectories with

a simple weight vector. For instance, a one-dimensional trajectory  $y_t \in \mathbb{R}$  can be represented with a weight vector  $\mathbf{v}$ :

$$y_t(\mathbf{v}) = \phi_t^\top \mathbf{v} + \epsilon_y \quad (2.1)$$

and the probability of observing this trajectory given a certain vector  $\mathbf{v}$  is given as a linear basis function model:

$$p(y_t|\mathbf{v}) = \prod_t \mathcal{N}(y_t|\phi_t^\top \mathbf{v}, \sigma_y) \quad (2.2)$$

where the variable  $\epsilon_y \sim \mathcal{N}(0, \sigma_y)$  is a zero-mean i.i.d Gaussian noise, and  $\phi_t \in \mathbb{R}^{n_{bf}}$  is a time dependent radial basis function vector for the trajectory positions. The general form of the  $i$ -th basis function  $b_i$  for stroke-based motions is given by:

$$b_i = \exp\left(-\frac{(z_t - c_i)^2}{2h}\right) \quad (2.3)$$

where  $h$  defines the basis' width and  $c_i$  is the basis' center; the basis' centers are uniformly distributed in  $[-2h, (1 + 2h)]$ ;  $z_t$  defines a phase variable in such a way that at the beginning of a motion  $z_{begin} = 0$ , and at the end  $z_{end} = 1$ . Then, we normalize the basis functions

$$\phi_t^i = \frac{b_i}{\sum_{j=1}^n b_j} \quad (2.4)$$

to maintain the same summed activation. In other words,  $y_t$  is represented as a weighted sum of  $n_{bf}$  normalized basis functions uniformly distributed in time.

To capture the variability of the movement,  $\mathbf{v}$  is also represented as a Gaussian variable,  $\mathbf{v} \sim \mathcal{N}(\boldsymbol{\mu}_v, \boldsymbol{\Sigma}_v)$ . Therefore, by marginalizing out the weight vector in 2.2 we get:

$$\begin{aligned} p(y_t|\boldsymbol{\mu}_v, \boldsymbol{\Sigma}_v) &= \int \mathcal{N}(y_t|\phi_t^\top \mathbf{v}, \sigma_y) \mathcal{N}(\mathbf{v}|\boldsymbol{\mu}_v, \boldsymbol{\Sigma}_v) d\mathbf{v} \\ &= \mathcal{N}(y_t|\phi_t^\top \boldsymbol{\mu}_v, \phi_t^\top \boldsymbol{\Sigma}_v \phi_t + \sigma_y) \end{aligned} \quad (2.5)$$

Then, we need to train the ProMP (2.5), that is, we need to estimate a mean ( $\boldsymbol{\mu}_v$ ) and variance ( $\boldsymbol{\Sigma}_v$ ) for the variable  $\mathbf{v}$  based on  $n_{demo}$  trajectory observations. Similarly to [125], we use a maximum likelihood estimation algorithm alongside a linear ridge regression to achieve the training. For each one of the trajectory demonstrations we compute a  $j$ -th weight  $\mathbf{v}_j$ :

$$\mathbf{v}_j = (\phi_t^\top \phi_t + \lambda \mathbf{I})^{-1} \phi_t \mathbf{Y}_j \quad (2.6)$$

where  $\mathbf{Y}_j$  contains the  $j$ -th trajectory demonstration, and  $\lambda$  is the ridge factor for the linear regression, here set to a very low value  $10^{-10}$  not to bias the regression results. Then,  $\mathbf{v}_j$  are used to estimate both  $\boldsymbol{\mu}_v, \boldsymbol{\Sigma}_v$ :

$$\boldsymbol{\mu}_v = \frac{1}{n_{demo}} \sum_j^{n_{demo}} \mathbf{v}_j \quad (2.7)$$

$$\boldsymbol{\Sigma}_v = \frac{1}{n_{demo}} \sum_j^{n_{demo}} (\mathbf{v}_j - \boldsymbol{\mu}_v)(\mathbf{v}_j - \boldsymbol{\mu}_v)^\top \quad (2.8)$$

By using ProMPs as trajectory references instead of the demonstrations directly, we are able to smooth the mean trajectories and capture their variability. Additionally, because of the phase variable  $z_t$ ,

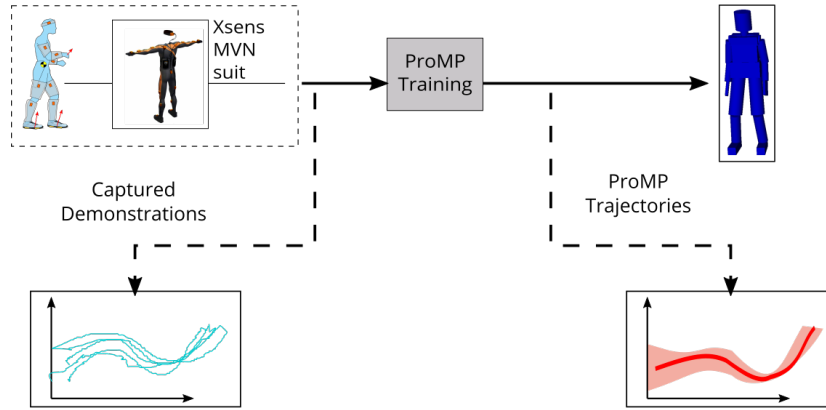


Figure 2.3: Process of extracting trajectories from demonstrations: 1) Acquisition of Cartesian position trajectories from a human wearing an Xsens suit; 2) Training a ProMP, smoothing the raw data and associating it with a variance of motion.

the trajectory demonstrations can also begin and end at different times and this will not affect the shape of the learned ProMP (Fig. 2.3).

Finally, for each coordinate of each selected Cartesian trajectory, *Selected*, a one-dimensional ProMP is learned using Eq. (2.7), Eq. (2.8), and they all are stacked into a single vector:

$$\mathbf{w} = [\mu_v^1 \dots \mu_v^{seg}] \quad (2.9)$$

From Eq. (2.9) all representative mean trajectories can be recovered using Eq. (2.5). Those mean trajectories are used as references for the DHM QP controller tasks Eq. (1.3). Since the QP controller commands all of the DHM joints while minimizing the reference tracking errors for all tasks, then  $\mathbf{w}$  effectively encodes the entire whole-body motion, and not just the motion in the set *Selected*. For this reason,  $\mathbf{w}$  is hereafter defined as our optimization variable, that we can modify in order to minimize the scores such as the ones in Tab. 1.1.

## 2.4 Constrained Trajectory Optimization

We optimize a selection of the DHM body segment trajectories,  $\mathbf{y}(\mathbf{w})$ , through its optimizable parameters,  $\mathbf{w}$ , w.r.t. one of the ergonomic scores in Tab. 1.1 with a single-objective optimizer, or for several scores with a multi-objective optimizer. The approach is equivalent to an episodic learning loop with the maximum number of  $K$  roll-outs (or episodes). Given an episode  $k$  in the optimization loop (Fig. 2.2), the point  $\mathbf{w}^k$  is considered feasible if, and only if, the executions of the whole-body trajectories  $\mathbf{y}(\mathbf{w}^k)$  respect some nonlinear constraints.

**Trajectory Constraints:** The DHM limbs and reference trajectories should always be within the environment workspace. That is, each ProMP weight is constrained to box boundaries that correspond to the DHM's reach in the workspace. Additionally, during the trajectories' execution, the DHM must never fall, and its hand(s) must reach all (activity-dependent) points of interest that are relevant for the activity. In order for the trajectory execution scores (Eq. (1.4)) to be comparable, the duration of every trajectory execution is always fixed for every episode. This trajectory optimization is a derivative-free problem with black-box non-linear constraints. In the next section, we briefly describe the different optimization algorithms we have tested with our framework.

### 2.4.1 Optimization Algorithms

We explore both single- and multi-objective optimization algorithms. For single-objective optimization the 3 following optimizers were considered: COBYLA, AGS, and CCMA-ES. The first two optimizers were already available within the NLOpt C++ library [69], and we implemented the latter in C++ especially for this work. All three optimizers are briefly described below.

- **COBYLA:** (Constrained Optimization BY Linear Approximation) is a deterministic optimization algorithm that constructs linear approximations of the objective function and then optimizes them at each roll-out [136].
- **AGS:** is a deterministic single-objective optimization algorithm proven to converge to a global optimum if the cost function satisfies the Lipschitz condition within the bound constraints [164].
- **CCMA-ES:** ((1+1)-CMA-ES with Constrained Covariance Adaptation) is a stochastic optimization algorithm. At every roll-out, it evaluates a set of samples drawn from a multivariate Gaussian distribution. If the samples violate any of the previously set constraints, it adapts the covariance matrix of the distribution and resamples from the new co-variance. This design ensures that the constraints are never violated [8] and demands that it has to start with a point that does not violate any constraints, otherwise the algorithm will get stuck and fail. This algorithm has already been used in learning soft task priorities for the iCub robot [107].

To optimize for multiple scores at the same time, we advocate for multi-objective optimization. The goal becomes not to find one single optimal solution, but rather, a *set* of Pareto-optimal solutions that provide trade-off trajectories for conflicting ergonomics scores, *i.e.* a Pareto front. By definition [32], within the Pareto front, all solutions are said to be dominant: given solutions  $w_1$  and  $w_2$ ,  $w_1$  is said to dominate  $w_2$  if and only if  $w_1$  provides better results for all objective functions; if one or more of  $w_2$ 's objectives is better than in  $w_1$ , then, both are dominant solutions with a trade-off between each other. For the multi-objective case, we chose the NSGA-II algorithm:

- **NSGA-II:** (Non-dominated Sorting Genetic Algorithm II) is a popular multi-objective evolutionary optimizer [32] with a fast non-dominated sorting approach. Its implementation was taken from the C++ library Sferes<sub>v2</sub> [111].

### 2.4.2 Single- and Multi-Objective Trajectory Optimization

Single-objective trajectory optimization (SOTO), and multi-objective trajectory optimization (MOTO) are handled differently due to differences in the selected optimizers. After Collecting  $n_{demo}$  motion demonstrations of a human subject, SOTO is initialized with the initial ProMP vector,  $w = w^0$  (Fig. 2.2). A score  $\varepsilon$  is chosen to evaluate execution of each one of the episodes in the optimization, then the whole episode execution is evaluated using Eq. (1.4). At last, a feasible optimal score is found by one of the aforementioned single-objective optimizers.

In the MOTO case, two or more scores are optimized simultaneously, however, in order to use the chosen optimizer, NSGA-II, some modifications are done to the formulation regarding: how to deal with the non-linear constraints; and how to bootstrap the initial demonstrations.

NSGA-II's implementation does not handle specifying feasible/unfeasible points directly, so we modify the objective function Eq. (1.4) to penalize the unfeasible points. Each ergonomics score is penalized in case the DHM falls or it does not reach the activity's points of interest:

$$\mathcal{J}_{obj} = T_{fall} \mathcal{P}_{obj}^{fall} + \mathcal{P}_{obj}^{via} + \sum_{t \in [0 \dots T]} \varepsilon_{obj}^2(t) \quad (2.10)$$

where  $T_{fall} \in \mathbb{R}^+$  is the period of time in which the DHM is fallen,  $\mathcal{P}_{obj}^{fall} \in \mathbb{R}^+$  is the fall penalty for a given score, and  $\mathcal{P}_{obj}^{via} \in \mathbb{R}^+$  is the point-of-interest penalty for a given score. Each score is associated with a different penalty value for they have different orders of magnitude.

Differently from the single-objective case, it is not possible to directly warm-start NSGA-II with the initial trajectories. To circumvent this issue, we modify the initial population sampling of NSGA-II instead. The  $i$ -th variable,  $w_i$ , of each initial individual is sampled using the initial ProMP  $i$ -th variable,  $w_i^{initial}$  using a Gaussian distribution:

$$w_i = \mathcal{N}(w_i^{initial}, \delta_i \beta) \quad (2.11)$$

where  $\delta_i$  is the largest distance between  $w_i^{initial}$  and any of its box boundaries, and  $\beta \in \mathbb{R}$  is a constant that modulates how much of the boundaries we want to sample initially. For instance, if  $\beta = \frac{1}{3}$ , then  $p(w_i = \text{boundary}_i) \leq 0.3\%$ , that is, we would sample the entire workspace with very low probabilities at each variable boundary. Here, we chose  $\beta = \frac{1}{12}$ , a low value, to keep the initial sample close to the initial demonstrations.

## 2.5 Humanoid Whole-body Motion Optimization from Retargeted Human Motions

We demonstrate our motion optimization methods with a humanoid robot model that initially replays retargeted human motions that are not optimal for the robot. Since the humanoid robot has similar kinematic chains w.r.t. a DHM, this is a proxy problem to optimizing whole-body motions for the DHM. In addition, we also benchmark different types of single-objective optimizers within this application to decide which type is more suitable to the whole-body optimization using our methods.

Kinesthetic teaching is widely used to demonstrate the motion required to perform a task to robotics manipulators. Motion retargeting [37, 127] implements this idea for humanoid robots by using human motion tracking data to demonstrate whole-body movements. While this approach is very powerful, it presents two main limitations. First, humans generate movements that may not be optimal for the robot mainly due to structural differences between them: different number of joints, or power generation at the joint level for instance. Second, because of the intrinsic variability of the human motion, the robot may not learn from the best possible representation of the task execution. The main insight is that even if a human demonstration enables the robot to perform a given task, i.e., lift a box, the retargeted motion will be hardly optimal for the robot from an energetic point of view: if a more efficient way to perform a task exists, it needs to be found.

Here, we used largely the same framework as the one devised for the DHM, but this time we retargeted the motion from the demonstrations before encoding them using ProMPs (Fig. 2.4 and 2.5). For the experiment, we proposed a lifting activity demonstrated by the human subject using the motion-tracking suit, where the retarget motion should minimize the joint torques at the iCub robot. All three single-objective optimization algorithms were benchmarked for different initial trajectories, and we show that our framework was able to minimize torque consumption by over 40%.

The human that executed the demonstrations and the iCub robot have different kinematic structures. Therefore, human trajectories have to be retargeted into feasible corresponding values for the robot. This is achieved by either retargeting the joint trajectories or by carefully choosing links and retargeting their Cartesian positions. Here, we chose the latter to decrease the number of trajectories that need to be retargeted to represent a whole-body task.

A way to retarget one link position is to consider its relative position w.r.t. a base link, and measure the length of such limb in both the human and the robot [127]. The relative position of the robot end

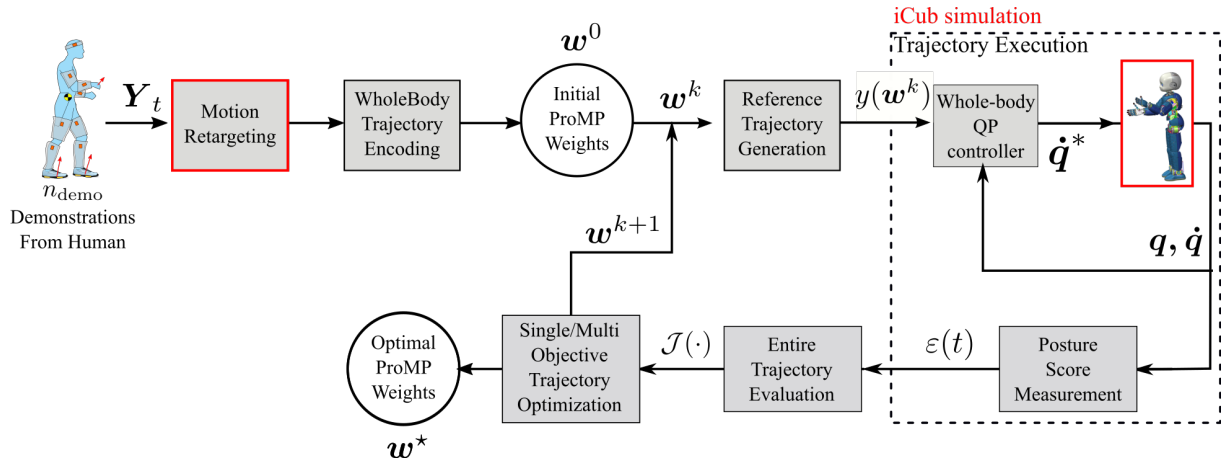


Figure 2.4: Modified whole-body motion optimization framework for the iCub robot. Here, the captured motion is retargeted to the iCub robot before the whole-body trajectory encoding.

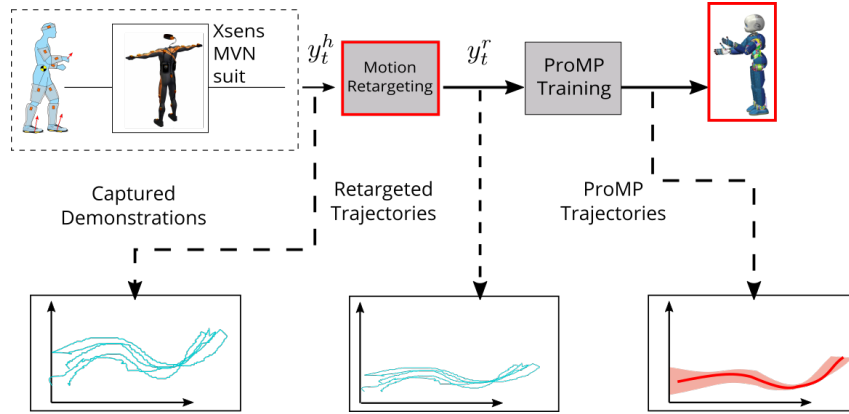


Figure 2.5: Process of extracting trajectories from demonstrations for the iCub Robot: 1) Acquisition of Cartesian position trajectories from a human wearing an Xsens suit; 2) Scaling the position trajectories for the iCub robot; 3) Training a ProMP, smoothing the raw data and associating it with a variance of motion.

effector is then computed as:

$$y_t^r = k_{rtg} (y_t^h - y_0^h) + y_0^r \quad (2.12)$$

where  $k_{rtg} \in \mathbb{R}$  is the ratio between the robot and the human limb lengths,  $r$  and  $h$  are superscripts related to the robot or human respectively, and  $0$  is a subscript indicating that this is the position for an initial instant. Effectively, Eq. (2.12) scales down the trajectory from the human to the child sized iCub robot (Fig. 2.5).

We define a pick and place activity where a human/iCub has to squat, grab a box, and stand up (Fig. 2.6). For the human demonstrations, the human grabs the box 9 times with variants of movement strategies. In particular, for the first 4 movement demonstrations, the human does not bend its back, while for the other 5 s/he does bend its back.

For this activity, the QP controller is set with a high-priority joint position task for the Head pitch angle, and high-priority Cartesian tasks for the feet (X,Y,Z), and Waist (X,Y,Z); and low-priority Cartesian tasks for the hands (X,Y,Z), and CoM (X,Y). The tasks, for the head, left foot, and right foot are fixed.

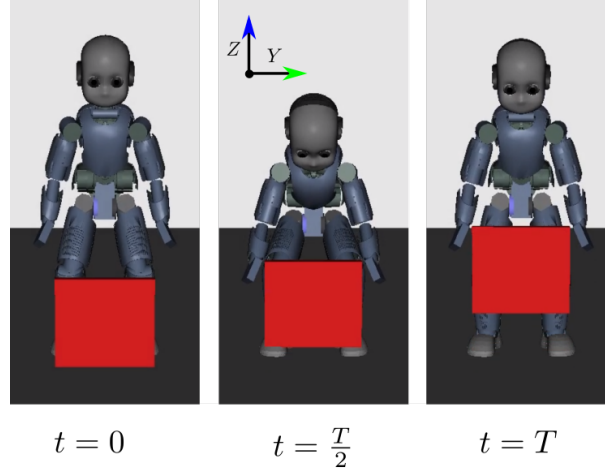


Figure 2.6: In our designed task, iCub has to squat, grab a box, and then stand up with the box.

Regarding the other tasks we modulate the following trajectories:

- $Z \mathbf{y}_t^{Waist}$ , Z-Axis of the waist;
- $X \mathbf{y}_t^{CoM}$ , X-Axis of the CoM;
- $X \mathbf{y}_t^{RH}, Z \mathbf{y}_t^{RH}$ , X- and Z-Axis of the right hand;
- $X \mathbf{y}_t^{LH}, Z \mathbf{y}_t^{LH}$ , X- and Z-Axis of the left hand;

however, to simplify the optimization using less parameters we assume the right hand trajectories to be symmetrical to the left hand

$$X \mathbf{y}_t^{RH} = X \mathbf{y}_t^{LH} \quad (2.13)$$

$$Z \mathbf{y}_t^{RH} = Z \mathbf{y}_t^{LH} \quad (2.14)$$

In this way, we only need to learn a ProMP for the right hand, and mirror it like in Eq. (2.14), totaling only 4 ProMPs to be learned.

Since in this application the iCub’s whole-body motion is being optimized, we do not optimize for ergonomics scores but rather a modified version of the normalized wholebody efforts to evaluate the iCub’s joint efforts:

$$\varepsilon_{icub} = \frac{1}{n_j} \sum_{i=1}^{n_j} \left( \frac{v_i \tau_i}{\tau_i^{\max}} \right)^2 \quad (2.15)$$

where  $\tau_i^{\max}$  is a known maximum value for the torque at the  $i$ -th joint, and  $v_i$  is a fixed weight for the  $i$ -th joint. Eq. (2.15) defines a sum of squared torques at every joint, therefore, as  $\varepsilon_{icub}$  decreases, so does the effort applied by the robot actuators. The weights are defined  $v_i = 1$  for every joint, except for the high priority and low priority joints. The high priority joints with  $v_i = 5$  are: left hip, right hip, torso, left shoulder, right shoulder. Furthermore, the low priority joints with  $v_i = 0.1$  are: left knee, right knee, left ankle, and right ankle.

As for the optimization parameters, we defined  $n_{bf} = 5$ , so for each ProMP there are 5 weight variables to be optimized. However, in order to further decrease the number of optimization parameters,

Table 2.1: Description of initial sets of human motion demonstration used on the benchmark.

Initial Set ID	Description
$r_1 - r_4$	Single Demonstration(s) w/ straight torso
$r_{all}$	ProMP from $r_1, r_2, r_3, r_4$
$s_1 - s_5$	Single Demonstration(s) w/ bent torso
$s_{all}$	ProMP from $s_1, s_2, s_3, s_4, s_5$
$all$	ProMP from every demonstration

we decided to optimize only for the CoM and waist trajectories (the Cartesian retargeted motions are still learned as ProMPs). It is important to note that the reduction of optimization parameters is taken solely to speed up the optimization computational process. Finally, the optimization variables are

$$\mathbf{w} = \left[ (\mathbf{w}_{waistZ})^\top, (\mathbf{w}_{comX})^\top \right]^\top \in \mathbb{R}^{10} \quad (2.16)$$

where  $\mathbf{w}_{waistZ}$  is bound between 0 and 1 and  $\mathbf{w}_{comX}$  is bound between -0.5 and 0.5, effectively, not allowing the Z component of the CoM trajectory to go below the inertial reference (ground) and the X component of the waist to go beyond 0.5 meters of the inertial reference.

Besides the standing-up at all times constraint, iCub’s hands have to achieve a specific set of targets at a particular order for the task to be considered executed. First, they have to reach the grasping box position:

$${}^X \mathbf{y}_t^{RH}, {}^X \mathbf{y}_t^{LH} > 0.15m \quad (2.17)$$

$${}^Z \mathbf{y}_t^{RH}, {}^Z \mathbf{y}_t^{LH} < 0.30m \quad (2.18)$$

and then they have to return to an initial position:

$${}^Z \mathbf{y}_t^{RH}, {}^Z \mathbf{y}_t^{LH} > 0.40m \quad (2.19)$$

If the robot’s hands do not reach those goals, then the entire execution is said unsuccessful, and a black-box constraint is violated. Furthermore, inside the simulation environment, whenever Eq. (2.17), Eq. (2.18) are satisfied for the first time, a virtual box of 1 kg is added to the robot, emulating a grasp. Note that the above inequalities are constant. This is done in order to fix the same kinematic task for different ProMP sets, allowing us to compare their performance.

### 2.5.1 Experiments

To demonstrate that our framework (Fig. 2.2) does not require a very specific ProMP as a starting point, different sets of demonstrations are used at the ProMP learning stage (Tab. 2.1), where the  $r_i$  sets correspond to demonstrations where the human did not bend his/her back to pick up the box, while the  $s_i$  sets correspond to the ones where the human did bend his/her back.

For AGS, the number of roll-outs was set to  $K = 2000$ . On the other hand, CCMA-ES and COBYLA would always converge to a solution much earlier (Fig. 2.7). Therefore, the number of roll-outs for them was reduced to  $K = 500$ . The hyperparameters for the CCMA-ES algorithm were set to  $\sigma = 0.1$ ,  $\lambda = 1$  (default values from the benchmarks in the original paper [8]). The hyperparameters for AGS and COBYLA were default values in the NLOPT library [69].

Table 2.2: Final  $\mathcal{J}$  scores after optimization, and  $\mathcal{I}$  compared with the initial score for each optimization algorithm. The initial sets  $s_1$ - $s_{all}$  are not able to complete the task of picking up the box, therefore, it is not possible to compute an initial score for the initial  $\mathcal{J}$  and for the improvement  $\mathcal{I}$  (marked with a /). Furthermore, CCMA-ES will also fail for them because the initial points violate the task constraints (marked with a /).

Initial Set	AGS, $K = 2000$		COBYLA, $K = 500$		CCMA-ES, 30 iterations with $K = 500$		
	Initial $\mathcal{J}$	$\mathcal{J}^*$	$\mathcal{I}$	$\mathcal{J}^*$	$\mathcal{I}$	$\mathcal{J}^*$ Median and IQR	$\mathcal{I}$ Median and IQR
$r_1$	188.55	188.55	00.00%	121.32	35.65%	116.12 (110.55 - 125.84)	38.41 (33.26 - 41.37)
$r_2$	229.72	215.21	6.32 %	125.01	45.58%	134.16 (127.97 - 143.32)	41.60 (37.61 - 44.29)
$r_3$	249.63	198.89	20.32%	202.90	18.71%	116.10 (105.10 - 145.40)	53.49 (41.76 - 57.90)
$r_4$	209.60	209.60	00.00 %	116.80	44.27 %	120.41 (109.50 - 134.24)	42.55 (35.96 - 47.76)
$r_{all}$	203.11	203.11	00.00%	102.68	49.44 %	114.94 (97.93 - 128.18)	43.41 (35.89 - 51.78)
$s_1$	/	213.15	/	412.61	/	//	/
$s_2$	/	202.47	/	350.33	/	//	/
$s_3$	/	213.68	/	409.34	/	//	/
$s_4$	/	213.55	/	279.12	/	//	/
$s_5$	/	186.55	/	206.68	/	//	/
$s_{all}$	/	223.28	/	383.62	/	//	/
$all$	223.52	223.52	00.00 %	120.71	45.99 %	111.80 (96.79 - 128.21)	49.98 (42.64 - 56.70)

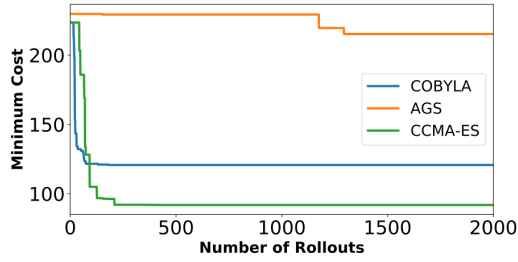


Figure 2.7: In our problem, COBYLA and CCMA-ES converge to a solution much faster than AGS. The figure shows the optimization of set  $r_2$ .

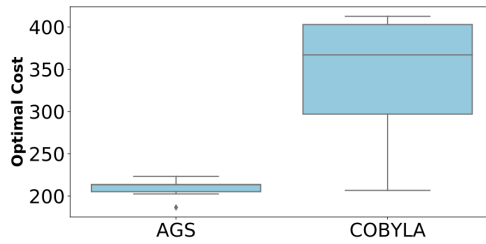


Figure 2.8: Optimal cost function from unfeasible starting sets  $(s_1, s_2, s_3, s_4, s_5, s_{all})$ .

To evaluate the performance of the algorithms in our optimization framework we measured the cost function value at the starting point (straight from the motion retargeting) and the optimal cost  $\mathcal{J}^*$  to calculate an improvement measurement:

$$\mathcal{I} = 1 - \frac{\mathcal{J}^*}{\mathcal{J}_{initial}} \quad (2.20)$$

## 2.5.2 Results and Discussion

The results for all optimization algorithms are displayed in Tab. 2.2. AGS and COBYLA are deterministic algorithms, so they were executed only once for every initial set. Whereas CCMA-ES is a stochastic algorithm, thus, in order to better evaluate the performance of the algorithm, it was executed 30 times. Additionally, we also show the torque values at the high priority joints (hips, torso, and shoulder) (Fig. 2.11).

During the execution of the benchmark, we found out that the sets  $s_1 - s_{all}$  did not pick up the box

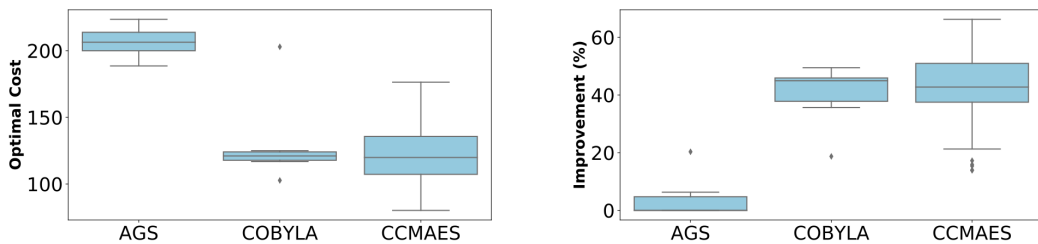


Figure 2.9: Optimal cost function, and improvement from feasible starting sets  $(r_1, r_2, r_3, r_4, r_{all}, all)$ .

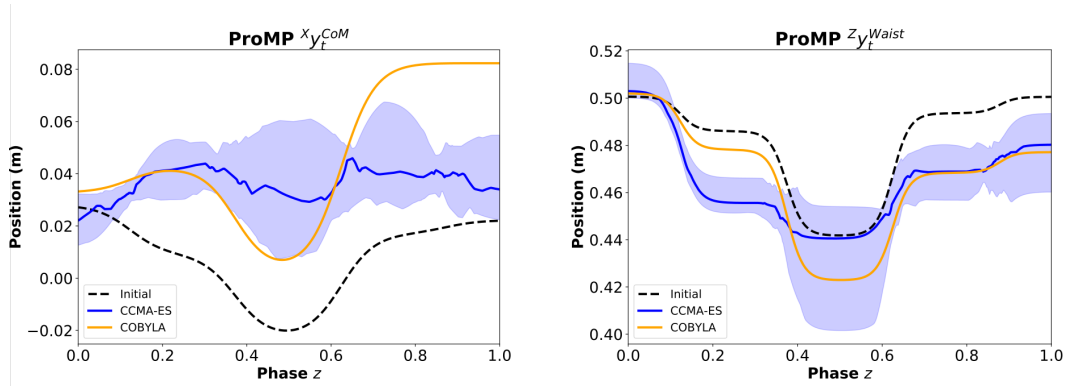


Figure 2.10: Reference trajectories: initial (from human demonstrations) and after optimization. Both CCMA-ES and COBYLA were bootstrapped from a ProMP that combined every demonstration, *all*. The 30 reference trajectories for CCMA-ES are represented with their median and IQR.

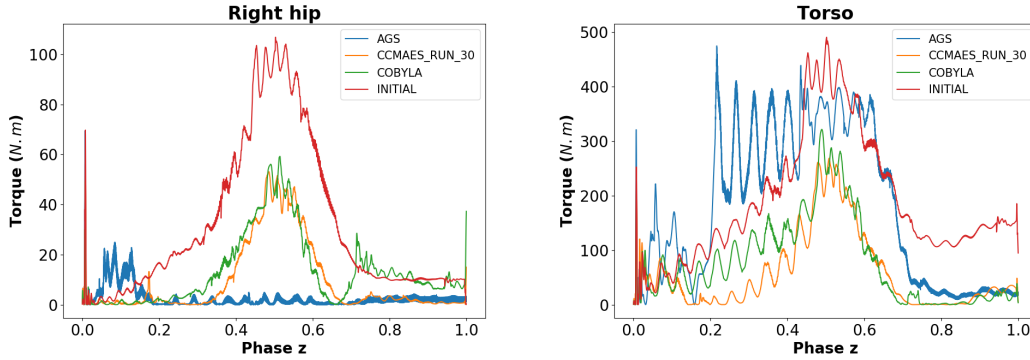


Figure 2.11: Torque values at the most critical joints in  $\epsilon_{icub}$ .

successfully according to Equations Eq. (2.17),Eq. (2.18),Eq. (2.19). Therefore, the initial cost function and improvements for those measures are inexistent. Moreover, those sets violated the task constraints from the start, so CCMA-ES cannot find a solution for them. However, contrarily to CCMA-ES, both AGS and COBYLA were able to find optimal values even when starting with unfeasible starting points. This different behavior within the sets of initial trajectories demands for a more careful comparison between the algorithms. For this reason, the analysis is first done concerning the unfeasible starting trajectories (Fig. 2.8) and posteriorly concerning the feasible starting trajectories (Fig. 2.9).

In Fig. 2.10, we show the optimized reference trajectories sent to the controller, for the different algorithms, compared with the initial solution with the ProMP that combined every demonstration, *all*. We do not show the result for AGS, as it behaved poorly when compared to the other ones (Tab. 2.2).

The AGS algorithm was only able to improve 2 feasible initial sets, with very little improvement (Tab. 2.2). However, AGS was remarkably able to find feasible solutions when starting from unfeasible points. These can be explained by AGS thoroughly and rapidly exploring the space, therefore, it is able to find a solution but it is not able to refine it.

COBYLA provided low-cost functions when starting from feasible solutions (Tab. 2.2), and like AGS, it also managed to find solutions even when starting from trajectories that violated constraints. It is noticeable, though, that COBYLA performs worse than AGS in the latter condition (Fig. 2.8). This

is likely caused by COBYLA being a local optimization algorithm, that works well at refining good solutions, but it does not perform well at exploring the search space.

Over 30 iterations, CCMA-ES was able to locate very good solutions in some of the initial sets (noticeably  $r_{all}$ , and  $all$ ). Additionally, all results from within the Interquartile Range (IQR) are better than the initial starting sets (Tab. 2.2). Interestingly, some of the solutions from CCMA-ES output a behavior that is known to be non-ergonomic for humans, e.g., bending the back while lifting, as shown in the accompanying video <sup>3</sup>. While this behavior is not desirable for humans, it is coherent with the fitness for which it is optimized on the robot. This is further indication that our framework indeed is suitable for motion optimization after retargeting from humans to humanoid robots.

When comparing the results from all three algorithms (Fig. 2.9) it is possible to verify that COBYLA and CCMA-ES have a very similar median behavior with improvements around the range of 40%. However, often, only the best trajectory is needed, and for this matter, CCMA-ES is more suitable, as their best results are better than the ones from COBYLA. AGS did not seem to produce good results even for 4 times more roll-outs than the other algorithms. Lastly, we can also verify that the cost function  $\epsilon_{icub}$  was able to minimize the torques at all of the high priority joints (Fig. 2.11).

In this work, we used a cost function that prioritized minimizing torques at selected joints. However, it is possible to define different weights ( $v_i$ ) at Eq. (2.15) and obtain different kinds of movements. Additionally, other cost functions like in Charbonneau *et al.* [23] can favor different movement aspects.

## 2.6 Multi-objective Trajectory Optimization to Improve Ergonomics in Human Motion

In this application, the goal is to generate whole-body motions that are ergonomically optimal according to one or more ergonomics scores. State-of-the-art human-robot applications that improve the human partner’s ergonomics usually take in consideration only one ergonomics score [15, 75, 96, 166]. However, single-objective optimization may not be sufficient to obtain ergonomically adequate whole-body motions, since optimizing for only one criterion often produces motions that are less ergonomic in other body regions; e.g., minimizing only the back flexion ignores the leg motion or efforts at the shoulder joints. Here, we use our optimization framework to generate several Pareto-optimal motions that simultaneously optimize several different ergonomics scores using a multi-objective optimizer (NSGA-II).

In the next sections, we empirically show that: 1) ergonomics optimization must be user-specific (experiment 1 in section 2.6.1-2.6.2); 2) optimizing for one single criteria may lead to non-ergonomic motions for other criteria, which means ergonomics criteria can enter in conflict (experiment 2 in section 2.6.1-2.6.2); 3) optimizing simultaneously for several criteria using multi-objective optimization leads to a rich set of trade-offs motions that are more reasonable in terms of ergonomics and realistic for a DHM.

### 2.6.1 Experiments

We optimize whole-body motions under a variety of body morphologies, ergonomics scores, and work activities. Two work activities commonly related to movements that are risky in terms of ergonomics were analyzed, A and B (Fig. 2.12), which are described hereafter.

**Activity A - Pick and Place Object from a Shelf:** In this activity, a human has to reach an object located on a shelf with its right hand, take the object, and move it laterally toward the right side to another point on the same shelf. If the worker’s shoulder level is below the shelf, this activity requires overhead work that could overload the worker’s right shoulder.

<sup>3</sup>Accompanying video is available at: [youtu.be/trJZVrVAVLMs](https://youtu.be/trJZVrVAVLMs).

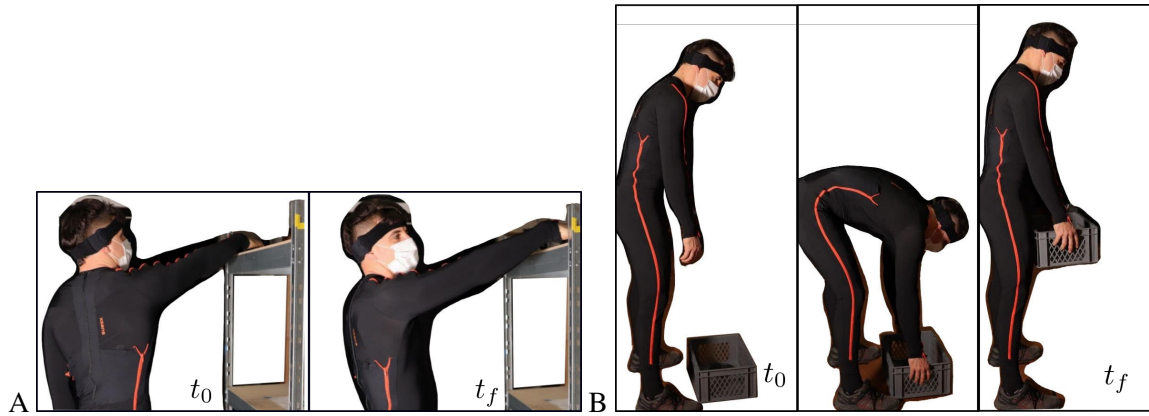


Figure 2.12: Demonstrations for work activities A and B captured with the motion capture suit XSens MVN. A: Pick and place a weight on a high shelf. B: Lift a box from the floor.

To execute this activity, the DHM QP controller includes an additional task that commands the head to always face the right hand position. The task weights in the QP controller are set as: 1.0 for the feet position (X,Y,Z), CoM position (X,Y), and hand position(X,Y,Z); 0.5 for the hand orientation (roll, pitch, yaw); 0.1 for Pelvis position (Z), and Head orientation; 0.05 for a reference body posture task; and 0.005 for a reference back lateral bending joint position task.

**Activity B - Lift Box from the Floor:** In this activity, a human has to reach a box situated on the ground, in front of her/him, and with both hands, lift it to the waist level height. This activity commonly requires a great amount of effort surrounding the human’s lumbar back area, which could be overloaded in the case of excessive back flexion, and/or excessive manipulated weights.

To execute this activity, the weights in the QP controller are set as: 1.0 for the feet position (X,Y,Z), CoM position (X,Y), hand position and orientation (X,Y,Z, roll, pitch and yaw); 0.05 for the pelvis position and orientation (Z, pitch), and reference body posture task; and 0.05 for reference joint positions at the ankles, knees, and back internal rotation and abduction joint positions.

### Experiment 1 - Effect of Varying Morphology

The goal of this experiment is to show that optimal ergonomic motions are user-dependent. We generated 9 different DHM morphologies with 3 different body heights, and 3 different body mass indexes corresponding to underweight, average weight, and overweight morphologies (Tab. 2.3). In this experiment, the right hand vertical position and the CoM ground projection trajectories were optimized for an activity A type of motion. The shelf is located at 1.5 m high and the start and end points for the hand are 30 cm apart. The initial hand trajectory was artificially generated as the minimum jerk trajectory between the start and end points. The hand trajectory was defined by a ProMP with 25 weights, and the CoM trajectory by a ProMP with 5 weights for each coordinate, X and Y, therefore,  $w \in \mathbb{R}^{35}$ .

For each morphology, we ran single-objective optimizations with 2 ergonomics scores for the shoulder: the RULA-C score (evaluates upper-body motions), and the shoulder torque score. The optimizer was set so that the optimization would converge. It was set to stop after 1500 rollouts or when the improvement in cost function between successive rollouts was below  $10^{-5}$ .

### Experiment 2 - Effect of Ergonomics Scores

The goal of this experiment is to show that SOTO with different ergonomics scores generates different optimal trajectories with possible negative impact on the overall ergonomics due to conflicting criteria.

We optimize the motion for both types of activities, A and B, and for each activity we run one SOTO for each ergonomics score listed in Tab. 1.1. Differently from experiment 1, here, the initial motion is captured from real human demonstrations (Fig. 2.12). In activity A, the shelf is located at 1.7 m high, and the start and end points are 0.64 m apart. The human demonstrator, as well as his DHM, are 1.85 m high, with 93 kg, therefore, here, activity A required oversoulder work. For both activities, we instructed the human demonstrator to perform a non-ergonomic demonstration (keeping hand above shoulder level in activity A and bending the back and not the knees in activity B), so that there was always a path for improvement in the optimization process. Additionally, weights of 1kg were used for both activities to limit the risk of injuries. In the simulation, however, we used a 5kg object (act. A) and a 10kg box (act. B) to assess demanding tasks where the choice of postural strategies might have a larger impact on ergonomics scores.

In activity A, the CoM, hand, and Pelvis QP reference trajectories are optimized with 10, 30, and 10 ProMP weights respectively, totaling 50 parameters to be optimized. In activity B, the CoM, and Pelvis QP reference trajectories are optimized with 10, 20 ProMP weights respectively, totaling 30 parameters to be optimized. For each parametrized trajectory, the initial values of the ProMP weights are learned from 5 human demonstrations. In both activities, the optimizer was set so that the optimization stopped after 1500 rollouts or when the improvement in cost function between successive rollouts was below  $10^{-5}$ .

### Experiment 3 - Multi-Objective Optimization

In this experiment, our goal is to show that MOTO generates motions with better trade-offs between several ergonomics scores than SOTO. We ran the MOTO on the same activities as in Exp.2, including the same constraints and parameters for the DHM QP controller. Instead of including all the ergonomics scores in the optimization, we selected the scores that are most relevant for each activity. Activity A demands a significant motion from the right shoulder, and it is predominantly an upper-body work activity, so we chose to optimize the motion w.r.t torques shoulder, normalized whole-body effort, and RULA-C scores. For activity B, both the shoulder and the lumbar joints are well demanded during the box lifting, so we chose to optimize the motion w.r.t. torques shoulder, and torques lumbar scores.

NSGA-II hyper-parameters are set as follows: cross rate = 0.5; population size = 100; number of generations = 600 (totalling 62000 rollouts per optimization execution). The mutation rates are set to 0.2, and 0.4 for activities A and B respectively, to take into account the different number of optimization parameters between activities. Since NSGA-II is a stochastic algorithm, we ran the optimization, in parallel, 20 times.

## 2.6.2 Results and Discussion

### Experiment 1

The optimization generated motions with improved ergonomics scores for each morphology with a median improvement of 16.9% and interquartile range (IQR) of 18.6% regarding the RULA-C score, as well as a median improvement of 25.2% and IQR of 10.7% for the torque shoulder score (Tab. 2.3). For both ergonomic scores, the hand trajectory of the short morphologies (m7, m8, m9) were distinguishingly lower than for the tall morphologies (m1, m2, m3), which is consistent with reducing the arm elevation angle. For the tall morphologies and the torque shoulder score, the hand vertical trajectory did not deviate much from the initial trajectory (straight line at 1.5m high). This was likely because the initial hand trajectory was already below the tall morphologies' shoulder level, and hence characterized a local minimum for this score. Indeed, lowering the arm even more would reduce the gravity torque at the shoulder, but it would require to move faster (since the task duration was fixed) thereby increasing the torque due

Table 2.3: Improvement of the ergonomics score from the initial movement after SOTO for different morphologies and scores (rula-c and torque shoulder).

$m_i$	Height (m)	B.M.I.	Weight (kg)	$\mathcal{J}_{rc}$	$\mathcal{J}_{tsh}$
1	2.0	18	72	8.3%	29.3%
2	2.0	22	88	8.4%	31.6%
3	2.0	30	120	8.1%	29.0%
4	1.8	18	58	16.9%	26.1%
5	1.8	22	71	17.6%	25.2%
6	1.8	30	97	14.3%	21.4%
7	1.6	18	46	33.5%	19.1%
8	1.6	22	56	25.9%	17.9%
9	1.6	30	77	28.0%	16.8%

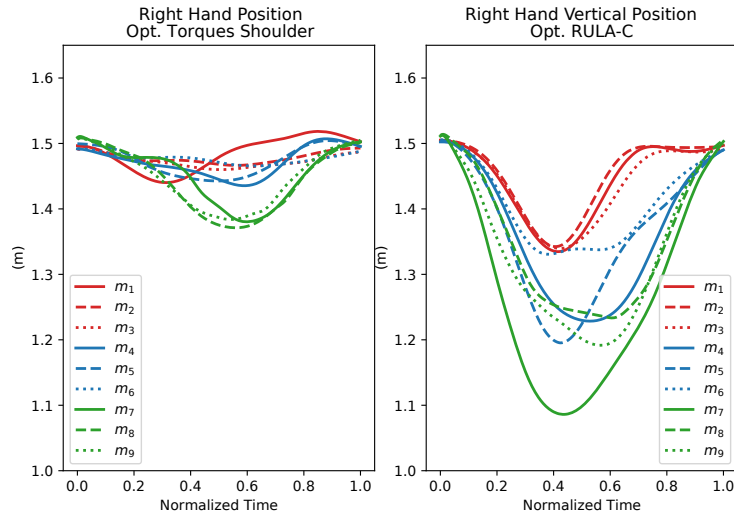


Figure 2.13: Optimized hand trajectories w.r.t. torques shoulder and RULA-C scores for the morphologies  $m_i | i \in [1 \dots 9]$  in Tab. 2.3 in experiment 1. Tall in red, medium in blue, and short in green.

to inertia. **These results confirm that each individual needs to have a custom motion optimization for his/her body morphology.**

### Experiment 2

Each optimization improved the initial motion according to its ergonomics score (Fig. 2.14). In Activity A, each optimization improved : back flexion by 99.37%, RULA-C by 4.52%, normalized whole-body efforts by 12.92%, torques shoulder by 60.36%, and torques lumbar by 77.24%. In Activity B, each optimization improved : back flexion by 93.42%, RULA-C by 30.02%, normalized whole-body efforts by 87.67%, torques shoulder by 64.97%, and torques lumbar by 67.32%.

Each one of the ergonomics scores have had a unique influence on the whole-body posture and efforts. For instance, the DHM's right elbow is more flexed during the optimal motion w.r.t. the torques shoulder score in comparison to the other motions during Activity A (Fig. 2.15). This is likely due to the fact that flexing the elbow brings the arm closer to the torso, hence, decreasing the torques caused by gravity on the shoulder. During activity B, the initial motion has excessively high lumbar torques (Fig. 2.14) due to the large back flexion (Fig. 2.15). This motion strategy was penalized by all ergonomics scores, which in turn favored motions that reduce the back torque decreasing the DHM's back flexion, and increasing the DHM's knee flexion instead. Interestingly, this is the case even for the torque shoulder optimal motion, where the lumbar torque is not directly penalized, although with a lesser amount of knee flexion than the others.

The results confirm that solutions optimized for a given score may degrade other scores (Fig. 2.14). In activity A, minimizing the torque shoulder score increases the whole-body effort and back flexion, while in activity B, minimizing back flexion increases the torque shoulder score. Additionally, conflicting ergonomics scores could happen when optimizing for scores that do not evaluate the activity's main load requirements. For instance, in activity A, whose main load is at the shoulder, optimizing for back flexion highly increased torques at the shoulder, while optimizing for lumbar torques increased the whole-body efforts in comparison to the initial motion.

**According to these results, optimizing for a single ergonomics score may not be advisable, and a more holistic approach concerning different ergonomics criteria must be sought for motion optimization.**

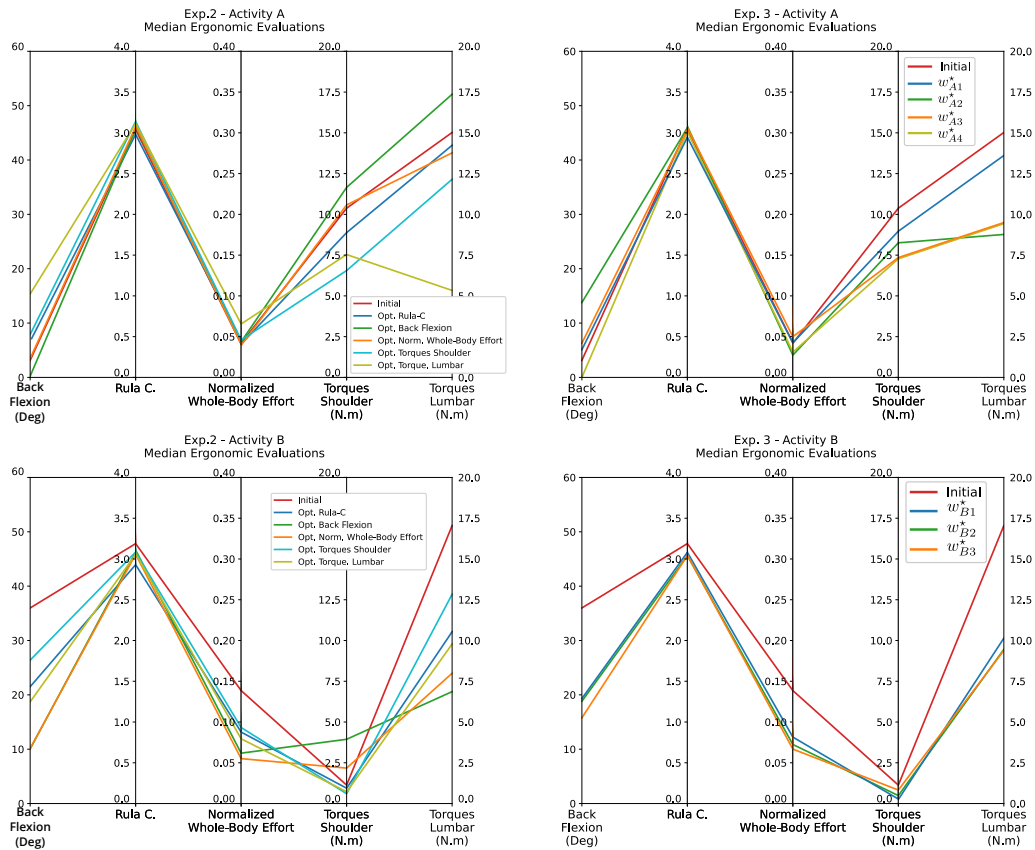


Figure 2.14: Experiment 2 (SOTO) and Experiment 3 (MOTO) - The median of the ergonomics scores during the execution of the initial and optimal motions. Lines of the same color represent one motion, and each axis represents one of the ergonomics scores. The motions in experiment 2 are taken from 5 independent single-objective optimizations for each activity. The motions in experiment 3 are taken from the respective Pareto fronts for each activity (Fig. 2.16 and 2.17).

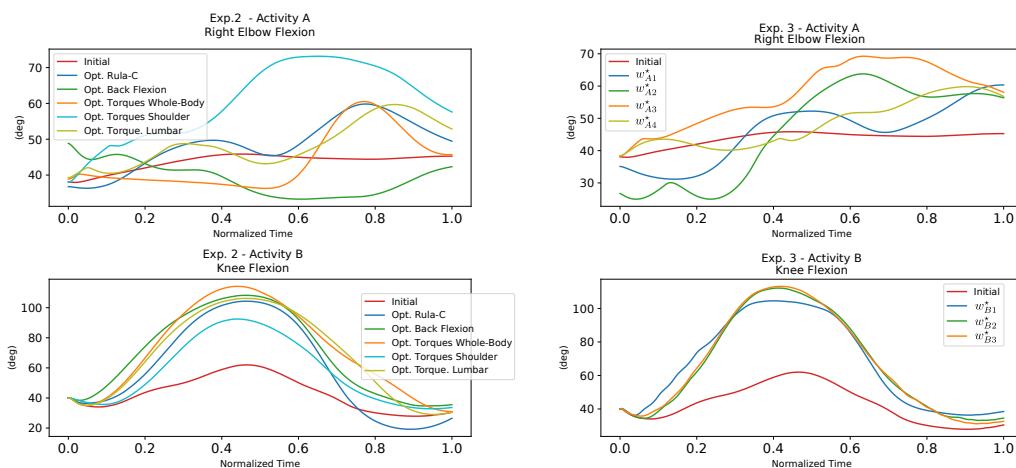


Figure 2.15: Experiment 2 (SOTO) and Experiment 3 (MOTO) - Time evolution of selected angles of the initial movement and the optimized motions: elbow flexion for activity A (Reaching); knee flexion for activity B (Lifting).

### Experiment 3

The Pareto front for both activities was computed for 20 MOTO replicates per activity (Fig. 2.16, and Fig. 2.17). The resulting Pareto fronts presented much starker score diversity between the Pareto-optimal solutions than the motions from the SOTO in Exp. 2 (Fig. 2.14). This likely happened because NSGA-II is a global optimizer, therefore, it explores the optimization space more efficiently than local optimizers. This diversity gives more options, and flexibility for the user to choose a Pareto-optimal solution according to given criteria.

To illustrate the advantage of using the MOTO approach, we visually selected some motions from each Pareto front of each activity with reasonable trade-offs between the scores (Fig. 2.16, Fig. 2.17), and compared them to the single objective solutions of the same scores (Tab. 2.4). For activity A,  $w_{A3}^*$  had similar elbow flexion trajectory to the SOTO w.r.t. torque shoulder score. As a matter of fact, this is a good solution if the user does not care about the generalized increase in the whole-body torques (indicated by  $\mathcal{J}_{nve}$ ). On the other hand, if both the whole-body torques and the torques at the shoulder are important for the user,  $w_{A4}^*$  could be a more interesting choice. Similarly for activity B,  $w_{B2}^*$  is a movement that optimizes both shoulder and lumbar torques simultaneously, but if the user would prefer the minimum shoulder torques from the pareto front, then  $w_{B1}^*$ , with less knee flexion, would be a better choice. Note that  $w_{B1}^*$ , also has a greater reduction on the lumbar torques than the SOTO solution for the shoulder torques. Additionally, most solutions from the Pareto fronts have improved their ergonomics scores, even for scores that were not being optimized (Fig. 2.15). This is likely due to those scores not being in conflict with the optimized ones.

**Video:** To show that Pareto-optimal solutions obtained by MOTO are better ergonomics trade-offs than those obtained by SOTO, we refer the reader to the accompanying video where we compare the different whole-body movements executed by our DHM<sup>4</sup>. Clearly, optimizing for a single criteria easily produces unrealistic movements that one could actually refer to as “non ergonomic”: for example, we point out the solution in activity A that minimizes only the lumbar torques with a very awkward non-ergonomic motion from other points of view. Movements generated by our MOTO approach are more feasible and ergonomically reasonable.

**In conclusion, generating whole-body motion with MOTO provides better trade-offs among several ergonomics criteria; and because many solutions are generated, we obtain a tool that enables a user (i.e., an ergonomist) to choose from a set of ergonomic motions that are often better than the ones generated with SOTO.**

---

<sup>4</sup>Accompanying video is available at: [youtu.be/vgQ0Ybs9TTo](https://youtu.be/vgQ0Ybs9TTo).

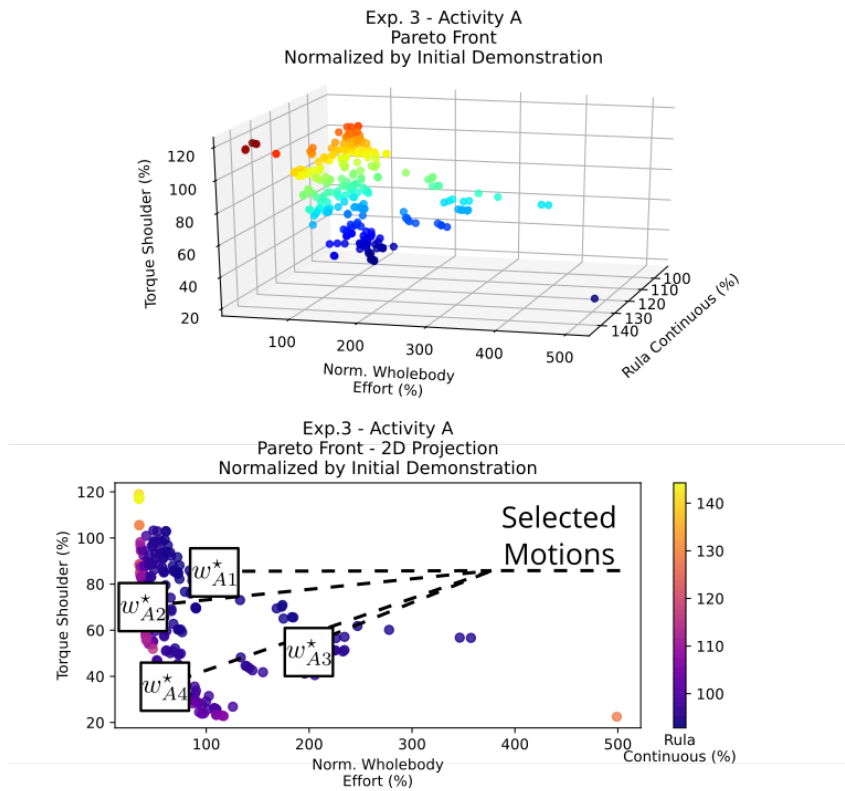


Figure 2.16: Experiment 3 - Activity A - Pareto front. The ergonomics scores values are normalized by those of the initial motion. The bottom image is a 2D projection of the 3D Pareto front, the third objective is represented by a color scale on each point.

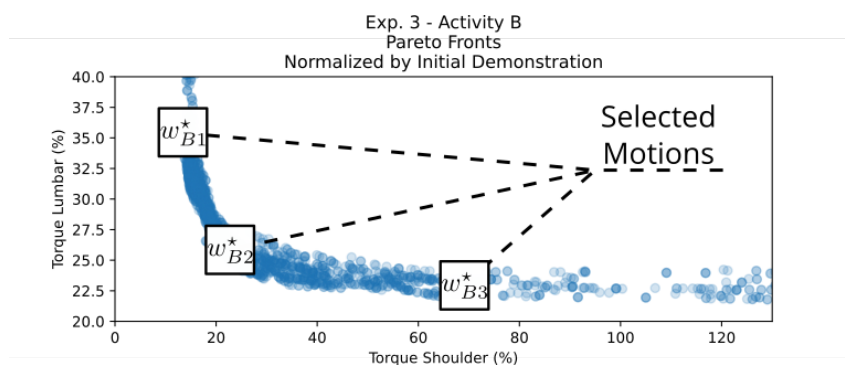


Figure 2.17: Experiment 3 - Activity B - Pareto front. The ergonomics scores values are normalized by those of the initial motion.

Table 2.4: Improvement of the ergonomics scores w.r.t. the initial motion after SOTO and MOTO. Worse performance in red. The multi-objective solutions are indicated in the Pareto fronts (Figs. 2.16 and 2.17).

(a) Activity A

<b>Motion</b>	$\mathcal{J}_{tsh}$	$\mathcal{J}_{nwe}$	$\mathcal{J}_{rc}$
<b>Initial</b>	100%	100%	100%
Single Obj. $\mathcal{J}_{tsh}$	39.4%	146.2%	105.7%
Single Obj. $\mathcal{J}_{nwe}$	99.1%	80.2%	102.4%
Single Obj. $\mathcal{J}_{rc}$	77.6%	90.8%	95.5%
Multi-Obj. $w_{A1}^*$	83.9%	115.9%	93.4%
Multi-Obj. $w_{A2}^*$	72.9%	41.2%	102.7%
Multi-Obj. $w_{A3}^*$	50.1%	198.0%	100.5%
Multi-Obj. $w_{A4}^*$	35.8%	53.4%	97.0%

(b) Activity B

<b>Motion</b>	$\mathcal{J}_{tsh}$	$\mathcal{J}_{tlb}$
<b>Initial</b>	100%	100%
Single Obj. $\mathcal{J}_{tsh}$	33.6%	70.6%
Single Obj. $\mathcal{J}_{tlb}$	78.8%	32.8%
Multi-Obj. $w_{B1}^*$	16.0%	36.9%
Multi-Obj. $w_{B2}^*$	22.4%	26.0%
Multi-Obj. $w_{B3}^*$	73.4%	24.4%

## 2.7 Discussion

In both applications, optimization of retargeted motions, and ergonomic motion generation, our trajectory optimization approach using ProMPs (Fig. 2.2) was able to improve the initial trajectories for different activities, body morphologies, and objectives. Bootstrapping the trajectory optimization with initial movements indeed seems to be a promising avenue to more efficient whole-body motion optimization regardless of the chosen optimizer. For instance, regarding the motion retargeting application, both single-objective optimizers COBYLA (deterministic), and CCMA-ES (stochastic) significantly improved the objective scores, even though they also require starting points that do not violate any constraints, as it was already observed in [108].

The motion retargeting application still has different ways in which can be expanded. Different whole-body motion patterns could be harnessed if different objectives other than the robot's effort are used, as it was better illustrated by the experiments on the ergonomic motion generation application. Our approach could also be used to optimize the design of a robot to accomplish tasks that were initially demonstrated by humans. In addition, our approach is inherently based on physical simulations, and therefore, it may still fail on tests with real robots, especially if the simulation environment and the real world have large discrepancies. A possible solution would be to input our optimized trajectories as priors for a reinforcement learning approach that deals with the real robot and its environment.

In the ergonomic motion generation application, we showed that single-objective optimization may not be sufficient to obtain satisfactory ergonomic motions, since optimizing for only one criterion often produces motions that are less ergonomic w.r.t. other criteria. Instead, in our approach we generate a set of Pareto-optimal motions with respect to multiple ergonomic scores. This allows us to simultaneously consider several criteria without requiring an ergonomics expert to preset weights for the different criteria prior to the optimization, as would be the case if the criteria were aggregated in a weighted sum. With our approach, solutions corresponding to any specific trade-off between the different ergonomic scores can be selected afterwards to match, for instance, the user preferences, or medical condition or the recommendations of an ergonomist. But importantly, this selection does not require to re-run the optimization, which represents a significant gain of time. Preliminary discussions with occupational ergonomists confirmed the potential of our tool, provided that we include learning implicit preferences for the Pareto-optimal solutions. This will be object of future work, possibly using preference learning algorithms [180].

Additionally, our approach has direct applications in human-robot physical interaction: a collaborative robot could be used to drive the human user towards an ergonomic posture when performing a joint task. For example, from the output of our optimization we can easily extract a user- and activity-specific optimal human hand trajectory, and then use it as the reference end-effector trajectory during a collaborative task. Nonetheless, to drive the human partner towards optimal one needs to comprehend how to coordinate the robot's actions with the human partner. The next chapter deals with studying a human dyad motor behavior during a physical interaction as a first step towards developing robot controllers to emulate such interactions.

# Human-Human Co-Manipulation

In this chapter, we present a study on the human motor behavior during an object co-manipulation task. First, we discuss about the many factors that can influence the human-human dyad’s motor behavior, in particular, the assignment of asymmetric responsibilities (roles) for each agent such as leadership. We propose to evaluate not only the kinematics of the motion, but also muscle activation signals from each agent and a task accuracy measurement for different leader/follower assignment conditions.

We find out that the condition in which no leadership was pre-assigned results in the best task accuracy despite also requiring more effort from both agents, as it was seen from the agents’ increased muscle activation signal. Surprisingly, the motor behavior of both agents resembled the behavior of a leader even if no leader was preassigned. At the end of the chapter, we discuss possible reasons for the results, and possible implications to human-robot applications, notably, to robot impedance control profiles.

## 3.1 Human Dyad Interactive behaviors

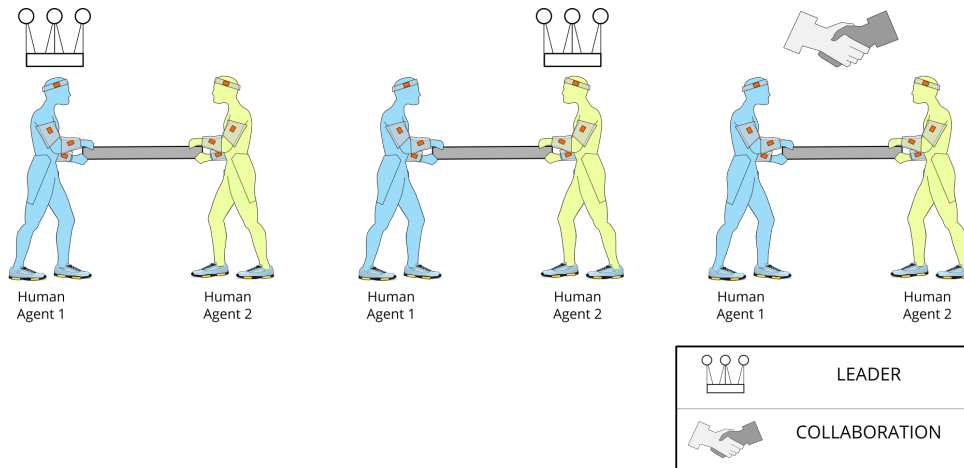


Figure 3.1: Human-human physical interaction study. The dyad executes a co-manipulation task under different leader/follower conditions: leader/follower; follower/leader; collaboration without pre-assigned leadership.

Humans in a dyadic interaction typically organize their movements around non-random, synchronized patterns in both timing and form [10, 12, 159]. Many factors may influence dyadic motor behavior, such as: sensory cues [109], roles [67], or skill level to execute a given activity [70]. When the human

dyad is haptically coupled, several studies use a leader/follower dichotomy [52, 95, 102, 103, 151, 170] to classify the roles of each agent based on haptic signals, such as force or stiffness. However, this premise may limit the understanding of the interaction, as recent studies in the neurology and psychology domains have reported that humans may see themselves as a dyadic interaction unit "greater than the sum of its parts" [36, 198].

According to Jarrassé *et al.*, physical interactive tasks between dyads (human or robots) can be classified in three categories [66]: competition, collaboration, and cooperation. During a *competition*, the benefit of an agent is detrimental to the other agent, therefore, they may work against each other if necessary. If prior to the task execution, the agents have been assigned, or agreed upon, different roles (asymmetric responsibilities) to execute the task, then the interactive task is classified as a *cooperation*. In contrast, during a *collaboration*, both agents form a coalition to accomplish the task [38]. The "activity is synchronized and coordinated in order to build and maintain a shared conception of a problem" [148]. That is, in a collaboration, the agents may deliberate and negotiate their roles in executing the task for the dyad common good.

Human-human dyads within a leader/follower dichotomy are actually a typical case of asymmetric role assignment in which the two cooperate to achieve a common goal [66]. Meanwhile, the follower is only there to support the actions of the leader. Many studies have associated this compliance regarding the other agent with different levels of stiffness for trajectory trackings [3, 17, 87, 95, 110]. For instance, if an agent has a high arm stiffness, then it is less compliant, and it acts as a leader, and vice-versa. However, to the best of our knowledge, no study has investigated the stiffness levels across leader/follower cooperation and collaboration conditions for the same human dyad. If the collaboration condition is where negotiations occur, can we identify a switching between leader and follower roles by looking at each agent's motor behavior? Or particular levels of stiffness that suggest a collaboration is established by the agents? Moreover, if the dyad organization also strongly affects the task execution, it could also have an effect on the task performance.

If a robot were to substitute one of the human agents, would the robot be able to drive the human towards more ergonomic trajectories? One solution would be to give complete autonomy of the task to the robot, with the robot as a leader and the human as follower. In this scenario the robot could track a trajectory that is known to be ergonomic for the human, possibly a trajectory from a single- or multi- objective optimization as in Chapter 2. However, humans may disagree with the robot leadership, be it for they judge the robot trajectory is incorrect, or for their own poor acceptability of the robot. A collaboration behavior that does not automatically impose the role of a follower to a human partner could prove to be the best solution. In this context, investigating the human motor behavior during collaboration conditions is key to reproducing the same behavior within a human-robot collaboration.

This chapter's goal is, hereafter, threefold. First, to evaluate if leader / follower cooperation, and collaboration conditions affect the stiffness levels of agents in a human dyad during a shared joint task. Secondly, to evaluate if the trajectory of the object being manipulated by the dyad is also affected. And lastly, if there is in fact a variation in performance with respect to a common goal for both agents in the dyad. For this matter, we have designed a precise object manipulation experiment, where a human dyad is organized in leader/follower configurations, as well as in a collaboration condition (Fig. 3.1).

## 3.2 Methods

### 3.2.1 Participants

Two experiments were designed with the same task and setup, but with different configurations regarding the human agents: the main experiment requires a human dyad (Fig. 3.2a), and a control complementary experiment requires a solo subject (Fig. 3.3). The dyad experiment was executed by 10 human dyads,

therefore 20 participants, of which 15 were male, and 5 were female. Their age ranged from 22 to 38 years old ( $M = 26.6$  years,  $SD = 3.61$  years). 17 participants were right-handed, and 3 were left-handed even though all manipulations were performed with the right hand.

The solo experiment was executed by 10 solo participants, of which 9 were male, and 1 was female. Their age ranged from 22 to 32 years old ( $M = 25.7$  years,  $SD = 2.16$  years). 2 subjects were left-handed. Participants from the dyad experiment did not participate on the solo experiment and vice-versa.

Every participant provided written informed consent for their participation in the experiment. No participant claimed any chronic motor disease or health condition that could influence in the experiment's results. The experiments were approved by INRIA's ethical committee (COERLE).

### 3.2.2 Task Description

The task consists in manipulating an object (pipe) to bring it from a start to an end point (Fig. 3.2a). The participants are instructed to avoid moving their back during the task execution (they are not strapped). They hold the pipe with their right hand with a power grasp, placing their hand on one of the designated handles. In the start (Phase 1), the pipe is within Tube 1 (the one closest to Agent 1), then the pipe has to be taken out of Tube 1 while avoiding contact with Tube 1's front wall. After extracting the pipe from the tube (Phase 2, free movement), the pipe has to be moved around a cylindrical obstacle towards Tube 2 (the one closest to Agent 2). Then, the pipe has to be inserted into Tube 2 (Phase 3)<sup>5</sup>, while avoiding contact with the front wall. By design, the task is always recorded and evaluated from Tube 1 to Tube 2, and the return motion is ignored. Even though there is no physical restriction on the pipe's motion after exiting Tube 1 and before entering Tube 2, the agent(s) are told not to move the pipe over the cylindrical obstacle. Effectively, this enforces a planar movement of the pipe.

If two human agents execute the experiment, then a black curtain is placed between the participants to prevent visual contact during the task execution. In addition, they are instructed not to talk during the task execution.

#### Duration

During the task execution, none of the agents saw a timer, but they were told that the whole manipulation (from Start to End) should not last longer than 15 s. If participants took significantly longer than 15 s then they were told so and the trial was canceled.

### 3.2.3 Apparatus

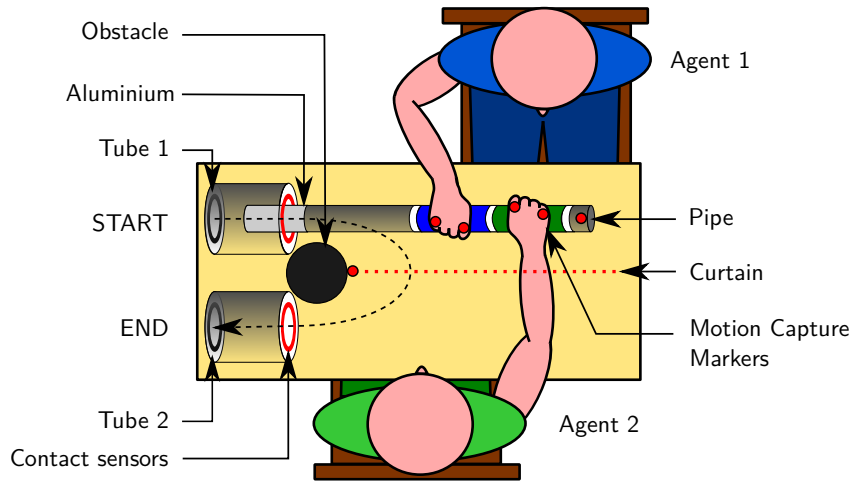
The manipulated object is a 218 g pipe of diameter 3 cm and length 50 cm (Fig. 3.4), with 10 cm wide handling areas for both agents. One end of the pipe is covered with 8 cm long of aluminum foil, which makes it possible to detect whenever the pipe touches any of the tube walls. On the other hand, since the tubes are 10 cm long, it is impossible to detect a contact between the front and back walls of a tube at the same time.

### 3.2.4 Experiment Description

#### Dyad experiment

In the *dyad* experiment, two agents shared the pipe manipulation. Each agent sat on one side of the table (Agent 1 and Agent 2 in Fig. 3.2a). Two handles were drawn on the pipe: Agent 1 held the pipe on Handle 1 (blue in Fig. 3.2a), while Agent 2 held the pipe on Handle 2 (green in Fig. 3.2a). The Agent

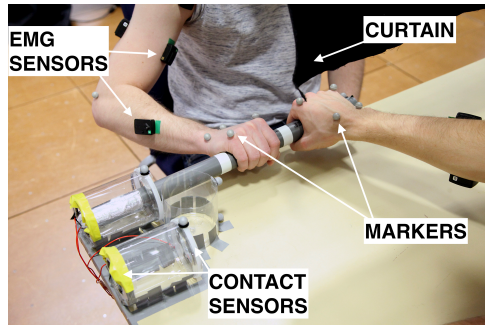
<sup>5</sup>The instant of the transition between phases is calculated in B.1



(a)



(b)



(c)

Figure 3.2: Main Experiment: Human Dyads. a) **Object co-manipulation by human dyad:** Top-down view of the experiment set-up. The black dashed line approximates the pipe trajectory. The red circles are metal rings attached to the walls of the tubes in order to detect contact with the aluminium that is wrapped around the end of the pipe. The red dashed line represents a curtain placed between both agents to prevent visual communication. b) **Experimental scenario:** Two participants performing the co-manipulation task. A black curtain blocks visual communication between agents. c) **Sensors:** surface EMG sensors placed on the agents' arms, motion tracking markers (on the agents' arms, the pipe, the obstacle, the targets) and contact sensors inside the tubes.

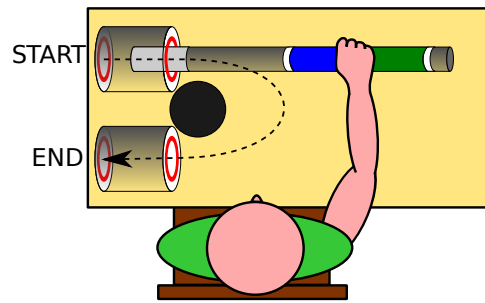


Figure 3.3: Complementary Experiment: Solo Human Agent. Top down view of the experimental set-up for the Solo Experiment. The human changes position between conditions.

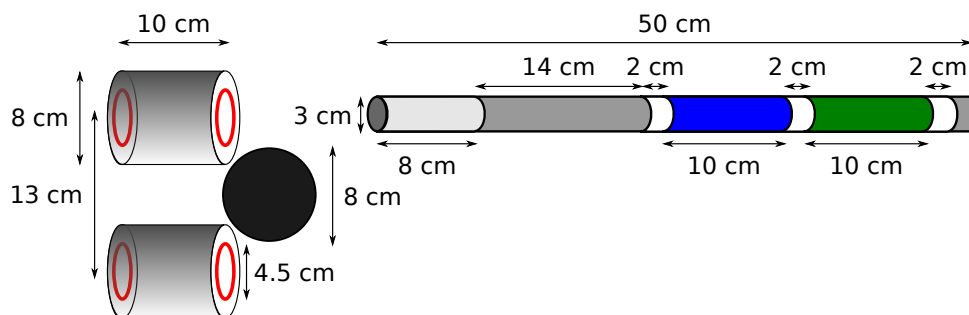


Figure 3.4: Dimensions of the pipe and tubes.

did not switch seat position, *i.e.* one Agent was always Agent 1, and the other always Agent 2. Each human-human dyad performed the task in all 3 conditions:

- *No specified roles:* Agents were only instructed to manipulate the pipe;
- *Agent 1 Leader and Agent 2 Follower:* Participants were instructed that Agent 1 must lead the movement, while Agent 2 was only there to support and follow Agent 1;
- *Agent 1 Follower and Agent 2 Leader:* Participants were instructed that Agent 2 must lead the movement, while Agent 1 is only there to support and follow Agent 2.

The order of the 3 conditions was randomized across dyads to counter-balance possible biases.

Before starting the recording for each condition the participants could practice for 2 trials. For each condition, 5 trials were recorded, resulting in a total of 15 trials. Since there were 10 recorded dyads, a total of 150 trials were recorded.

There was an approximate 45 s break between each trial, in which the participants could rest their arm, but the exact duration of the break was not imposed (participants decided when they wanted to start the next trial).

### Solo experiment

In the *solo* experiment, there was only 1 agent (Fig. 3.3 ). The Agent held the pipe between Handle 1 and Handle 2. There were 2 conditions in the *single* experiment:

- *Position 1:* The participant sat in Agent 1's position;
- *Position 2:* The participant sat in Agent 2's position.

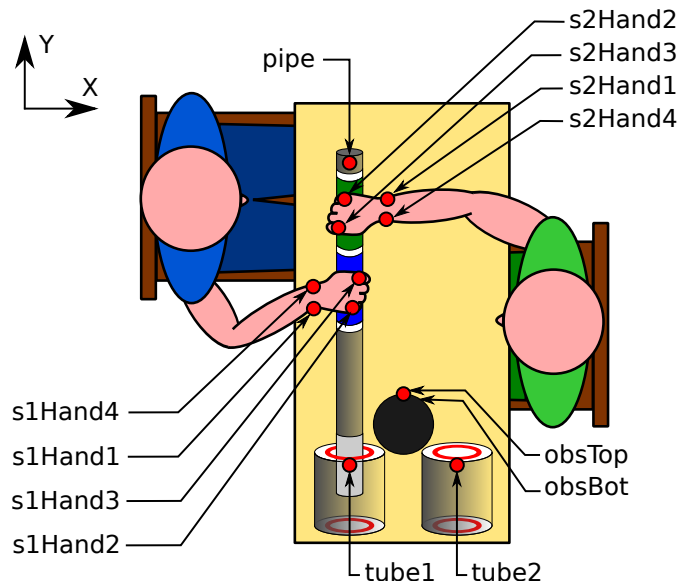


Figure 3.5: Positions of the Qualisys reflective markers: 4 markers are set on each agent’s right hand, and 5 markers are set on the pipe, tubes and obstacle. Note that the *obsBottom* marker set on the obstacle is not visible, because it is vertically aligned with the *obsTop* marker.

The order of the 2 conditions was randomized across participants to counter-balance biases.

All participants performed 5 trials for each condition, and 10 trials in total. Similarly to the *dyad* experiment, the trials were separated by an approximate 45 s break, and 2 practice trials were allowed at the beginning of each condition.

### 3.2.5 Data Collection

During both experiments, we gathered data on each agent’s arm, motion and muscle activity. And to assess how accurate the agent (or the dyad) was in executing the task, we also measured how many times the pipes would touch the tube walls.

#### Motion capture

The motion of the participants’ right arm was recorded with a Qualisys optical motion capture system (at rate of 150 Hz). Four reflective markers were placed on the participant’s hand (Fig. 3.5) to track their 3D Cartesian positions:

- 1 marker on the Ulnar-Styloid Process
- 1 marker on the Head of the 5th Metacarpal
- 1 marker on the Head of the 2nd Metacarpal
- 1 marker on the Radial-Styloid Process

In addition, 5 markers were placed on the pipe, tubes and obstacle (Fig. 3.5):

- 1 at the tip of the pipe which does not go inside the tubes (opposite to where the aluminum foil is). Agents were told to hold the pipe so that this marker was facing up (referred to as *pipe*);
- 1 at the top of the front wall of each tube (referred to as *tube1* and *tube2*);

- 1 at the top of the obstacle wall, farthest away from both tubes (referred to as *obsTop*);
- 1 at the bottom of the obstacle wall, farthest away from both tubes (referred to as *obsBot*);

### **Electromyography**

In the *dyad* experiment, 6 wireless Delsys Trigno EMG sensors were placed on the participant's right arm, on the following muscles:

- Flexor Carpi Ulnaris;
- Extensor Carpi Ulnaris;
- Biceps Brachii;
- Triceps (lateral head);
- Deltoid, Anterior;
- Deltoid, Posterior.

The EMG sensors are placed on the subject following guidance rules from the European project SENIAM [171], as well as location cues from Perroto, 2011 [128]. After locating a muscle, the subject is asked to contract it to confirm the location of the "muscle belly", that is then marked with a pen. For each muscle, an EMG sensor is assigned, and annotated in our EMG acquisition software.

Before placing a sensor on a muscle location, the area surrounding the pen mark is prepared accordingly. The subject's skin is cleaned with alcohol until it acquires red tones, which indicates good skin impedance. After the alcohol dries out, the EMG sensor is placed on the skin at the muscle fibers direction with the help of a double-sided sticker provided by the sensor manufacturer.

Prior to the task execution, each agent is asked to perform maximum voluntary contractions (MVC) during isometric exercises for each selected muscle [171] for 3 s. The exercise is performed 3 times, with a 1 minute interval between them to decrease fatigue biases. After the 3 trials, the maximum EMG signal is then stored and used for posterior post-processing of the EMG signals during the task execution.

In the *solo* experiment, only the 2 muscles in the forearm (Flexor Carpi Ulnaris and Extensor Carpi Ulnaris) were recorded. All of the EMG recordings, in both experiments, were taken at a rate of 2 kHz.

### **Contacts**

The designed task requires the solo agent, or human dyad, to avoid contact between the pipe and the tube walls. We then use contact sensors to detect those contacts, and posteriorly use this information as a performance measure.

To detect the contacts between the pipe and the tubes, we wrapped the end of the pipe with aluminum foil, and metallic rings were placed inside the walls of both tubes. It is important to note, that those contact sensors are essentially mechanical switches which are known for their bouncy signals, so to circumvent this issue we debounce the input through software. After we detect a signal onset (a contact) no other onset is stored as a contact for the next 100 ms window (roughly half of the average human simple reaction time [202]).

## Data Synchronization

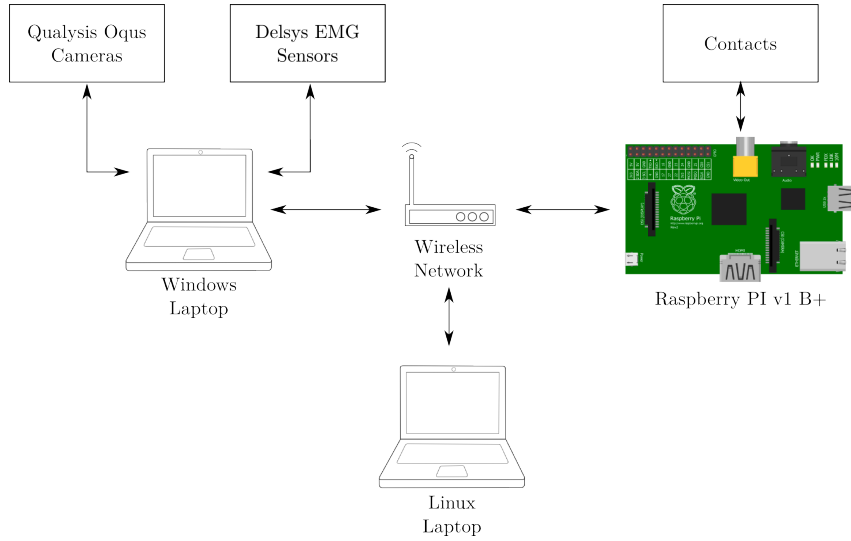


Figure 3.6: Equipment used for data collection. The Qualysis system collects the motion capture data; the Delsys system collects the EMG data; and a custom contact sensor collects the number of contacts between the pipe and the tube walls.

The data collection of the EMG and motion data is synchronized, that is, they start and end at the same instant, and are both taken from the same Windows computer (Fig. 3.6) using Delsys and Qualysis respective proprietary softwares. The Linux laptop was used to collect data from the contact sensor, and it additionally executes a graphical interface for acquisition of EMG signals corresponding MVCs <sup>6</sup>. Since here we are only concerned with the number of contacts during the task execution, the contact sensor data does not require a precise synchronization with the other sensors, so it is simply done manually.

### 3.2.6 Data Analysis

#### EMG Processing

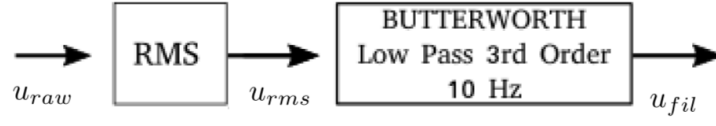
Surface EMG signals are easy to capture, but require careful pre-processing before analysis [93]. Here, the EMG signal for the  $i$ -th muscle,  $u_i$ , was passed through a 100 ms RMS window, and filtered by a low-pass third order Butterworth filter with a 10 Hz cutoff frequency (Fig. 3.7a) to generate a filtered signal  $u_i^{fil}$ . However, the filtered signal alone is only proportional to its respective muscle activation, or contraction.

To obtain an index of the muscle activation, between 0 and 1, we needed to normalize the signal with respect to its stored MVC value:

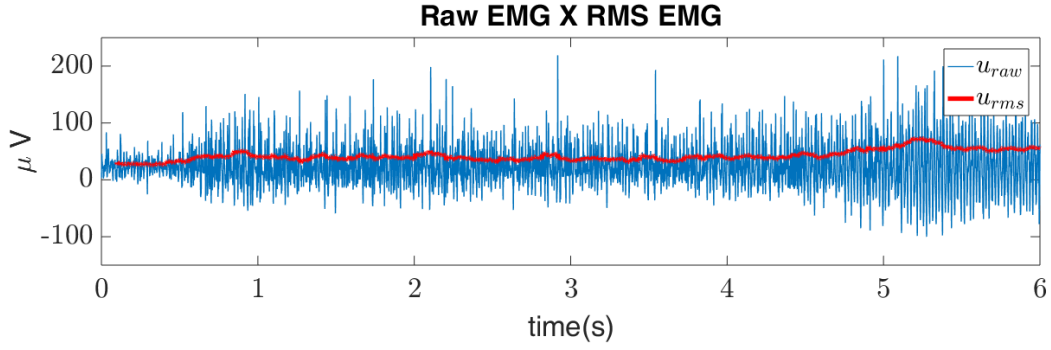
$$u_i^{norm} = \frac{u_i^{fil}}{u_i^{MVC}} \quad (3.1)$$

where  $u_i^{norm}$  can finally be used to provide information on the arm stiffness modulation.

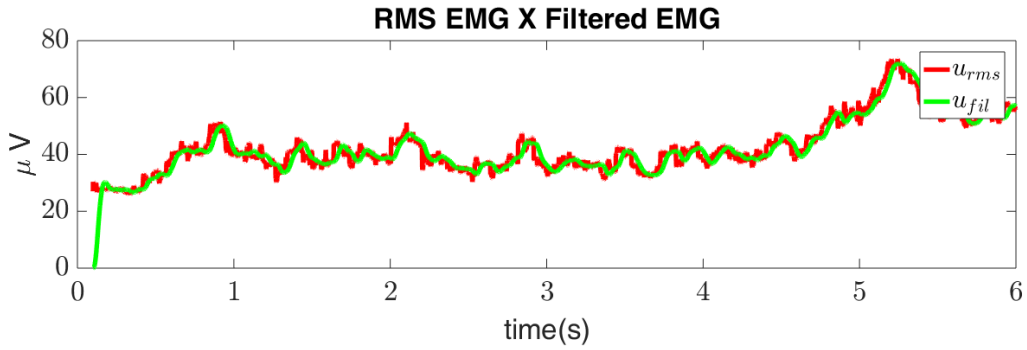
<sup>6</sup>This GUI can be found in: <https://github.com/inria-larsen/emg-processing>



(a) EMG signal processing steps: acquisition from sensor  $u_{raw}$ ; RMS window of 100 ms ( $u_{rms}$ ); Butterworth low pass third order filter with 10 Hz cutoff frequency ( $u_{fil}$ ).



(b) Comparison between  $u_{raw}$ , and  $u_{rms}$ . It can be seen that  $u_{rms}$  is an envelope of  $u_{raw}$ .



(c) Comparison between  $u_{rms}$ , and  $u_{fil}$ . The Butterworth filter smooths the RMS signal.

Figure 3.7: Steps to obtain an enveloped EMG signal for this work.

### Index of Co-Contraction

Instead of generating movement at a given joint, equivalent contraction from antagonist muscles tend to increase joint stiffness. Given the activation levels from two antagonist muscles,  $i, j$ , we can calculate an Index of Co-Contraction (ICC) for their respective  $k$  joint [14, 51, 185]:

$$icc_k(t) = \min(u_{norm}^i(t), u_{norm}^j(t)) \quad (3.2)$$

where  $icc_k(t) \in [0, 1]$ .

In both experiments, we processed the EMG signals from only two antagonist muscles with respect to the wrist joint movement (Flexor Carpi Ulnaris and Extensor Carpi Ulnaris). Due to muscle synergy [60], the ICC for both muscles should reflect the arm stiffness modulation for the entire arm. For simplicity, hereafter, we will refer to the ICC corresponding to both of those muscles as ICC.

### Deviation Angle $\alpha$

From obstacle avoidance motor planning, we expected humans to plan their arm trajectories while taking into account inertial and kinematic properties of their arms, likely favoring motion plans with their hands

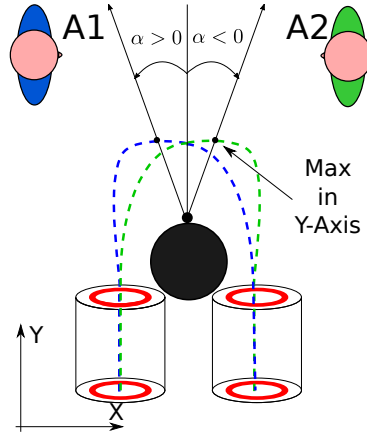


Figure 3.8: Angle of trajectory deviation,  $\alpha$ : It is the angle between the vertical line that divides the setup symmetrically, and the line from the obstacle marker to the point of the trajectory with maximum value in the Y-Axis.

closer to their bodies [150]. During a leader/follower cooperation, leaders were expected to try to impose their own intended trajectories to the pipe trajectory. Therefore, since in our case the agents were seated facing each other (Fig. 3.2a), we expected the intended leader trajectories to be different from the follower trajectories. In the cooperation scenario, the resulting pipe trajectory should have roughly translated to the intended leader trajectory<sup>7</sup>, however, there was no clear expectation for what could have happened in the collaboration scenario.

To quantify how the pipe trajectories favor one agent or another, we defined a trajectory deviation angle  $\alpha$ . Positive values of  $\alpha$  mean that the trajectory deviates towards agent 1, and negative values mean deviation towards agent 2 (Fig. 3.8). Specifically,  $\alpha$  quantifies the skewness of the pipe trajectory with respect to the Y-axis that divides the experimental setup symmetrically. Given a dyad or agent's hand markers centroid trajectory,  $\vec{r}(t)$ , we calculated the point in which the position is maximum in the Y-axis

$$t_{max} = \arg \max(r_y) \quad (3.3)$$

$$\vec{r}_{max} = \vec{r}(t_{max}) \quad (3.4)$$

and the position of the marker in front of the obstacle  $\vec{r}_{obs}$  to be able to calculate a vector that indicates the direction of the skew.

$$\vec{r}_{dir} = \vec{r}_{max} - \vec{r}_{obs} \quad (3.5)$$

Then,  $\alpha$  is the smallest angle between the Y-Axis vector and  $\vec{r}_{dir}$ :

$$\text{atan2}((\vec{r}_{dir})_x / (\vec{r}_{dir})_y) \quad (3.6)$$

### 3.2.7 Methods for Statistical Analysis

#### Index of Co-Contraction Data

Each agent's ICC is in fact a time series (Fig. 3.9), however, for the purpose of this study, we decided to obtain a representative value of the ICC for every task execution calculating an RMS value. In addition,

<sup>7</sup>All resulting trajectories can be found in B.3

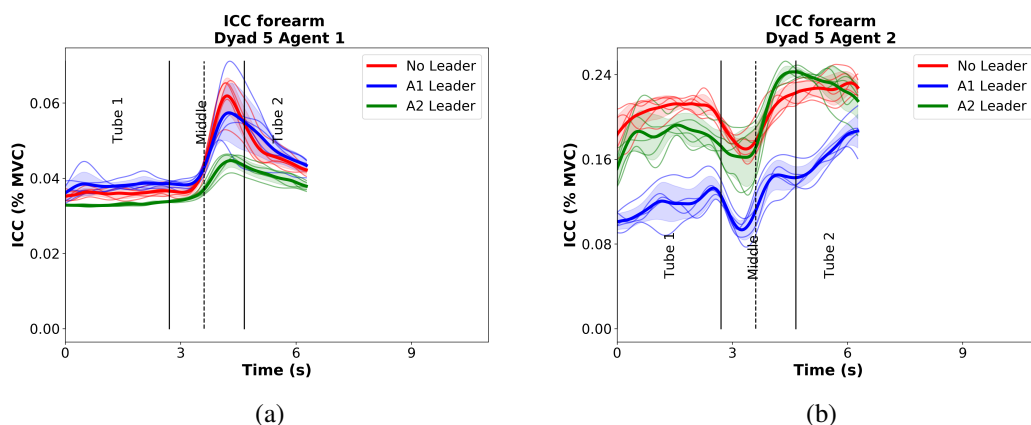


Figure 3.9: **Dyad Co-Manipulation Experiment**: Index of Co-Contraction (ICC) for the muscle pair Extensor/Flexor Carpi Ulnaris at the subject’s forearms, for both agents in dyad 5 of the main dyad experiment. Phase 1: pipe is within Tube 1. Phase 2: Pipe is out of the tubes. Phase 3: Pipe is within Tube 2. The plots for all other time series can be found in B.2

during phases 1 and 3 of the task, while the pipe is within any of the tubes, the agents have to act more precisely to avoid contacting the tube walls, so it is likely that the co-contraction will be higher than in phase 2. Therefore, we decided to calculate the RMS value,  $icc_{rms}$ , only for the phases 1 and 3 of every task execution.

In the dyad experiment, there is one source of  $icc_{rms}$  data from each agent. To evaluate the effect of the roles on the RMS values, we re-grouped them into 3 new conditions:  $icc_{rms}$  of a leader,  $icc_{rms}$  of a follower, and  $icc_{rms}$  during collaboration without pre-assigned leadership. Since there were 5 trials per dyad and 2 agents per dyad, each role condition included 10 ICC measurements, therefore, 30 measurements per dyad, and 300 in total. Finally, for the statistical analysis in the *dyad* experiment, since the ICC data was not Gaussian (Shapiro tests with  $p < 0.001$ ), the median for each new condition was calculated in order to enable the usage of Friedman tests.

### Deviation Angle Data

The deviation angle in both experiments had a normal distribution (Shapiro-Wilk normality test: dyad manipulation,  $p = .39$ ; solo Manipulation,  $p = .05$ ), therefore, a regular analysis of variance with repeated measures (or a paired t-test for the solo experiment) was done to verify the effect of the conditions on the deviation angle.

### Contact Sensor Data

The data from the contact sensors is made of natural numbers, therefore, the sample measures are in fact classified as *count data*. After verifying that the count data was overdispersed (variances larger than means) in both experiments, we used a general linear mixed model with negative binomial distributions [19], with random effects to account for the repetitions in the same condition. Since there are 3 conditions, post-hoc tests with Tukey correction were used to evaluate if the different conditions affected the number of contacts.

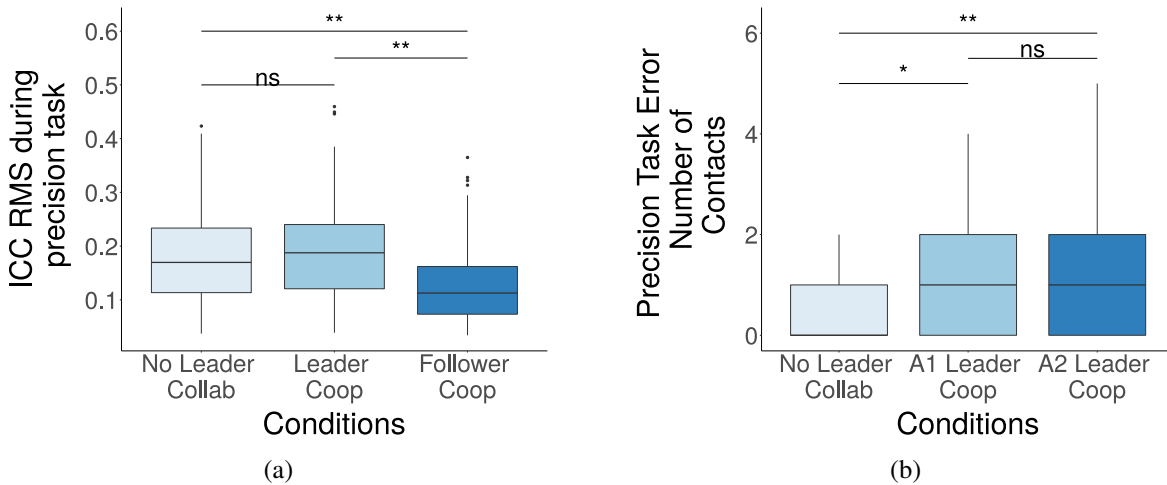


Figure 3.10: **Dyad Co-Manipulation Experiment**: Both agents increase their muscle co-contraction in the collaboration condition when the trajectory execution is more precise which is when the pipe is within any of the tubes. a) Root Mean Square index of co-contraction removing and inserting the pipe inside the tube for every condition: Collaboration condition (no leader) is not significantly different from the leader condition, however, both of them are different from the follower condition b) Number of contact errors in the tube walls per condition: No significant difference in the number of contact errors is found between the cooperation conditions, but there is a significant difference in the number of contact errors for both of them and the collaboration condition.

### 3.3 Results

#### 3.3.1 Collaboration leads to muscle co-contraction as high as in leaders

In the dyad experiment, we expected that different role assignments to a human dyad would affect each agent's arm stiffness. Then, we estimated an ICC for each agent as the ICC and the arm stiffness are directly proportional. Friedman tests indicated that the ICC RMS value,  $icc_{rms}$ , was significantly different between the groups of leaders, followers, and agents in collaboration,  $\chi^2(2) = 24.7, p < .001$ . However, posterior post-hoc Friedman tests revealed that there was no significant difference between the leader  $icc_{rms}$  and the collaboration  $icc_{rms}$  ( $p = .246$ ) while both of them were significantly different from the follower  $icc_{rms}$  ( $p = .005$ ) (Fig. 3.10a).

Since the median of  $icc_{rms}$  is the smallest of the 3 conditions, the inferential statistical analysis suggests that the co-contraction was increased both when the human took the leadership, and when he/she collaborated.

#### 3.3.2 Trajectories are deviated towards the dyad's leader

The trajectory deviation angle,  $\alpha$ , quantifies how much an agent deviates the dyad trajectory towards him/herself. An analysis of variance with repeated measures was applied to the deviation angle  $\alpha$  for the 3 coordination conditions. There was indeed a significant effect on  $\alpha$ , ( $F(2,18) = 10.85, p = .0008, \eta^2 = 0.13$ ) across the experiment conditions, and, Bonferroni corrected post-hoc t-tests showed a significant difference in  $\alpha$  between every condition, from collaboration to Agent 1 being the leader ( $p = .002$ ), from collaboration to Agent 2 being the leader ( $p = .001$ ), and between both cooperation conditions ( $p < .0001$ ). As expected, the median values for all conditions (Fig. 3.11b) suggests that the trajectory of the object deviated towards the agent who was the preassigned leader of the task (fig.

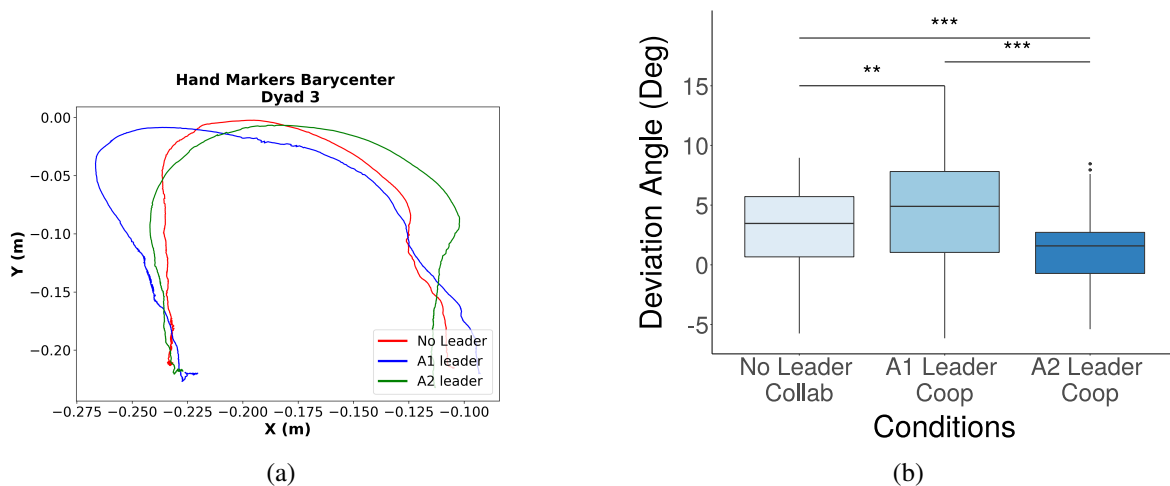


Figure 3.11: **Dyad Co-Manipulation Experiment**: a) Typical trajectories for the different conditions executed by one of the dyads in the experiment (Dyad 3); b) Deviation angle per condition: as can be seen by the median values, during cooperation, the deviation angle  $\alpha$  exhibited values towards the leader of the task, and in collaboration,  $\alpha$  had values in the middle of the leadership extremes.

Fig. 3.11a). Furthermore, in the collaboration condition, the median of  $\alpha$  was between the medians for the other two conditions.

The main dyad experiment also raised the question of how different would the object's trajectory be if the agents were moving the object on their own, and most importantly if the trajectory would still deviate towards the agent when he/she is the only one doing the task, therefore, no partner bias. To answer these questions, we verified the deviation angle of the trajectories per position of the agent (Fig. 3.12) during the solo experiment. The statistical analysis ( $t(49) = 13.06, p < .001, d = 2.59$ ) showed that the deviation angle does change per position, and in the solo experiment, the means of the deviation angle showed a more accentuated deviation towards the solo agent than the deviation angle towards the leader agent in the main dyad experiment. Furthermore, the means of  $\alpha$  for each condition (Fig. 3.12) are even greater than on the main dyad experiment when the leaders were in the same positions. This also reinforces our argument that the leaders had an intended trajectory shaped closer to their bodies.

### 3.3.3 Fewer errors during collaboration than during cooperation conditions

Since the contacts were undesired per task definition, every contact at any of the walls is considered as an error committed by the dyad. The medians for every condition suggested that the dyad committed less errors during collaboration than in cooperation (Fig. 3.10b). We verified that the different task conditions had a significant effect on the total error count for the dyad ( $\chi^2(2; 149) = 13.8, p = .001$ ). Furthermore, Tukey corrected post-hoc tests revealed a significant difference between the collaboration condition and cooperation conditions (when Agent 1 was the leader  $p = .02$ ; and when Agent 2 was the leader  $p = .002$ ), and without any difference between cooperation conditions ( $p = .67$ ).

In our setup, the seating positions and the grasping handling positions are not symmetric. Depending on the position, each agent has a different view of Tube 1 or Tube 2. This could introduce a bias for errors in one tube or the other depending on how close the tube is to the leader of the task, in the dyad experiment, or the solo Agent, in the solo experiment. First, we analyzed if the distance of any of the tubes to the leader in the dyad experiment would have an influence on the number of errors for each tube, and no significant effect was found,  $\chi^2(1, 199) = 2.0322, p = 0.154$  (Fig. 3.13). Second, we analyzed

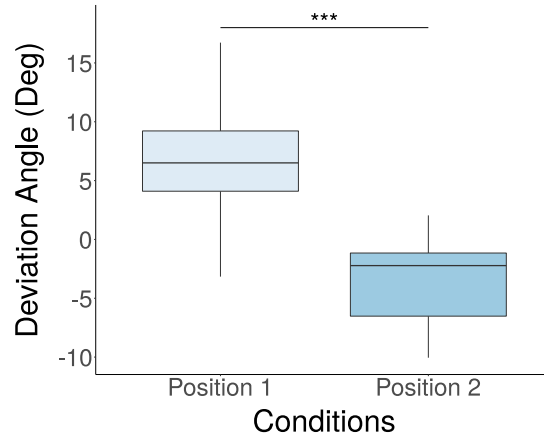


Figure 3.12: **Solo Manipulation Experiment:** Deviation angle  $\alpha$  per agent position. The agent in position 1 deviates the object trajectory position 1 ( $\bar{\alpha} > 0$ ), and agent 2 deviates its trajectory towards position 2 ( $\bar{\alpha} < 0$ ).

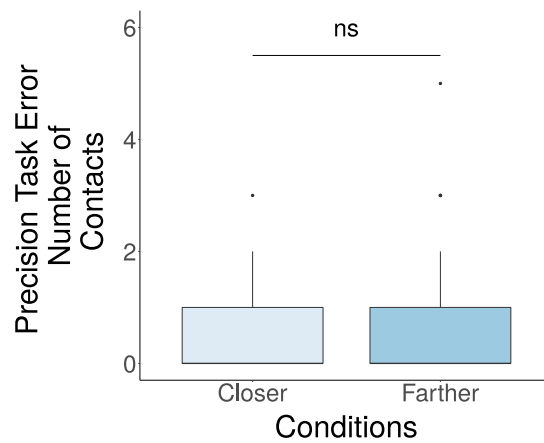


Figure 3.13: **Dyad Manipulation Experiment:** Number of touches in the wall, i.e. errors, per tube position w.r.t. the leader of the task. If the leader is on Position 1, Tube 2 is the closer tube, and vice-versa. No significant difference is found between conditions ( $p = 0.154$ ).

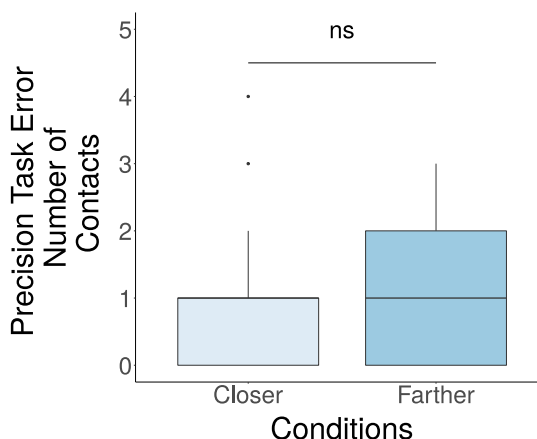


Figure 3.14: **Solo Manipulation Experiment:** Number of touches in the wall, i.e. errors, per tube position w.r.t. the agent. If the agent is on Position 1, Tube 2 is the closer tube, and vice-versa. No significant difference is found between conditions ( $p = .24$ ).

if the distance of any of the tubes to the agent in the solo experiment would have an influence on the number of errors for each tube, and once again, no significant effect was found  $\chi^2(1, 199) = 1.409$ ,  $p = .24$  (Fig. 3.14). Both results indicate that the better performance for the collaboration condition on the dyad experiment is not biased by our task setup.

### 3.4 Discussion

Our results in the cooperation condition agree with recent research on human dyadic interaction that suggests that when they are not competing, humans try to convey their intended trajectories for the object by modulating their stiffness in the space [109, 178], while also estimating the partner's goal [175, 177]. However, we did not expect that without pre-assigning leader/follower roles, in a collaboration, the stiffness levels of both agents would be similar to the leaders' stiffness levels. On one hand the agents could have been increasing their stiffness as a result to perceiving the other agent as a disturbance. On the other hand, this could mean that the agents established a bi-directional communication, eventually co-adapting to a trajectory that blends the intended trajectories of both agents.

Whenever there was a leader, the deviation angle,  $\alpha$ , indicated a trajectory closer to the leader as it was expected from the literature on obstacle avoidance for humans acting solo [150]. However, during collaboration, the angles indicated trajectories in-between the leadership trajectories for each agent. This suggests that, in their achieved pipe trajectory, the leaders dominated the outcome trajectory, meanwhile, when in collaboration, there was no clear dominance for neither agent. This lack of dominance throughout the entire task execution discards the possibility that during collaboration there could have been plasticity between leader/follower roles during the task execution [113].

There are already several indications that for individual motion planning the motion is a result of an underlining optimization process that could take into account several kinds of cost functions, such as speed or physical effort [44, 54, 63, 130, 188, 196]. So it is not surprising, that the agents would try to minimize the contacts with the walls, given it was one of the task objectives, and to do so, the agents need to be more precise, and therefore co-contract their muscles. On the other hand, it was surprising that the collaboration outcome significantly decreased the number of contacts in comparison to the cooperation conditions. Additionally, in collaboration, each one of the agents had RMS ICC levels on the same high-level as in the preassigned leader conditions, therefore, the overall arm stiffness and muscle effort were

also at a high level. So, why did the agents chose a strategy that spends more energy?

There is evidence that while interacting, humans may use the sensorimotor channel to coordinate joint actions [193] among two or more agents [177] even if it means increasing the agents' efforts. Some studies have reported that in an object co-manipulation, in a situation analogous to the collaboration defined here, the human dyad develops a shared sense of control (capability of an individual to influence the surrounding environment), in opposition to their own sense of agency [36]. Even more, there is already behavioural and neurological evidence that humans visually perceive dyadic interactions differently, and more so, that interacting individuals are seen as a dyad interaction unit rather than separate individuals [124, 140, 197, 198]. Hence, it is possible that during collaboration, the agents needed to shift into a "we-mode" [36], where they self-coordinated towards a collective target [177], and evaluated the dyad's performance over achieving their own desired trajectories.

Alternatively, Jagau and van Veelen [64] used game theory to model the behavior of cooperating agents showing that there is a variety of possible strategies that can emerge as a consequence of different combinations of intuition and deliberation, which in the literature are considered as the main drives to explain cooperation. Intuition is the automatic, fast, effortless and often emotional process; deliberation is the rational, controlled, slow and effortful process. Rand [143] explains that "decisions made under time pressure are more heavily influenced by intuition, whereas decisions made under time delay are more heavily influenced by deliberation". In time-constraint studies, where subjects are required to make their decisions quickly before a given amount of time elapses (which is the case of our study), intuitive behavior is preponderant. This suggests that the increase of co-contraction in the two agents of the dyad could be an intuitive behavioral response influenced by our explicit instructions telling subjects not to make errors and to be fast. Considering that the human motor control literature shows that humans co-contract the arms when moving under physical perturbations [14] it is possible that in the collaboration condition of our experiment the partners were co-contracting because they were considering the other partner as a disturbance rather than an agent whose behavior is predictable or could be predicted, which is the case of the cooperation condition where the agent knew about the role of the other partner and therefore could have a prediction of his/her behavior.

It is reasonable to argue that when in collaboration, both partners seemed to be actively trying to correct each other through its stiffness levels and intended trajectory. Collaboration in a shared haptic task may indeed naturally develop into a role beyond the usual leader/follower dichotomy for dyadic interactions [104, 113]: A collaborator role. This collaborator role would take into account individual environment information, requirements, and expertise from both agents encoded by their intended trajectories to form a more efficient trajectory according to a given *common criteria*, in here, the indication to not touch the tubes' walls. This role may even be the reason why several other studies have reported improvements when executing tasks as a human dyad against executing them alone [45, 70, 145].

In the last chapter, we mentioned the possibility of driving the human towards a more ergonomic trajectory using a physical human-robot interaction. In such scenario, at first glance, we could use a leader-follower coordination where the robot leader is fully aware of the human state, and has the complete autonomy of the task execution. However, as it was seen during the dyad co-manipulation experiment, even when both agents have the exact same goals, this type of coordination may not be optimal. This inefficiency could be even more accentuated, and potentially dangerous to the human agent if the autonomy of the task is never shared, that is, if the human can never correct the robot's actions. Therefore, a scenario, in which both agents have a shared autonomy of the task and possibly arbitrate over the best course of action should be preferred over the leader-follower paradigm. In the dyad co-manipulation experiment we verified strong indications that the haptic channel, notably through the modulation of stiffness, is used by the human agents to arbitrate their joint actions. In the next chapter we propose control laws to modulate the robot's stiffness during a physical human-robot interaction where the robot is aware of the human stiffness modulation.

### **Data Availability**

The raw data for EMG signal, motion measurements, and number of wall touches is freely available in Zenodo at the DOI: 10.5281/zenodo.3989616 [183].

### **Code Availability**

The custom code used to obtain the MVC values for the EMG signals can be found on <http://github.com/inria-larsen/emg-processing>.



# Human-Robot Co-Manipulation

This chapter presents an object co-manipulation study where the dyad is now composed of a human and a robot. To emulate the human collaboration motor behavior, different variable impedance control profiles are presented and tested on a pilot experiment. We report on preliminary results of a pilot study that investigates the dyad's efficiency under different cooperation and collaboration conditions. It was possible to verify a trend suggesting that the robot collaboration profiles are more efficient than the robot cooperation ones, especially when the robot is a follower.

## 4.1 Introduction

Human-robot interaction could be used to improve the efficiency of work activities, or to reduce physical and cognitive workload of the human co-worker [4, 24, 133]. The human-robot co-activity may leverage the robot superior task precision or movement repeatability alongside the human cognitive skills and more knowledgeable situation awareness. Each agent is usually given a clear division of responsibilities, or roles, that is, they have autonomy over different aspects of the task. However, recent advancements in sensing, inference, modeling and learning methods, have been gradually refocusing this design paradigm from this clear division, to a scenario in which the human and the robot share the autonomy of a task. In this scenario both the human and the robot share the autonomy or the leadership of a task according to specific criteria, such as the robot's awareness of the environment or the human partner. In a recent

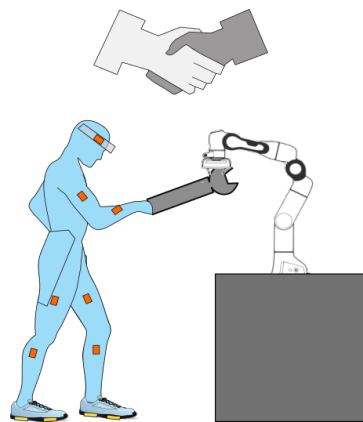


Figure 4.1: Human-Robot physical interaction study. Two human-aware robot control profiles are proposed for dyadic collaboration.

survey, Selvaggio *et al.* [163] defined the spectrum of applications in which the roles are fixed as a Shared Control (SC) approach, whereas applications in which the roles are not preassigned are defined to be within a Shared Autonomy (SA) approach. As a matter of fact, these SC or SA approaches are also well within the definition of a dyadic cooperation or collaboration [66]. A controller for a human-robot collaboration shares the autonomy of the task (SA), while a controller for human-robot cooperation consider fixed roles within the dyad (SC).

The leader-follower SC approach in which the human is always the leader of the task is likely the most traditional coordination strategy in physical Human-Robot Interaction (pHRI) [92]. In this case in particular, the robot may be controlled to guarantee only certain aspects of the task execution, such as rejecting disturbances, or sustaining forces and positions in different axes from the ones controlled by the human [199]. Ficuciello *et al.* [42] uses a more sophisticated strategy that explores the null-space of a redundant robot in order to decouple the apparent inertia at the robot end-effector, reportedly improving the intuitiveness of the task for the leader. Even though the SC approach meets great success in some applications such as robotic surgery [122, 142], and telemanipulation, there are instances in which SA could be preferred [67].

Cherubini *et al.* [24] alternates the leader and follower roles of a robot in a pHRI application for industry according to visual and haptic cues by the human co-worker. Khoramshahi and Billard [73] propose a method to automatically detect when the human co-worker is physically trying to guide a robot that is executing an autonomous task. After the intent detection, the robot switches into a follower mode, and only goes back to leader mode when the human stops correcting the robot. Agravante *et al.* [3] interpolate between a humanoid robot's behavior from a total leader to a total follower (each behavior corresponds to a different walking pattern generator to the humanoid robot). During the leader behavior the robot controller minimizes the errors for the desired trajectory (high-impedance), whereas for the follower behavior it minimizes the forces applied at the human operator (low-impedance).

In the following section, we present an impedance controller that can be used either in a leader-follower SC approach, or in a SA approach that is arbitrated by the human. Inspired by the results of the previous chapter, we decided to arbitrate the autonomy of the task according to the human arm muscle co-contraction under two different variable impedance profiles. Then, the object co-manipulation experiment from chapter 3 is modified to consider a human and a robot agent; the goal is to investigate whether or not the variable impedance profiles are able to emulate the motor behavior observed during the collaboration condition in the human-human experiment.

## 4.2 Impedance Control and Role Definition

A robot manipulator with  $n$  DoF ( $\mathbf{q} \in \mathbb{R}^n$ ) is chosen to execute the accurate task from Chapter 3. In the human-human experiment, the human agents modulated their arm co-contraction (known to be directly proportional to the arm stiffness) according to leadership roles they were assigned. Similarly, here, the robot's role in the co-manipulation is defined by its desired end-effector Cartesian stiffness. A desired robot high stiffness defines the robot as a leader while a low stiffness defines the robot as a follower. These behaviors can be achieved by changing the robot's impedance. For instance, let the robot's equation of motion (EoM) [112] be:

$$\mathbf{M}(\mathbf{q})\ddot{\mathbf{q}} + \mathbf{C}(\mathbf{q}, \dot{\mathbf{q}})\dot{\mathbf{q}} + \mathbf{g}(\mathbf{q}) = \boldsymbol{\tau}_c - \mathbf{J}^\top \mathbf{F}_{ext} \quad (4.1)$$

where  $\mathbf{M} \in \mathbb{R}^{n \times n}$  is the robot's inertia matrix;  $\mathbf{C} \in \mathbb{R}^{n \times n}$  is the Coriolis matrix;  $\mathbf{g}(\mathbf{q}) \in \mathbb{R}^n$  is the vector representing the gravitational torques at each robot's joint;  $\mathbf{J} \in \mathbb{R}^{6 \times n}$  is the robot Jacobian;  $\boldsymbol{\tau}_c \in \mathbb{R}^n$  is a control vector; and  $\mathbf{F}_{ext} \in \mathbb{R}^6$  is the interaction wrench at the end-effector. Using feedback linearization,

$\tau_c$  can be set to achieve a desired mechanical impedance at the robot's end-effector:

$$\mathbf{F}_{ext} = \mathbf{K}(\mathbf{e}_d) + \mathbf{D}(\dot{\mathbf{e}}_d) \quad (4.2)$$

$$\mathbf{e}_d = \mathbf{x}_{ee} - \mathbf{x}_d \quad (4.3)$$

where  $\mathbf{K} \in \mathbb{R}^{6 \times 6}$  is the desired Cartesian stiffness;  $\mathbf{D} \in \mathbb{R}^{6 \times 6}$  is the desired Cartesian damping; and  $\mathbf{x}_{ee}, \mathbf{x}_d$  are respectively the actual and desired end-effector Cartesian poses.

The desired Cartesian damping  $\mathbf{D}$  is proportional to  $\mathbf{K}$  and to  $\mathbf{M}$  using *factorisation design* as in [5].

### Human-aware Variable Impedance Control

In the object co-manipulation of Chapter 3, the dyads were the most effective at executing the task during the collaboration condition. Therefore, it is possible that a simple follower/leader paradigm is also not the optimal role configuration for human-robot co-manipulation. One of the major results from the human-human experiment was that during the collaboration condition both human partners exhibited high levels of co-contraction for the entire task execution. In addition, their arm co-contraction was significantly higher than in the followership conditions, but not significantly different from the leadership conditions.

To try to emulate the collaboration condition in the human-human dyad, we propose to test two variable impedance control (VIC) profiles that respond not only to the task trajectory execution but also to the human arm co-contraction modulation [131]. For this study, we measure the co-contraction w.r.t. a pair of antagonist muscles at the right forearm. To integrate the co-contraction modulation from a pair of antagonist arm muscles into the controller, the  $icc(t)$  signal from Eq. (3.2) needs to be mapped into desired Cartesian stiffness for the robot.

First, a sigmoid function inspired on the work of Peternel *et al.* [131] is used to map the joint stiffness trend,  $c_h \in \mathbb{R}$ , and the index of co-contraction related to that joint,  $icc(t)$ :

$$c_h(t) = b_1 \frac{1 - e^{-b_2 icc(t)}}{1 + e^{-b_2 icc(t)}} \in [0, 1] \quad (4.4)$$

where  $b_1, b_2 \in \mathbb{R}$  define the amplitude and shape of  $c_h$ , and are determined experimentally to reflect the actual operational range of the  $icc$  of a given participant during the task execution. During the measure of a MVC, the respective EMG muscle signal is likely to be much higher than the ones necessary during a task execution, therefore, the actual values of  $icc(t)$  should be well below 1. As a consequence, the experimental scaling is necessary to effectively modulate the robot behavior from one role to the other.

The first VIC profile implements a **reciprocal** behavior regarding the ICC modulation:

$$\text{Reciprocal: } \mathbf{K}(t) = \mathbf{K}_{cte} + \mathbf{S} \left( (1 - c_h(t)) (\mathbf{K}_{\max} - \mathbf{K}_{\min}) + \mathbf{K}_{\min} \right) \quad (4.5)$$

where  $\mathbf{S}$  is a selection matrix that defines the axis where the Cartesian stiffness is modulated by  $icc(t)$ ;  $\mathbf{K}_{\max}, \mathbf{K}_{\min}$  are the maximum and minimum desired Cartesian stiffness for those axes; and  $\mathbf{K}_{cte}$  is a matrix that contains the constant stiffness for the axis that are not modulated by  $icc(t)$ . In this case, the robot behaves as a leader if the human is compliant. However, if the human decides to co-contrast, which s/he is likely to do in order to decrease disturbances, or to be more accurate during a task execution, then the robot will effectively cede the autonomy of the task to the human.

The second VIC profile implements a **mirrored behavior** regarding the ICC modulation:

$$\text{Mirror: } \mathbf{K}(t) = \mathbf{K}_{cte} + \mathbf{S} \left( c_h(t) (\mathbf{K}_{\max} - \mathbf{K}_{\min}) + \mathbf{K}_{\min} \right) \quad (4.6)$$

In this case, the more the human co-contracts her/his arm, the higher the robot stiffness will be. Here, the robot and the human are always equally sharing the task autonomy, which could be analogous to the

Table 4.1: Robot’s role definition according to the scaled index of co-contraction,  $c_h$ , and the robot’s reference trajectory.

Robot’s role	Stiffness Profile	$K_{\min}$ ( $N.m^{-1}$ )	$K_{\max}$ ( $N.m^{-1}$ )	Reference Trajectory
Follower	$K = K_{\min}$	500	-	No
Leader	$K = K_{\max}$	-	1000	Yes
Reciprocal	$K(t) \propto (1 - c_h)$	100	1000	Yes
Mirrored	$K(t) \propto c_h$	100	1000	Yes

similar ICC level in the human-human dyad experiment. All robot stiffness profiles are summarized in Tab. 4.1.

Note that during the follower condition, the robot stiffness has a higher stiffness value than its minimum stiffness during the collaboration condition. Prior to the data collection, we found that the middle-valued stiffness was beneficial to executing the task while it was not detrimental to the robot follower behavior. When the robot is assigned a complete follower behavior, the impedance controller does not have a reference trajectory, therefore, the impedance is applied to the current end-effector position,  $x_{ee}$ , and the stiffness effectively acts as a damper to the end-effector motion. For this reason, the follower condition can have a higher stiffness value than the minimum stiffness for the reciprocal and mirrored profiles without being detrimental to the robot follower behavior.

## 4.3 Human-Robot Experiment

### 4.3.1 Participants

The experiment consists of a human-robot object co-manipulation task that was executed by 5 human participants alongside a Franka Emika Panda robot. 2 of the human participants were female, and 3 were male. Their age ranged from 23 to 27 years old ( $M = 25.4$  years,  $SD = 1.5$  years). All participants were right-handed. No participant claimed any chronic motor disease or health condition that could influence in the experiment’s results. None of the participants were involved in the human-human experiment of the previous chapter. The experiments were approved by INRIA’s ethical committee (COERLE).

### 4.3.2 Task Description

The task goals and description are identical to the task described in Chapter 3. It consists in manipulating an object (pipe) to bring it from a start to an end point (Fig. 4.2a). The experiment starts with the pipe within a tube (Tube 1). First the pipe is taken out of Tube 1, and contact with the front wall of Tube 1 should be avoided. Then, the pipe is moved around an obstacle to the entrance of a second tube (Tube 2). Finally the pipe is inserted inside Tube 2, and contact with the front wall of Tube 2 should be avoided. The motion is always performed from Tube 1 to Tube 2. The return motion is not recorded nor evaluated.

While in free space (after exiting Tube 1 and before entering Tube 2), there is no physical restriction on the tube motion. However, the human is told to move around the obstacle, and not above. In both experiments, the participants were instructed to avoid moving their back during the task execution, however, they were not strapped to the chair. In addition, they were not allowed to support their right or left arm on the setup’s table, which would make the task easier to execute. They hold the pipe on Handle 2 with their right hand with a power grasp.

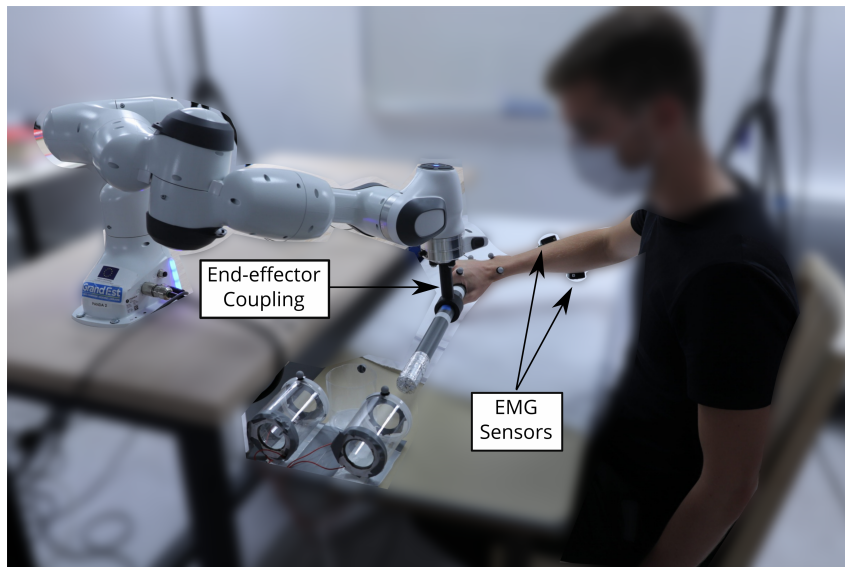
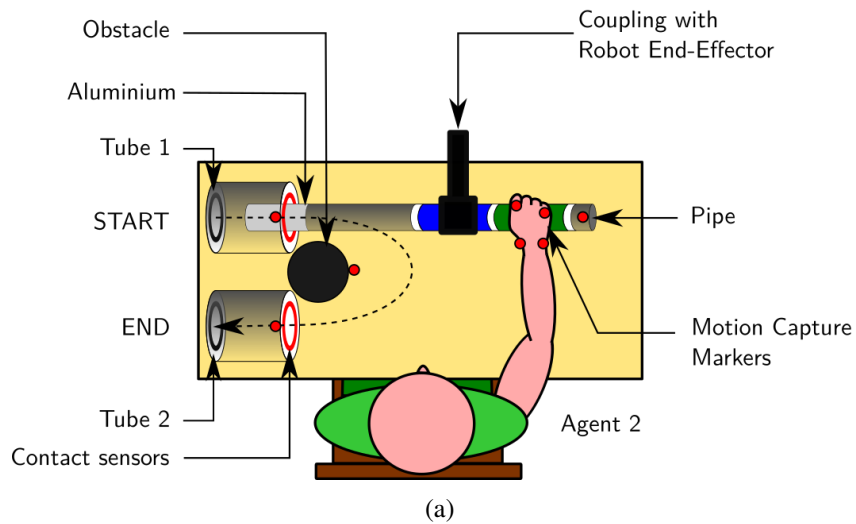


Figure 4.2: Human-robot object co-manipulation setup. In this setup, a Franka Emika Panda robot manipulator is coupled with the manipulated pipe through a 3D-printed part. The robot is made aware of the human behavior not only from the pipe displacement, but also from the EMG sensors signal. In this setup, the human is always in position 2 (corresponding to Agent 2).

### 4.3.3 Duration

During the task execution, the human agent does not see a timer, but s/he is told that the whole manipulation (from Start to End) should not last longer than 30 s. If the task execution takes significantly longer than 30 s then the trial is canceled. The humans are also informed that a trial starts when the human listens to a *beep* sound signaling him/her that either the robot will start moving, or s/he should start moving.

### 4.3.4 Apparatus

The manipulated object and the setup is similar to the one described in Chapter 3 (Fig. 3.4), with the important addition of a robot agent, and its physical coupling to the pipe (Fig. 4.2). The coupling is a 3D-printed part that was custom designed to couple the robot end-effector with the pipe manipulated by the human.

The Franka Emika Panda Robot has 7 torque-actuated revolute joints ( $q \in \mathbb{R}^7$ ), weighting 18 kg, and a payload at the end-effector of 3 kg. The robot is controlled through the manufacturer's C++ interface, Franka Control Interface (FCI) [46]. The FCI runs at 1 kHz, and allows the user to control the robot's joint positions and velocities through the manufacturer's trajectory generator and controller, or through torque control where the user is the sole responsible for providing the desired torque vector  $\tau_d$ . Conveniently, the FCI outputs important numerical values to implement the impedance control in Eq. (4.2): its estimated inertia matrix  $\bar{M}(q)$ , Coriolis matrix  $\bar{C}(q, \dot{q})$ , gravity vector  $\bar{g}(q)$ , and Jacobian  $\bar{J}$ .

### 4.3.5 Experiment Description

Both human and robot agents shared their autonomy over the object depending on their role coordination. The robot is coupled to the pipe on Handle 1, that corresponds to Agent 1 in the human-human experiment. Meanwhile, the human agent grasps the pipe on handle 2, that corresponds to Agent 2 in the human-human experiment (Fig. 4.2a).

The participants performed the task under 4 different conditions, where the robot behavior is dictated by the stiffness profiles in Tab. 4.1:

- *Condition 1 (Robot Follower and Human Leader)*: Participants were instructed that they must lead the movement, while the robot is completely compliant to the human motion;
- *Condition 2 (Robot Leader and Human Follower)*: Participants were instructed that the robot would lead the movement, while they are completely compliant to robot's motion.
- *Condition 3 (Robot Reciprocal Stiffness)*: Robot starts as a leader with high end-effector stiffness, but its stiffness modulation is proportionally inverse to the human index of co-contraction modulation (Eq. (4.5)). Participants are not explicitly made aware of the robot's policy.
- *Condition 4 (Robot Mirrored Stiffness)*: Robot mirrors its end-effector stiffness modulation w.r.t. to the human index of co-contraction (Eq. (4.6)). Participants are not explicitly made aware of the robot's policy.

The order of conditions 1 and 2, with fixed desired impedance, is random in between them, but they are always the first 2 conditions to be executed. They are used to estimate the scaling parameters,  $b_1, b_2$ , for the variable impedance controllers during conditions 3 and 4. The order of the last 2 conditions is also randomized between them.

For each condition, 5 trials were recorded, resulting in a total of 20 trials per participant. Since there were 5 recorded dyads, a total of 100 trials were recorded. There was an approximate 60 s break between each trial to allow the participants to rest their muscles, but the exact duration of the break was not forced.

### 4.3.6 Data Collection

#### Motion capture

The motion of the participants' right arm was recorded with a Qualisys optical motion capture system (at a rate of 150 Hz). Four reflective markers were placed on the participant's hand (Fig. 4.2a) to track their 3D Cartesian positions:

- 1 marker on the Ulnar-Styloid Process
- 1 marker on the Head of the 5th Metacarpal
- 1 marker on the Head of the 2nd Metacarpal
- 1 marker on the Radial-Styloid Process

In addition, 4 markers were placed on the pipe, tubes and obstacle (Fig. 4.2a):

- 1 marker at the tip of the pipe which does not go inside the tubes (opposite to where the aluminum foil is). Participants were told to hold the pipe so that this marker was facing up;
- 2 markers on the tubes. 1 at the top of the front wall of each tube;
- 1 marker at the top of the obstacle wall, farthest away from both tubes;

#### Electromyography

Two wireless Delsys Trigno EMG sensors were placed on each participant's right arm, on the following antagonist muscles:

- Flexor Carpi Ulnaris;
- Extensor Carpi Ulnaris;

The EMG signal was captured at 2 kHz, and filtered as in Fig. 3.7. For each participant, the maximum voluntary contraction (MVC) of each muscle was recorded prior to the experiment during an isometric exercise according to SENIAM recommendations [171]. Only the EMG signal was recorded during the MVC; the actual force produced was not recorded. The value of the EMG signal during the MVC was used to obtain an index of co-contraction like in Eq. (3.2). The  $icc(t)$  signal was streamed to the robot at the same frequency of the robot's control loop, 1 kHz. As it was the case for the human-human dyad experiment, due to muscle synergy [60], the  $icc(t)$  for both muscles should reflect the arm stiffness modulation for the entire arm.

#### Contact Sensor

The contact sensor was the same used in the human-human experiment from Chapter 3, and so it was its data collection.

#### Franka Emika Panda Robot

Using the FCI, the following measurements were recorded from the robot: end-effector position,  $\mathbf{x}_{ee}$ , joint positions and velocities,  $\mathbf{q}$ ,  $\dot{\mathbf{q}}$ , and the effect of  $\mathbf{F}_{ext}$  at the robot's joints,  $\boldsymbol{\tau}_{ext} = \mathbf{J}^\top \mathbf{F}_{ext}$ . Additionally, the calculated stiffness from Eq. (4.5) or Eq. (4.6) is also stored at each timestep.

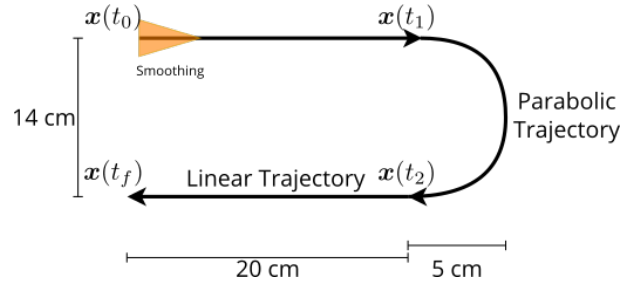


Figure 4.3: Trajectory designed for the robot to execute the task in the human-robot coordination experiment.

### 4.3.7 Desired Robot Trajectory and Stiffness

The robot follower role is the only role that does not require a reference trajectory (Tab. 4.1). For all other roles, we designed a reference trajectory,  $x_d$  for the robot (Fig. 4.3). The robot desired orientation  $x_d^o$  and vertical position remain fixed for the entire task execution, while the X-Y planar trajectory is defined by straight lines and a parabolic curve:

$$x_d^p(t) = \begin{cases} [x(t_0) + (t - t_0)v_0, y(t_0), z(t_0)]^\top & \text{if } t_0 < t \leq t_1, \\ [a_1((t - t_1)v_1)^2 + a_2(t - t_1)v_1 + x(t_1), y(t_0) - (t - t_1)v_1, z(t_0)]^\top & \text{if } t_1 < t \leq t_2, \\ [x(t_2) - (t - t_2)v_2, y(t_2), z(t_0)]^\top & \text{if } t_2 < t \leq t_f \end{cases} \quad (4.7)$$

where  $v_0, v_1, v_2, a_1, a_2 \in \mathbb{R}$  define the speed and shape of the trajectory (Fig. 4.3). The trajectory is designed to be executed in 25 s.

According to our experiment protocol, the participant manually inserts the tube at its initial position. The placement is never exact w.r.t. the initial position defined by Eq. (4.7), then, because of this, the impedance control could generate excessive rapid motions in the beginning of the task execution. Since the pipe is within tube 1 at this stage, motions could be detrimental to the integrity of the tubes. To mitigate this issue, we smoothed the initial error trajectory  $e_d$  during the first  $T_S = 2.5$  seconds of the trajectory:

$$e_d(t) = \begin{cases} \left(\frac{t-T_S}{T_S}\right) e_d(t) & \text{if } t \leq T_S, \\ e_d(t) & \text{if } t > T_S \end{cases} \quad (4.8)$$

Follower and leader roles represent small and high desired Cartesian stiffness for the robot (Tab. 4.1). This effectively modulates the robot role between a leader or follower behavior depending on  $c_h(t)$ .

### 4.3.8 Statistical Analysis

Both the index of co-contraction,  $icc(t)$ , and the norm of the interaction torques of the robot,  $\|\tau_{ext}\|(t)$ , are timeseries. A single RMS value is computed for each task execution to evaluate how they are affected by the experiment conditions. Similarly to the human-human experiment, their RMS value is computed taking in consideration only phases 1 and 3 of the task, that is, when the pipe is inside the tubes. Additionally, for the statistical analysis both the ICC and the  $\tau_{ext}$  data were not Gaussian (Shapiro-wilk normality tests with  $p < 0.001$ , and  $p < 0.001$  respectively), then the median for each condition is calculated prior to the usage of Friedman tests.

The deviation angle data,  $\alpha$ , was once again normally distributed (Shapiro-wilk normality test with  $p = 0.301$ ). An analysis of variance with repeated measures is done to verify the effects of the conditions on the deviation angle.

The count data from the contact sensors was overdispersed (variances larger than means), therefore, a negative binomial distribution in a general linear mixed model with random effects [19] is once again used for the statistical analysis. Additionally, post-hoc tests with Tukey correction are used to further evaluate the conditions.

## 4.4 Results

Similarly to the dyad experiment in Chapter 3, we verified the effect of all conditions on the arm ICC (stiffness modulation), number of contacts between the pipe and the tubes (task accuracy), and trajectory deviation. Additionally, given the robot F/T sensors, the  $\|\tau_{ext}\|$  was also calculated and posteriorly analyzed.

Friedman tests indicated no statistically significant difference between the ICC RMS values across all conditions,  $\chi^2(3) = 7.32$ ,  $p = 0.06$ . Although we cannot draw precise conclusions from these preliminary results (5 participants only), the ICC RMS across all conditions (Fig. 4.5) suggests that the human agents co-contracted her/his arm muscles much less during the robot collaboration conditions than in the robot follower condition (where the human was the leader). In addition, the co-contraction during robot collaboration seems to have assumed low values as a default behavior, only increasing when the human agent deemed necessary and with much less intensity than in the case where the human agent was the leader (Fig. 4.4). These results suggest that **robot collaboration may demand less muscle co-contraction from the human partner**.

As for the interaction torque vector, Friedman tests indicated statistically significant difference between the RMS values of  $\|\tau_{ext}\|$  across the conditions  $\chi^2(3) = 8.28$ ,  $p = 0.04$ . Even though corrected post-hoc tests do not indicate significant differences between the conditions, descriptive statistics indicates a higher external torque application on the robot collaboration condition (Fig. 4.6, Fig. 4.7), which **could suggest that interaction torques/forces with the robot are greater during robot collaboration**.

The trajectory deviation angle,  $\alpha$  (Eq. (3.6)), that quantifies how much the agent, human or robot deviates the trajectory towards the self, is used to quantify if the trajectories (Fig. 4.8) in the experiment were similar. An analysis of variance with repeated measures was applied to  $\alpha$  for all coordination conditions. Differently from the previous experiment, no condition significantly affected  $\alpha$  ( $F(3, 12) = 1.27$ ,  $p = 0.33$ ,  $\eta = 0.19$ ) (Fig. 4.9). On the other hand, the resulting planar trajectories (Attachment C) are not similar for all conditions.

Regarding the number of contacts between the pipe and the tube, the medians for every condition, the statistical analysis indicates a significant effect on the error count by the robot conditions,  $\chi^2(3) = 14.017$ ,  $p = 0.003$ . In addition, Tukey corrected post-hoc tests indicate differences between some robot collaboration conditions and the cooperation conditions. Between the robot follower and reciprocal condition there is a significant effect ( $p = 0.005$ ), on the other hand, between the robot follower and mirrored condition ( $p = 0.061$ ) as well as for between robot leader and reciprocal conditions ( $p = 0.107$ ) the calculated  $p$ -values are above the usual threshold of  $p = 0.05$ . However, by inspecting the median and IQR values for the conditions Fig. 4.10, it is still possible to infer a trend towards the conclusion that **there were less contacts (task errors) during the robot collaboration conditions than during the robot cooperation conditions**.

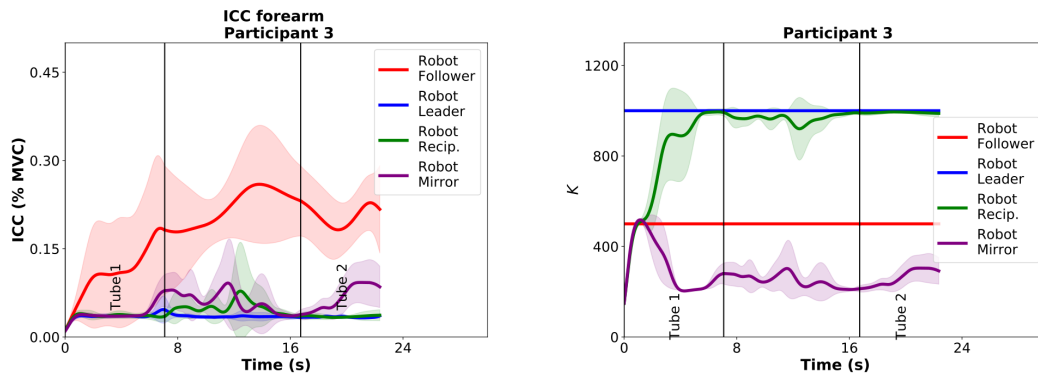


Figure 4.4: Example of index of co-contraction, and robot stiffness modulation during human-robot co-manipulation for a given participant for different robot behaviors. Human seems to co-contract the arm in much more intensity when s/he is the leader than in other conditions.

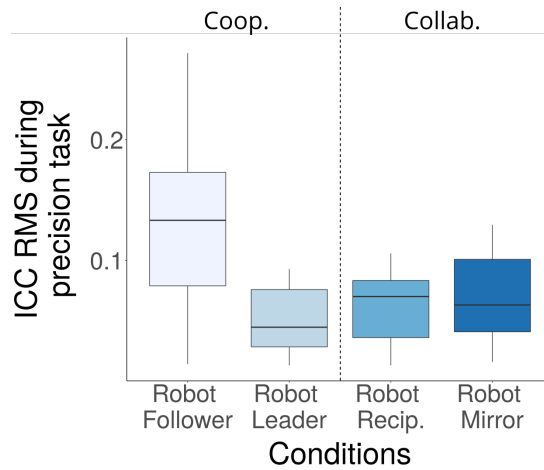


Figure 4.5: Boxplot of the RMS values of the index of co-contraction for each trial during the human-robot co-manipulation. The robot collaboration conditions had an overall co-contraction similar to the condition in which the robot is the leader (and by consequence the human is a follower).

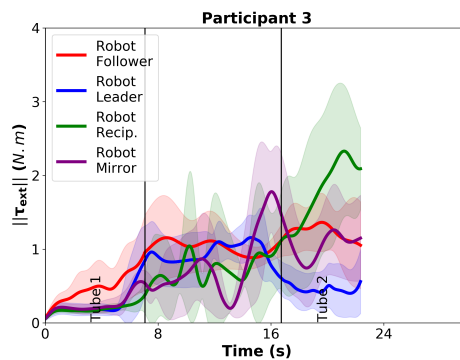


Figure 4.6: Example of the modulation on the perceived external torque during human-robot co-manipulation.

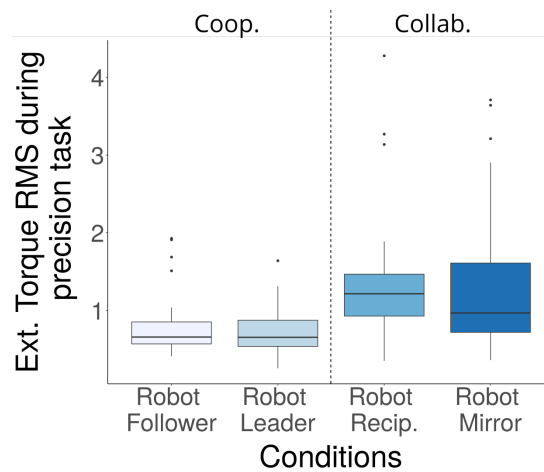


Figure 4.7: RMS values of  $\tau_{ext}$  during human-robot co-manipulation. The robot F/T sensor perceived higher external torques during the robot collaboration conditions.

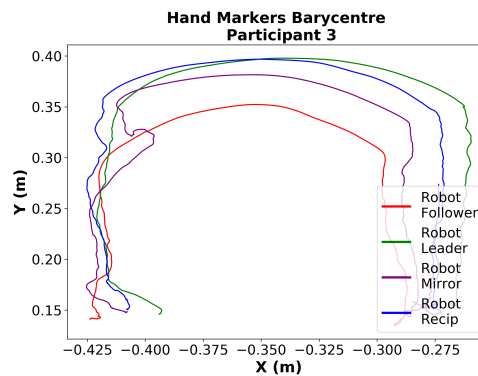


Figure 4.8: Example of Planar Trajectory for a Subject's Hand during the Human-Robot Object Co-Manipulation.

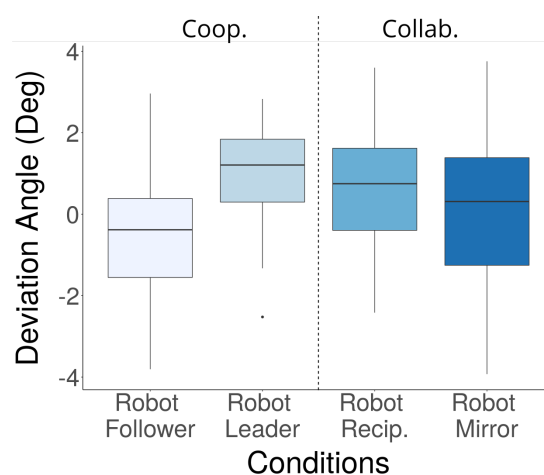


Figure 4.9: Deviation Angle during Human-Robot Co-manipulation. No significant difference was observed among the conditions. Furthermore even when the robot was a follower and the human a leader, the deviation angle was still very close to 0.

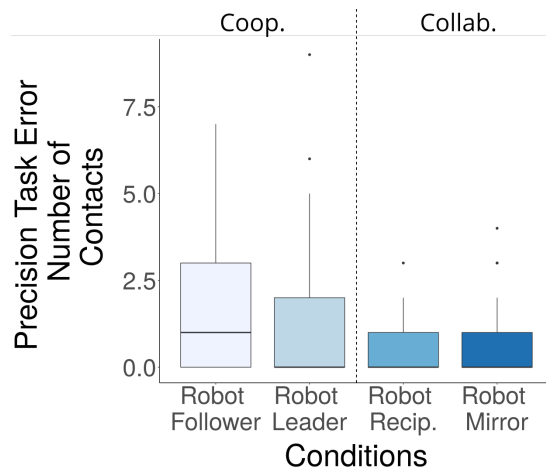


Figure 4.10: Precision Task Error During Human-Robot Co-manipulation. During both robot collaboration conditions, the human was more precise at executing the task.

## 4.5 Discussion

We proposed two variable impedance profiles for robot collaboration (robot shares the task autonomy with human) based on the muscle co-contraction of the human co-worker: a reciprocal and a mirrored profile. In a pilot experiment, with 5 subjects, as it was done in the human-human experiment, leader-follower cooperation was compared with human-robot collaboration, and it was already possible to verify a few important trends that may be significant if more subjects are taken into consideration.

When analyzing the muscle co-contraction, it seems clear that when the human is the leader of the task, s/he will have a higher level of muscle co-contraction than when the human is simply following the robot trajectory. In contrast with the high level of co-contraction during human-human collaboration, during both human-robot collaboration conditions the humans seemed to have just slightly increased their muscle co-contraction. Despite not having the same outcome with regards to the muscle co-contraction, the human-robot collaboration seemed to have been even better than the condition in which the robot is the leader, and similarly effective in comparison to the human-human collaboration, with less errors, or contacts between the pipe and the tube wall. The robot perceived more external torques during the collaboration conditions, this was due to the higher torque peaks present in the collaboration conditions. Those peaks were even more prominent when the pipe was inside the tubes, likely because the human perceived the necessity to correct the robot trajectory in order not to touch the tube walls.

In a human-robot experiment, Gombolay *et al.* [48] affirms that users were willing to cede the decision making to the robot if it resulted in a greater team fluency, however, in a later study they verified that this sort of behavior could be detrimental to the human environmental awareness [47]. Similarly, other works in SC/SA have also reported that exchanging forces with the robot increased awareness of the robot status [94, 162, 163]. Since in the cooperation condition the human was aware that s/he was only following the robot, it is possible that the human agents have indeed decreased their attention to the execution of the precision task at hand. During our experiment, whenever the robot had a reference trajectory, (robot as a leader, and both collaboration conditions) the human agent could have been inclined to cede the decision making to the robot, as in those conditions the human-robot dyad was more effective than when the human was the sole leader of the task execution. Moreover, during the robot collaboration condition, because the human still shares the autonomy of the task with the robot, on top of potential benefits from taking the leadership (reciprocal profile) or increasing the overall stiffness (mirrored profile), the human may have just been more aware of the task execution, yet, this is a hypothesis that needs

further experiments to be validated.

For this human-robot experiment, the deviation angle,  $\alpha$ , does not seem to be sufficient to analyze the trajectory differences between the conditions (attachment C, and Fig. 4.9) and further analysis should be pursued in the near future.

The variable impedance control profiles proposed here were inspired on recent works from the literature both in SC/SA [50, 131] and in motor behavior studies [14, 176, 178], however, more sophisticated approaches for modulating the impedance could be taken. For instance, Li *et al.* [88] uses differential game theory to continuously move the robot from a follower to a leader state. Moreover, there are also other SA approaches where the robot not only changes its stiffness, but also its reference trajectories. For instance, in many studies, the robot first tries to predict the human behavior, and then changes its behavior including its reference trajectories, or goals according to human motion or intent [68, 92, 144]. One possible research direction would be to integrate the index of co-contraction signal into those aforementioned approaches. In addition, even with only 5 subjects the results from this pilot experiment are already promising, in such a way that we expect to conduct in the near future a more comprehensive version of this experiment with a larger and more diverse sample of the population prior to testing new variable impedance control profiles or other control laws.



## 5

# Conclusions

In this closing chapter, we elaborate on the main discussions presented throughout the thesis. Posteriorly, the body of work is put into perspective with possible future research on the topics of ergonomics and human-robot interaction.

### 5.1 Discussion

The work in this thesis stems from a multi-disciplinary approach that results in a set of tools for improving whole-body motion ergonomics. **The human motor behavior is evaluated from a robotics perspective, but not exclusively, concepts from both ergonomics and biomechanics fields are also key to our approach.** This human-centered approach is justified to propose methods in which a robot can collaborate with a human partner in an ergonomic fashion while being able to physically interact effectively with him/her.

The first two chapters of this thesis deal with the problem of analyzing the whole-body motion of a human during a specific work activity according to a given set of ergonomics scores. The whole-body motion is parameterized, replayed, evaluated and finally optimized for ergonomics. This ergonomic motion, or set of ergonomic motions may be leveraged in different ways; in this work, a human-robot interaction is proposed. However, before driving the human towards known optimal ergonomic trajectories, a robot controller has to be able to coordinate its actions with the human partner in a task-effective and engaging manner. The last two chapters follow on this human-centric path by investigating the human motor behavior during an object co-manipulation task. The human motor behavior is analyzed both in a human-human dyad, and in a human-robot dyad where the robot tries to emulate the human behavior from the human-human dyad.

**Digital Human Model Simulation and Optimization:** in chapter 1, we took inspiration on recent works on the simulation of DHMs [98, 156]. We proposed a DHM of our own whose whole-body control is defined by a velocity-based QP controller. Simulating the DHM in a lightweight physics engine makes it possible to quickly and simultaneously evaluate several whole-body motion trajectories according to ergonomics scores that evaluate not only the motion kinematics but also its dynamics. The whole-body motion optimization is feasible as long as an adequate initial parameterization of the motion is obtained, both in the number of parameters and in the quality of the motion reproduction. The whole-body motion parameterization and optimization is done in chapter 2.

Our DHM mimics the anatomical frames of the human body, and therefore, contains 43 revolute joints. If the whole-body motion parameterization is taken for this high number of revolute joints, then a very high number of parameters is to be expected. To avoid this problem, the QP formulation is used to

our benefit here. The QP controller can essentially track multiple Cartesian positions while respecting all of the DHM joint constraints. Therefore, instead of parameterizing all joint trajectories directly, a handful of Cartesian trajectories are sufficient to represent the whole-body motion. The parameterization itself is realized using Probabilistic Movement Primitives, ProMPs [125], which are particularly interesting for the parameterization of human movements as they encode both the human motions, and its variance as they are trained from different trajectory demonstrations with different time-lengths. As a matter of fact, a ProMP can be compactly represented by a single weight vector, and this one vector can be used to generate the encoded mean trajectory. The whole-body trajectory is then represented by a stack of individual ProMPs. This whole-body representation using a stack of Cartesian ProMP weights while leveraging the QP controller properties to maintain the joint-level constraints is part of the contributions of this thesis, as it allows for a very compact, yet, easy to grasp, representation of the whole-body motion. Having proposed a solution to the whole-body parameterization problem, we turn back to the optimization of human whole-body motions w.r.t. ergonomics scores.

**Personalized and Multi-objective Ergonomics Motion Optimization:** the human body is capable of executing motions in many different ways due to the body's high number of DoF and efficient musculoskeletal system. Furthermore, the human population has a very large variety of body morphologies with even more diverse power capabilities. Therefore, if two people with very different body morphologies attempt to execute an identical set of Cartesian trajectories, then an ergonomics evaluation, as the ones from chapter 1, could yield widely different results. Furthermore, each person can also have special constraints, such as a limitation on flexibility, or a handicap for instance. These individual factors, or special constraints are not taken into account by classic ergonomics scores. In a nutshell, a motion that is ergonomic for an individual may be different to another, and many individual requirements may be hard to grasp with classic ergonomics evaluations. Even though some strategies or patterns could be devised, we show in chapter 2 that optimal ergonomic motions are individual.

In addition to the uniqueness of each body morphology, optimizing a whole-body trajectory w.r.t. ergonomics scores needs to be handled carefully. Work-related musculoskeletal disorders, WMSDs, are multi-factorial and may be developed at different body segments. For this reason, there are many possible ways to quantify the risk of developing any WMSD<sup>8</sup>, and this still may happen in different parts of the human body. Therefore, if the goal of the trajectory optimization is to decrease the overall risk of developing any WMSD, then optimizing for a single ergonomics score may not be sufficient nor optimal in an ergonomics sense. Our simulation results with single-objective trajectory optimization make it clear that optimizing for a single ergonomics score is not sufficient to obtain an overall ergonomics motion from the optimization. To solve this issue, instead of a single-objective optimization, a multi-objective optimization is proposed instead. In the multi-objective optimization experiment, the simulation conditions are kept the same, and two or more ergonomics scores are chosen for the optimization. The output of any multi-objective optimization approach is a set of non-dominated solutions, a Pareto front, that typically highlights potential trade-offs between the chosen objective functions. As it turns out, this was the case for our experiment as well. The multi-objective trajectory optimization highlighted trade-offs between different ergonomics scores. Not only that, but from a Pareto front, it is possible to pick whole-body motions that simultaneously improve many ergonomics scores. This multi-objective approach is in contrast with state-of-the-art solutions for ergonomics trajectory optimization [166, 190] that only take into consideration single-objective optimization.

**Human Motor Behavior during Cooperation and Collaboration:** to drive a person towards an ergonomically optimal whole-body posture using a physical human-robot interaction, the reference tra-

---

<sup>8</sup>Some of such ergonomics scores are exposed in chapter 1.

jectory itself is just part of the solution: the robot needs to coordinate its actions with the human in an efficient way and eventually drive him/her to the ergonomic trajectory. In chapter 3, the approach is to investigate how humans coordinate their actions in a co-manipulation task under different leadership coordination conditions: leader/follower cooperation, or no leaders (collaboration). In the devised task, the human dyad has to perform a challenging manipulation that requires precise movements. The experiment setup only allows haptic communication between the human agents, otherwise the results of the experiment could have been biased by other forms of communication that were not tracked by the setup, like speech, or eye gaze. The agents' motor behavior is tracked using motion capture markers, and muscle activation signals, as well as a measure for the task execution efficiency. The results of the experiment confirm that when a human leads the task, its arm muscle co-contraction is significantly higher than when the agents are followers, that is, leaders increase their arm stiffness in comparison to followers. We found that when no leadership is assigned, in a coordination akin to a collaboration as defined by Jarrassé *et al.* [66], both agents have arm co-contraction levels similar to their leadership condition. The human-human dyad is more effective at executing the challenging co-manipulation task than when one of the agents is assigned as a leader.

The motion of the dyad's hands also suggest that when each human agent leads the task, their desired trajectories to achieve the task's goal are significantly different, which means that in this case they could be also favoring individual biomechanical goals such as arm manipulability [150] for instance, yet, further experiments are needed to confirm this hypothesis. Meanwhile, when no leader is assigned, the resulting trajectory seems to be an arbitration between the trajectories from the other two conditions. Alongside the stiffness modulation and task efficiency results, this could mean that during the collaboration, the agents are haptically communicating their intentions of motion by modulating their arm stiffness [109], while possibly estimating each others goals for arbitrating their desired trajectory and improving the task execution [176]. This sort of human motor behavior during leader/follower cooperation and collaboration conditions fit into the unified shared control/shared autonomy classification as defined by Selvaggio *et al.* [163].

**Human-Robot Collaboration:** in chapter 4, a human-robot dyad executes the same task as the human-human counterpart did previously. The goal in this experiment is twofold: investigate the human motor behavior for the same task but with a robot; and try to emulate the such behavior on the robot control side. Given the results from the human-human experiment, whenever the robot is assigned a leadership, the robot is considered to have full autonomy over the task, while the robot and the human share that same autonomy during a collaboration. Both behaviors are expressed by changing the desired Cartesian stiffness of the robot's end-effector: robot leader at high stiffness, robot follower at low stiffness. Moreover, in this experiment the autonomy of the task is arbitrated by the human arm co-contraction, using two different variable impedance control profiles: reciprocal and mirrored.

The reciprocal profile turns the robot behavior from a leader to a follower while the human co-contracts his/her arm, and consequently, turns from a follower to a leader. Therefore, in this case, the autonomy is taken from the robot into the hands of the human so to speak. This profile is similar to the one implemented in Peternel *et al.* [131] that was arbitrated by the sum of the muscle activation signals from a pair of antagonist muscles, while in chapter 4, an index of co-contraction was used. This is an important difference as muscle co-contraction is a phenomenon associated with increased movement stability and accuracy [14, 51] while the sum of antagonist muscles efforts has not been associated with such outcome. The mirrored profile considers that the robot and the human should always share the task in equal parts, there is never a total leader nor a total follower. In this profile, the robot's desired Cartesian stiffness is directly proportional to the human arm co-contraction. This is a similar behavior to the one observed for human-human collaboration behaviors where both agents had high values of arm co-

contraction. Furthermore, this profile is also similar to the one in Grafakos *et al.* [50], with the difference that in this related work the robot was always a follower, and the arm co-contraction only increased the desired Cartesian damping of the robot, which was intended to simply intensify the Cartesian movement stabilization and not to share the autonomy of the task like it was done in chapter 4. On one hand the reciprocal profile uses a leader/follower smooth interpolation approach for shared autonomy similar to other works in literature [3, 88, 110], and on the other hand the mirrored profile is closer in resemblance to what was observed during the proposed human-human experiment for the same task. Both variable impedance control profiles are tested.

The human-robot experiment was executed by a small number of subjects, hence, we cannot draw precise conclusions from the preliminary results, however, an important trend seems to appear. During the collaboration conditions, reciprocal and mirrored profiles, the human-robot dyad executed the task more accurately than when the human or the robot were given full autonomy to the task. Moreover, it seems like the arm co-contraction during the collaboration conditions decreases in comparison to the leader/follower conditions, which could be related to the human engaging on the task only in specific times, as if it perceives that a robot trajectory may not be sufficient to accomplish the task goal for example. The leader-follower behavior corresponds to what was expected, with sub-optimal task efficiency, and the human presenting a low arm co-contraction when acting as a follower, and a high co-contraction when acting as a leader. However, it is yet not clear which of the variable impedance profiles is more adequate for the task. It is possible, nonetheless, that just by having a shared autonomy the human keeps its engagement to the task, and situational awareness at high levels. This may not to be the case when the robot has complete autonomy of the task [47] and it could incur in task inefficiency if the robot execution can not be trusted or the robot has a lower situational awareness potential than the human partner.

Overall, during the course of this PhD thesis it was possible to develop tools that can serve as a basis for a physical human-robot interaction that aims to improve human ergonomics. In our approach, the next step beyond this thesis is to put those pieces together in a single application (Fig. 6), where optimized human motion is used as a reference for the variable impedance profiles proposed in chapter 4. First, the DHM should be coupled with a robot in simulation so that the DHM efforts better reflect reality. This will also be facilitated by the fact that the DHM is simulated on an engine typically used for robot simulations [85]. Second, more data should be collected for the human-robot experiment in order to verify if the observed trends indeed show significant effects. Last, the task devised for the human-human and human-robot experiments is already very challenging on the point of view of accuracy, however, successful movements are already very constrained, so there is not much margin for trajectory ergonomics optimization. Consequently, another co-manipulation task should be designed; one of which its execution would require accuracy at certain periods of time, while in other periods of time the motion would be unrestricted enough to allow the ergonomics optimization to produce meaningful results. In other words, the task needs to be challenging enough so that the robot assistance is required to achieve both precision and ergonomics of motion.

The development of both the motion optimization methods and variable impedance profiles were made possible by taking a human-centric approach with strong emphasis on measuring and understanding the human status. In addition, both the motion optimization and the dyad coordination through physical interaction topics themselves are also in position for improvements. Perspectives of future works in these topics are then discussed in the next section.

## 5.2 Perspective

### 5.2.1 Whole-Body Trajectory Optimization w.r.t Ergonomics

The whole-body optimization methods presented in chapter 2 optimize a vector of ProMP weights corresponding to several Cartesian Trajectories. This approach is more efficient than optimizing ProMPs for the entire DHM configuration space with 43 DoFs, however, it could be improved in several ways. One possible line of work is to optimize the whole-body motion in a latent space, of low-dimensionality, related to the DHM's configuration space and mapped to a given ergonomics score, in other words, the Latent Ergonomics Maps (LEMs) defined in chapter 1. Given an initial and a final whole-body configuration, finding a path of postures that minimize an associated ergonomics score over that path would be straightforward using path-planning techniques such as the classic rapid-exploring random trees (RRT) family of algorithms [84]. The optimizers used in chapter 2 could still be used alongside LEMs instead, and given the low-dimensionality of the LEMs, it is likely that the optimization would be very efficient. In addition, LEMs also can be used for multi-objective optimization as long as many different LEMs are trained for many different ergonomics scores. For instance, one could use a similar multi-objective approach to the one used in this thesis with multi-objective optimizers. Alternatively, different LEMs could be combined into one latent space where gradient-based optimizers could be used to find the ergonomic motion.

In chapter 2, it was mentioned that ProMPs are an adequate way of representing biological motions such as the ones from human beings due to its stochastic nature. Nevertheless, the optimization process only modulated the mean trajectories of the learned ProMPs. The data from the prompts could be used to infer trajectory constraints for a given work activity. The ProMPs learned from activity demonstration will have low standard deviations at activity constraint points. Since it is also possible that the demonstrator is biased towards a certain type of trajectory due to their own experience, or there is some kind of individual or environmental constraint, this sort of inference is therefore not trivial, and for this reason it was not pursued in chapter 2, but it remains as a possible future work perspective.

The optimization algorithms used in this thesis were classic optimizers with readily available, and convenient, C++ implementations. In the case of the multi-objective optimization in particular, only one optimizer was tested, NSGA-II [31], whose implementation unlike the tested single-objective methods did not handle black-box constraints directly. Therefore, other more suitable optimizers should be tested under the same methods from chapter 2, for instance, NSGA-III [65] is an extension of the NSGA-II algorithm that directly handles black-box constraints. In addition, NSGA-III is also reportedly more efficient than NSGA-II in finding Pareto fronts for problems with more than three objective functions, which may be the case when optimizing trajectories for multiple ergonomics scores.

The methods devised here for trajectory optimization are not *only* useful for human-robot applications. Being able to automatically generate optimal motions is a desired feature also for the ergonomics field. In preliminary conversations with ergonomics experts, it was suggested that the Pareto front from the multi-objective optimization would be of particular interest. It was indicated in chapter 2, that ergonomists could pick the best solutions from the resulting Pareto fronts. Additionally, it would be even better to include in our methods a way of learning implicit preferences from an ergonomics expert in order to automatically select those trajectories from the Pareto Front. That is, given a work activity, its Pareto front of optimal ergonomic solutions, and the choices from an ergonomics expert from within this Pareto front, preference learning algorithms could be used to automate the selection of ergonomics solutions [180].

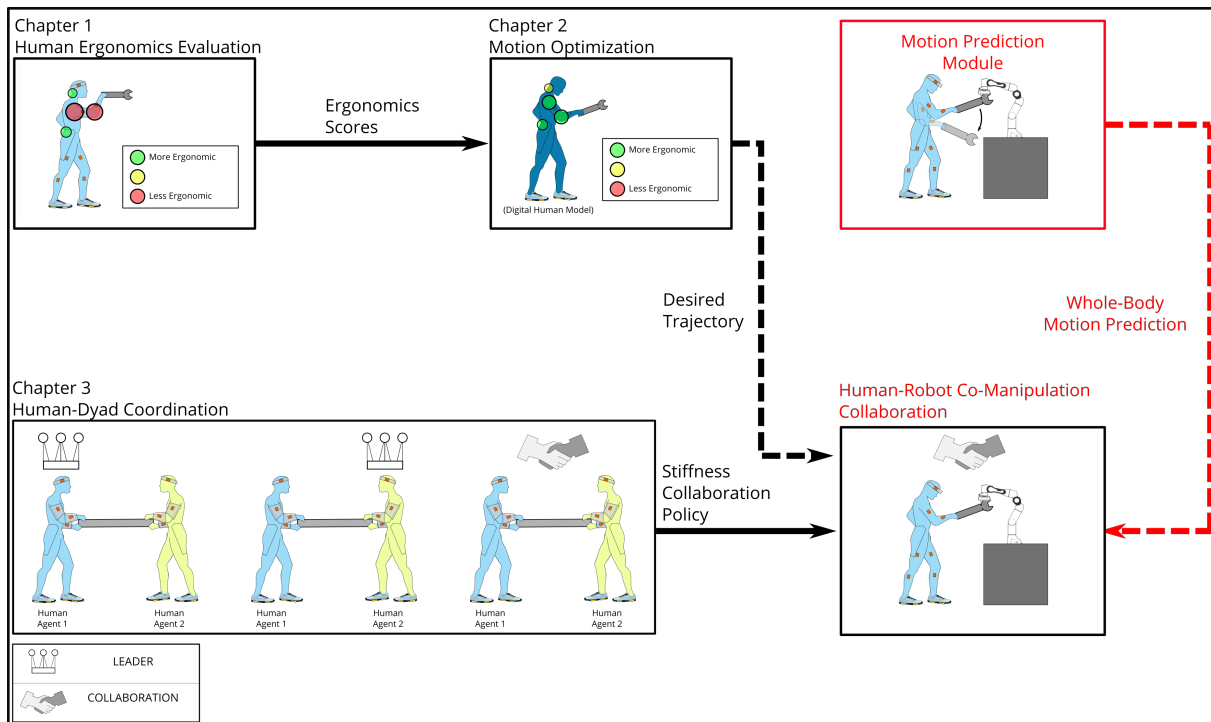


Figure 5.1: Perspective Future Work. To achieve the same sensorimotor control mechanisms a human utilizes during human-human collaboration, the robot needs a complementary whole-body (or partial) motion prediction module.

### 5.2.2 Human-Robot Interaction with Shared Task Autonomy

Successful integration of the variable impedance control profiles presented in chapter 4 still requires careful safety and ethics considerations before they can be certified for use in the real world. For this matter, the profiles still need a proof of stability, as both the desired stiffness and damping matrices for the mirrored and reciprocal profiles are not constant in time (although they are symmetrical and positive definite). Other works have already proved stability for similar variable impedance control profiles [49, 81] and could serve as a starting point.

The human-robot interaction within chapter 4 is a collaboration with a shared autonomy control as defined by Jarrassé *et al.* and Selvaggio *et al.* [66, 163], however, it still does not use all three of the human sensorimotor control mechanisms for physical interaction [18]. Adding the DHM from chapter 1 would include a human representation, and the haptic channel is open in both direction with the impedance control, but the motion prediction is still missing. To complete it, one could use whole-body motion prediction motions based on the same ProMPs presented in this thesis [34, 35] (Fig. 5.1).

# A

## Exoturn Exoskeletons

For the pilot study on chapter 1, we have selected 4 exoskeletons as potential candidates: Corfor, Laevo, CrayX, BackX. During the study, beyond of the actual the assistance of the exoskeletons, only the Laevo exoskeleton received a positive qualitative feedback from the hospital personnel.

The participant perceived a reduction on physical effort for all exoskeletons with the exception of CORFOR (Fig. A.1). In addition, for all exoskeletons the participant did not perceive a reduction on its performance. However, the participant reported that CrayX and BackX were too cumbersome be worn in the ICU, or would be unpleasant to perform the PP maneuvers (Fig. A.2 and A.3) In contrast the participant was satisfied with Laevo in terms of perceived assistance during bent postures, easiness of equipment, and freedom of movements (Fig. A.4).



Figure A.1: Evaluation of the Corfor exoskeleton by the prone-positioning team. A Corfor system was assigned to each participant by choosing the size according to their height and the manufacturer's recommendations. Two participants are also equipped with the Xsens MVN suit to have their motion recorded. The device was reported as not helpful for the PP maneuver.



Figure A.2: CrayX worn by the participant. The arrows highlight the external parts of the exoskeleton that add constraints to the workspace. The CrayX was considered too cumbersome to be used around patients, and very difficult to tune. The participant perceived it required additional concentration effort during back flexion to enable the active support, which they couldn't improve even after changing the sensitivity parameter. Furthermore, the participant also reported a critical discomfort due to a part of the CrayX applying a force on the dorsum.



Figure A.3: BackX worn by a participant. The arrows point to the metallic arcs that are constraining the arms during the PP gestures: the participants pointed out that this was one of the main reasons for not choosing to use this exoskeleton for this particular gesture. The BackX was perceived similar to the LAEVO in terms of assistance, but both participants reported that the metallic curved bars from the sternum to the hip were preventing several arm movements necessary to complete the PP maneuver, and as such they felt they could not execute the entire maneuver with this equipment in real conditions.

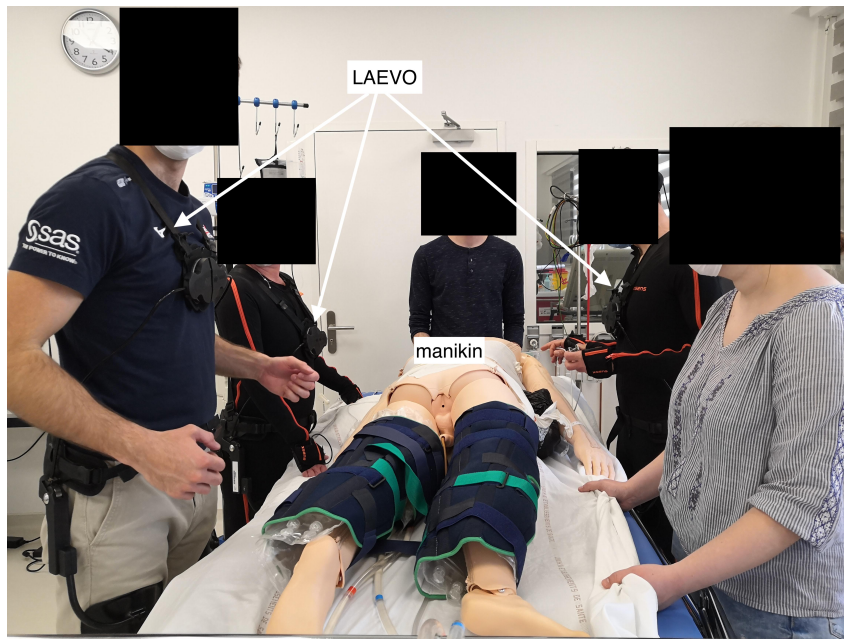


Figure A.4: evaluation of the Laevo exoskeleton by the PP team. We only had three Laevo v1, one for each size (small, medium, large). Each exoskeleton was attributed to the participants according to their height and following the recommendations of the manufacturer. The Laevo exoskeleton was immediately perceived helpful and intuitive. One participant reported a slight discomfort on the sternum during back flexion and on the thighs during walking, noticing it would be better to unlock it to walk normally. This issue was solved in later versions of the Laevo exoskeleton, such as the v2.5 that was purchased and used in the 2nd wave of the pandemic in the ICU (since October 2020).

## B

# Human Co-Manipulation Data

### B.1 Timing Measurements

In order to define phases 1, 2 and 3 of the task execution, there are three important timing measurements:  $t_{EXIT}$ ,  $t_{MID}$ ,  $t_{ENT}$  (fig. B.1). They are the instants in which the pipe exits tube 1, in which the pipe goes around the obstacle, and in which the pipe enters tube 2. In order to obtain those instants, first, we calculate the centroid of hand markers of both participants  $\vec{r} = (r_x, r_y)$ , and then we obtain

$$t_{EXIT} = t(|r_y - tube_{1y}| < 0.35) \quad (B.1)$$

, where  $tube_{1X}$  is the Y component of the tube 1 position, and 0.35 is the distance from the middle of the handles to the end of the tube (fig. 3.4). The same is done for  $t_{ENTER}$ :

$$t_{ENTER} = t(|r_y - tube_{2y}| < 0.35) \quad (B.2)$$

Finally,  $t_{MIDDLE}$  is the instant after  $t_{EXIT}$  and before  $t_{ENTER}$  in which  $r_y$  starts decreasing instead of increasing.

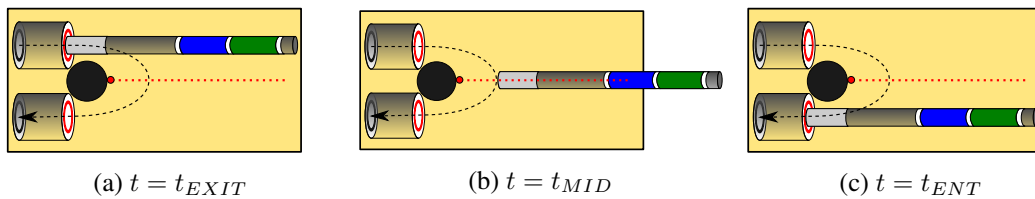


Figure B.1: Sequence of key instants during the manipulation

## B.2 Index of Co-Contraction

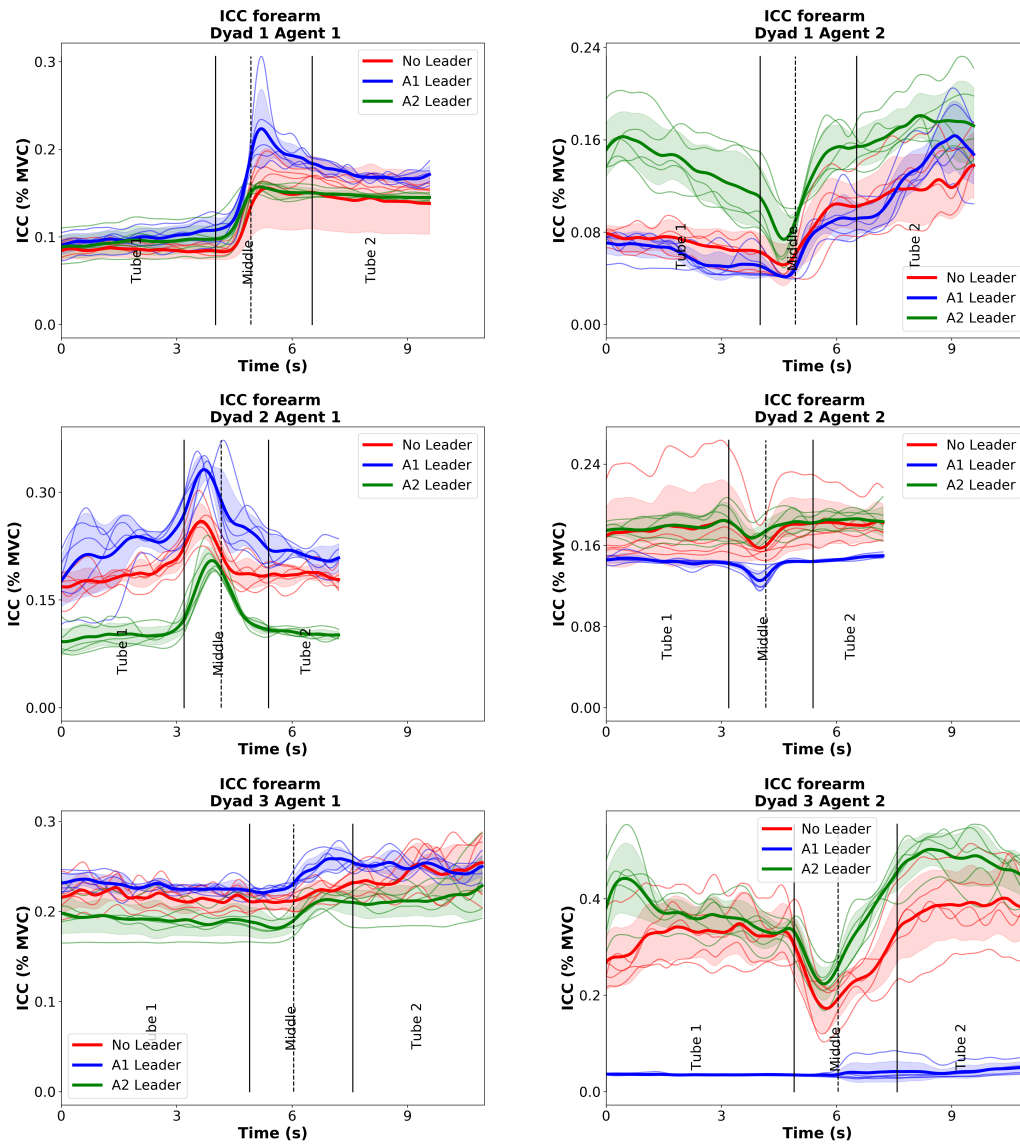


Figure B.2: Average Index of Co-Contraction for dyads 1,2 and 3 for all conditions on the Dyad Experiment

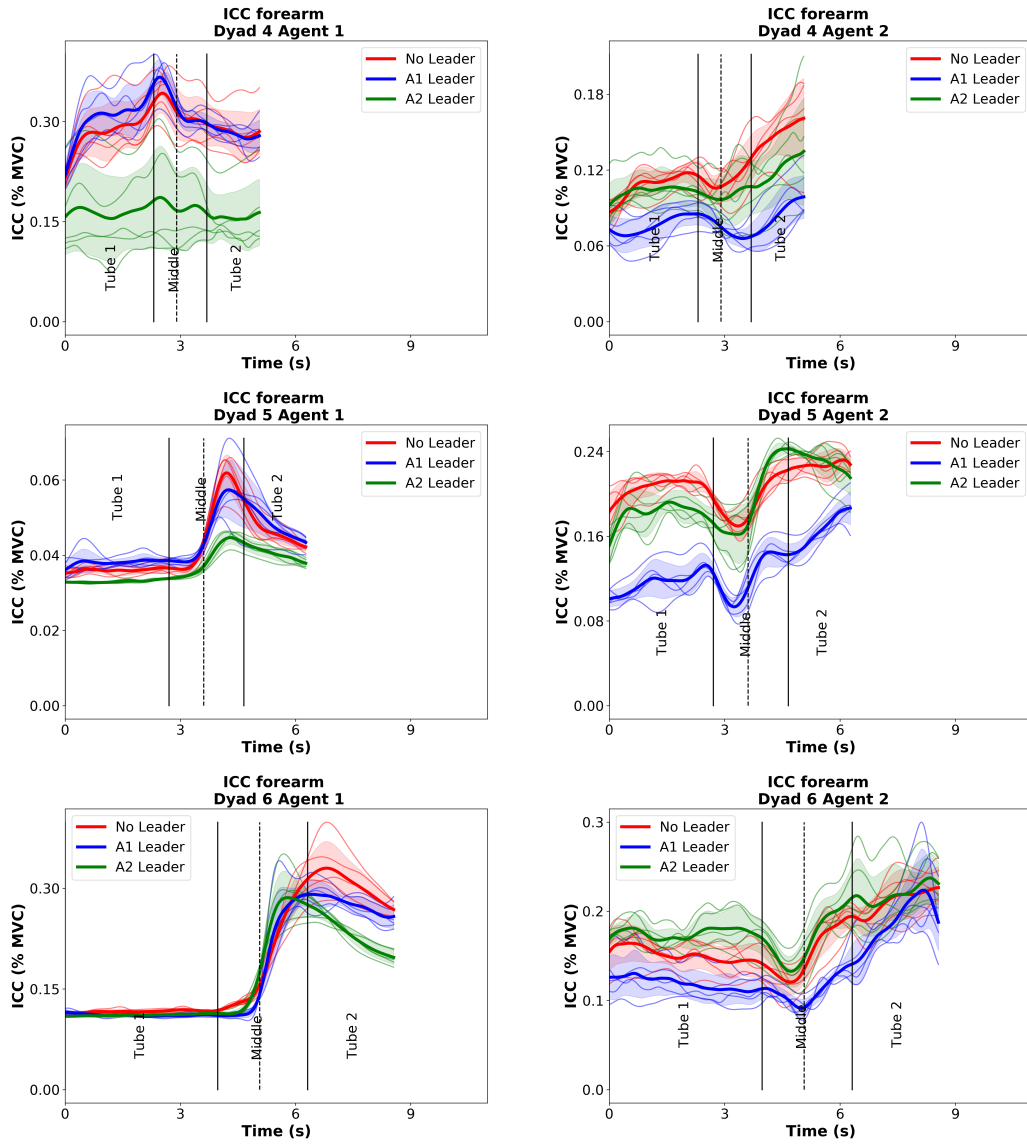


Figure B.3: Average Index of Co-Contraction for dyads 4,5 and 6 for all conditions on the Dyad Experiment

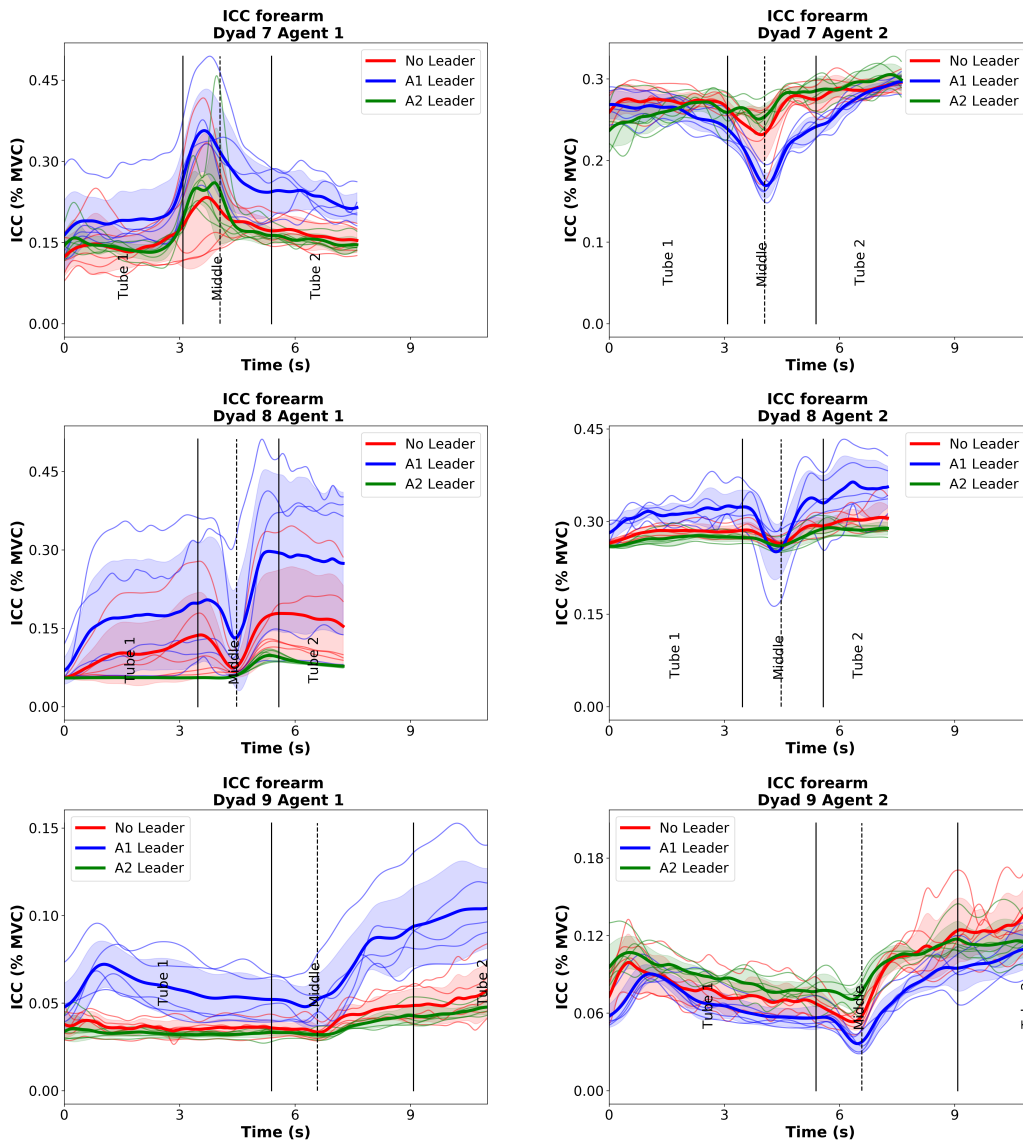


Figure B.4: Average Index of Co-Contraction for dyads 7,8 and 9 for all conditions on the Dyad Experiment

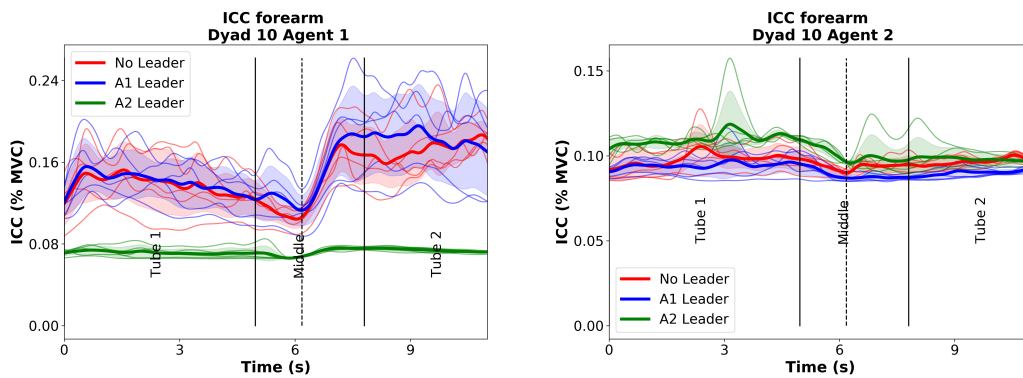


Figure B.5: Average Index of Co-Contraction for dyad 10 for all conditions on the Dyad Experiment

## B.3 Pipe Trajectory

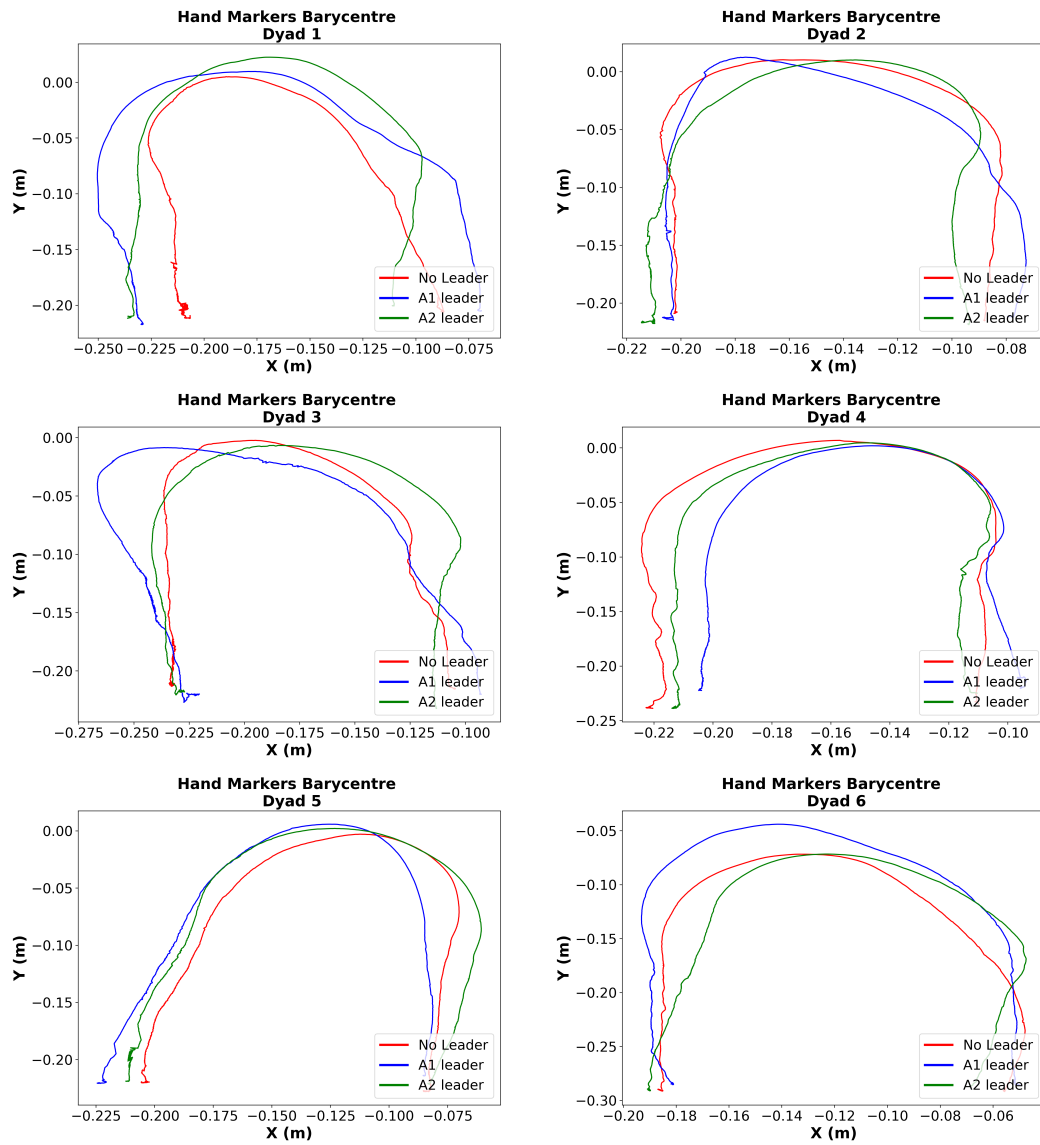


Figure B.6: Trajectory of the barycentre of the agents' hands as a proxy to the center of the pipe. Dyads 1 to 6

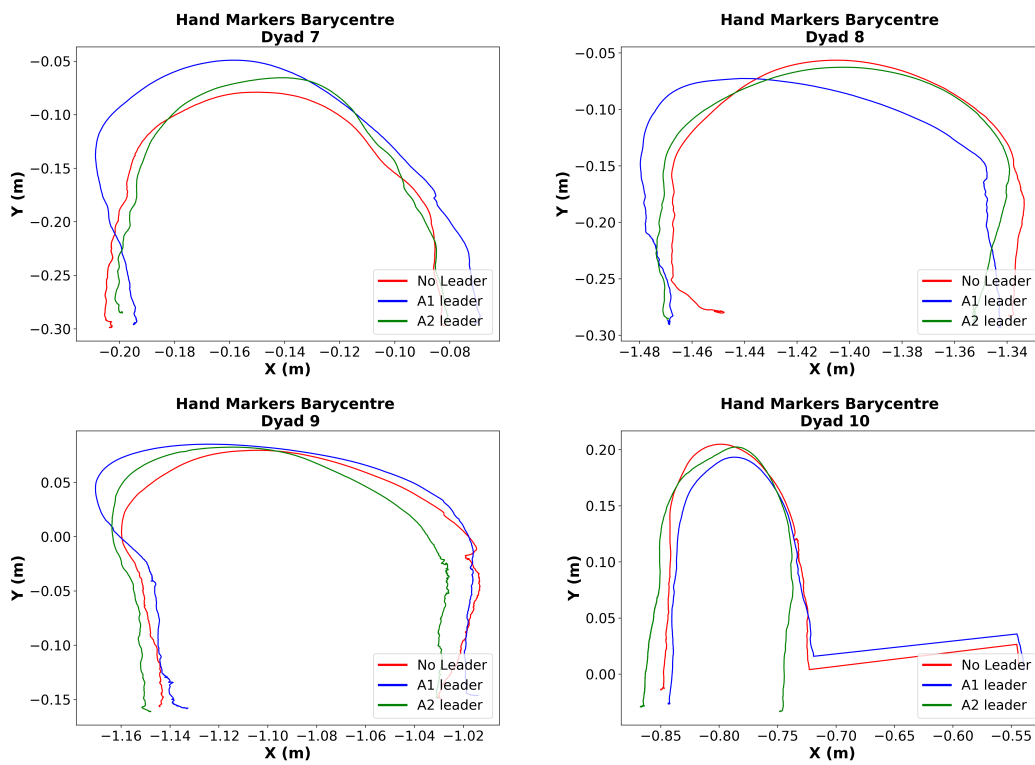


Figure B.7: Trajectory of the barycentre of the agents' hands as a proxy to the center of the pipe. Dyads 7 to 10

# C

## Human-Robot Co-Manipulation Data

### C.1 Index of Co-Contraction

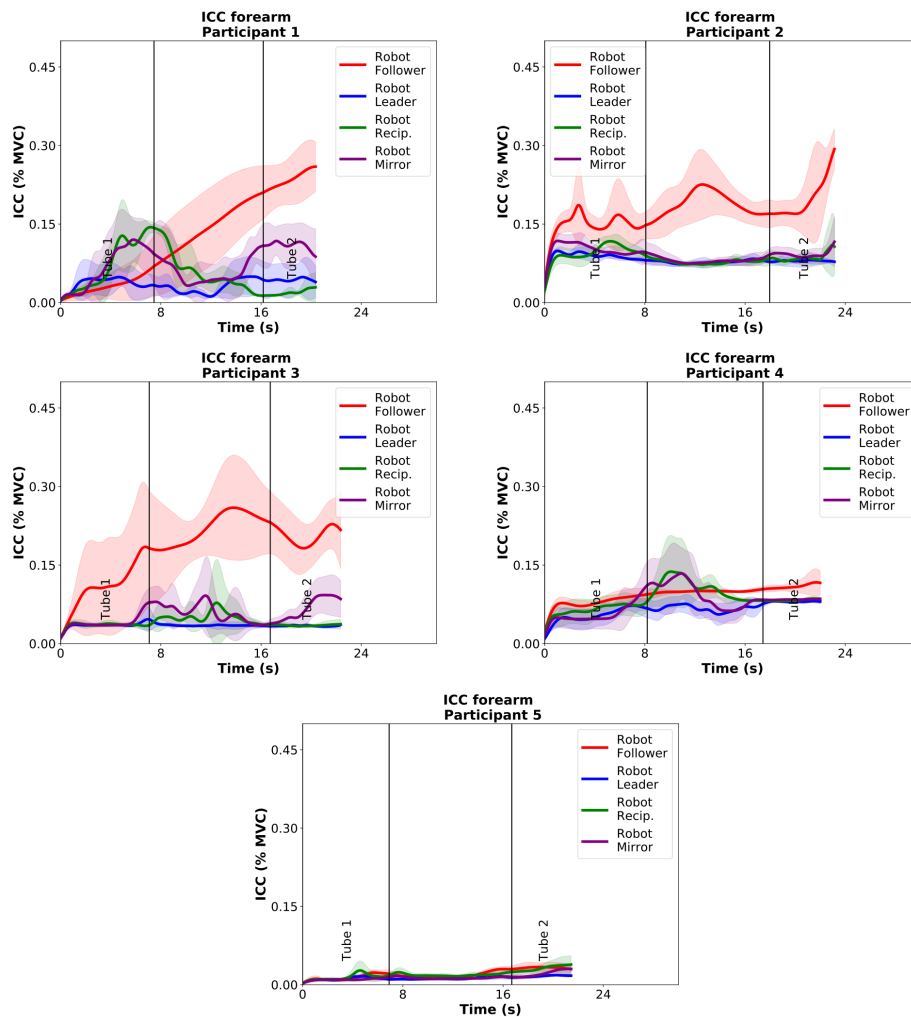


Figure C.1: Average Index of Co-Contraction for Human-Robot Co-Manipulation Experiment

## C.2 Pipe Trajectory

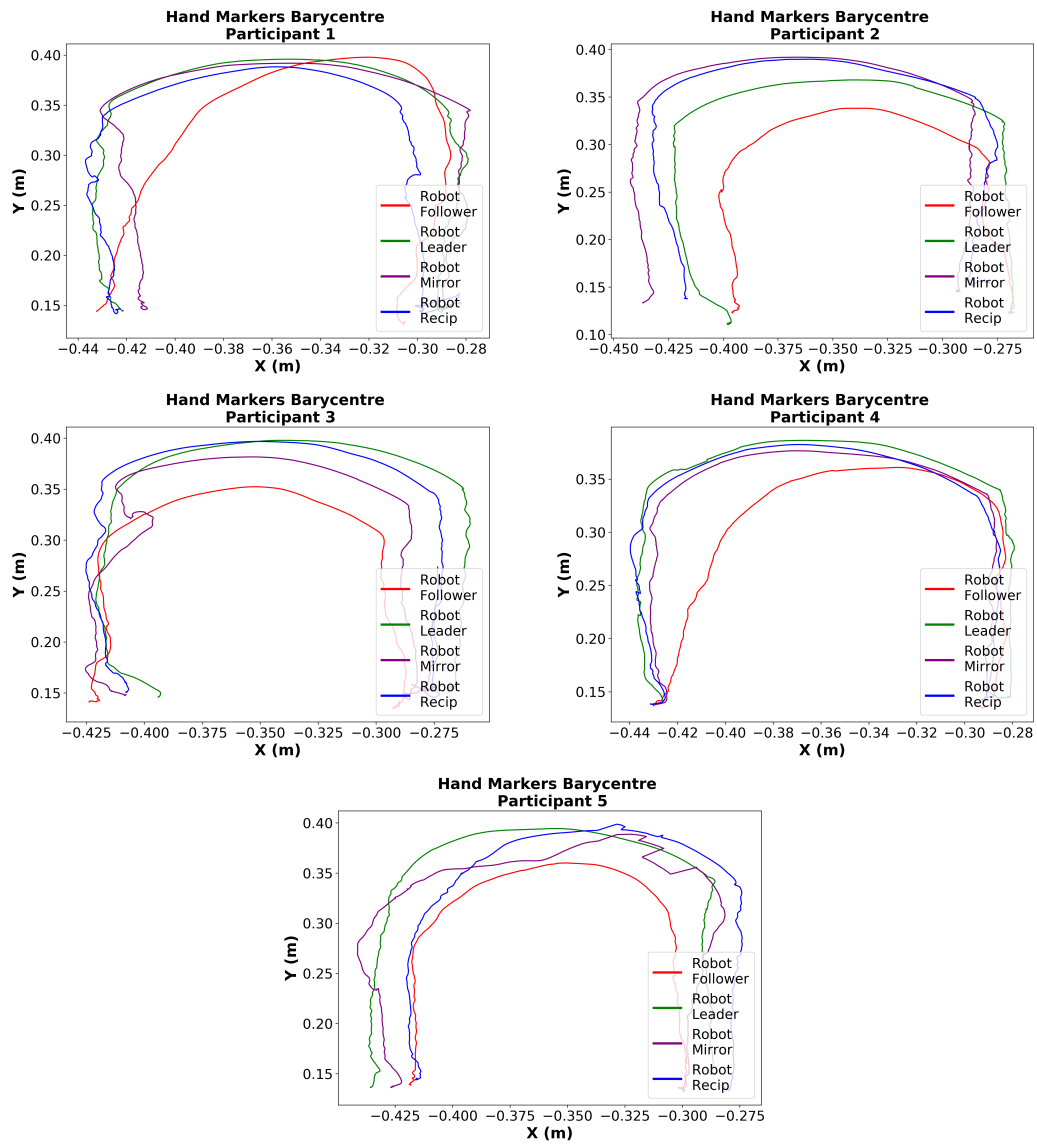


Figure C.2: Trajectory of the barycentre of the agents' hands for HR Co-Manipulation

### C.3 Interaction Torque

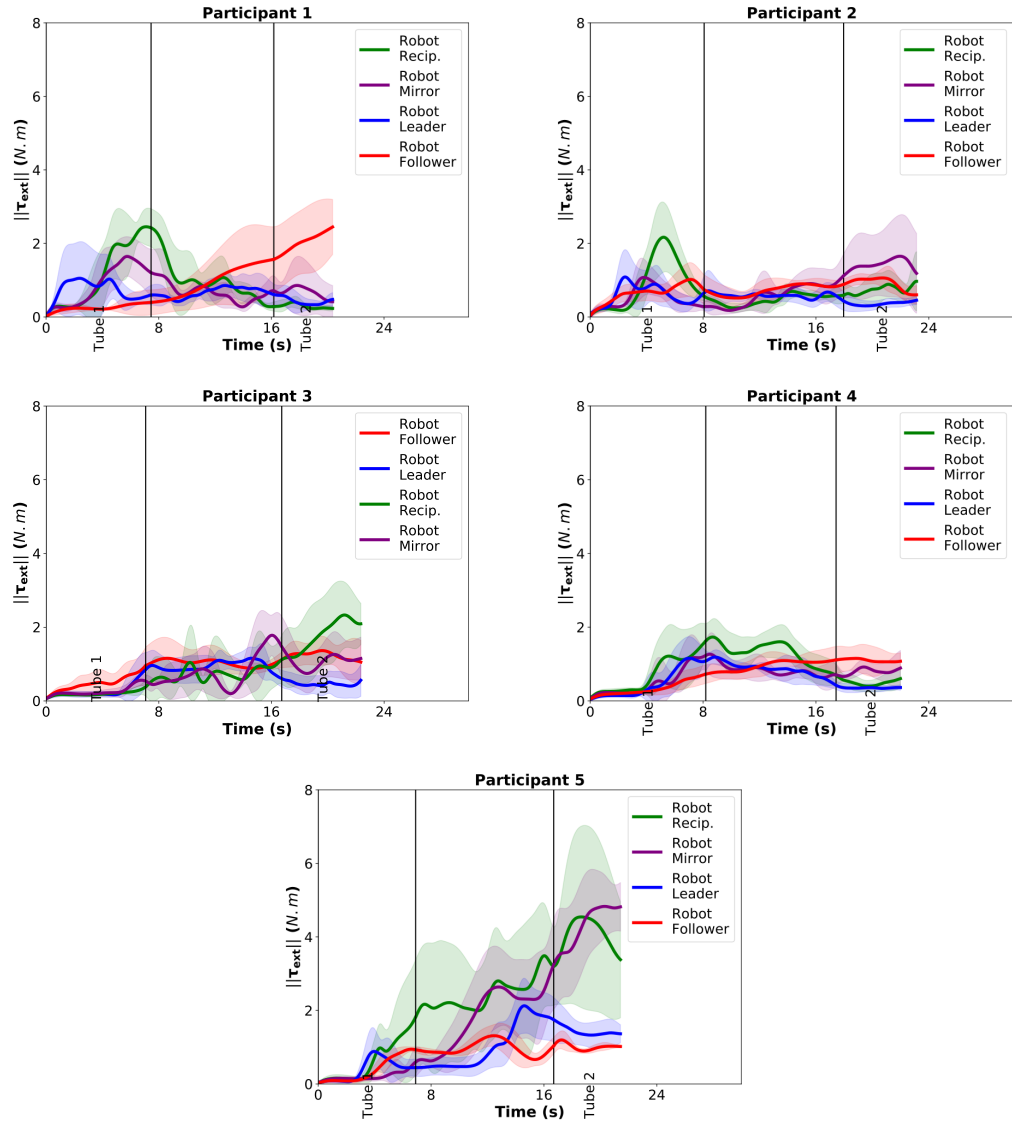


Figure C.3: Interaction torque during human-robot co-manipulation



# Bibliography

- [1] Robotics 2020 Multi-Annual Roadmap. <https://www.eu-robotics.net/sparc/about/roadmap/index.html>. Accessed: 2021-10-16.
- [2] Karen E Adolph and John M Franchak. The development of motor behavior. *Wiley Interdisciplinary Reviews: Cognitive Science*, 8(1-2):e1430, 2017.
- [3] Don Joven Agravante, Andrea Cherubini, Alexander Sherikov, Pierre-Brice Wieber, and Abderrahmane Kheddar. Human-humanoid collaborative carrying. *IEEE Transactions on Robotics*, 35(4):833–846, 2019.
- [4] Arash Ajoudani, Andrea Maria Zanchettin, Serena Ivaldi, Alin Albu-Schäffer, Kazuhiro Kosuge, and Oussama Khatib. Progress and prospects of the human–robot collaboration. *Autonomous Robots*, 42(5):957–975, Jun 2018.
- [5] Alin Albu-Schaffer, Christian Ott, Udo Frese, and Gerd Hirzinger. Cartesian impedance control of redundant robots: Recent results with the dlr-light-weight-arms. In *2003 IEEE International conference on robotics and automation (Cat. No. 03CH37422)*, volume 3, pages 3704–3709. IEEE, 2003.
- [6] DM Andrews, AM Holmes, PL Weir, TA Arnold, and JP Callaghan. Decision times and errors increase when classifying trunk postures near posture bin boundaries. *Theoretical Issues in Ergonomics Science*, 9(5):425–440, 2008.
- [7] Dan Anton, Lee D Shibley, Nathan B Fethke, Jennifer Hess, Thomas M Cook, and John Rosecrance. The effect of overhead drilling position on shoulder moment and electromyography. *Ergonomics*, 44(5):489–501, 2001.
- [8] Dirk V Arnold and Nikolaus Hansen. A (1+1)-CMA-ES for constrained optimisation. In *GECCO*, pages 297–304, 2012.
- [9] Jimmy Baraglia, Maya Cakmak, Yukie Nagai, Rajesh Rao, and Minoru Asada. Efficient human-robot collaboration: when should a robot take initiative? *The International Journal of Robotics Research*, page 027836491668825, 02 2017.
- [10] Frank J. Bernieri and Robert Rosenthal. Interpersonal coordination: Behavior matching and interactional synchrony. 1991.
- [11] Antonio Bicchi, Giovanni Tonietti, Michele Bavaro, and Marco Piccigallo. Variable stiffness actuators for fast and safe motion control. In *Robotics research. The eleventh international symposium*, pages 527–536. Springer, 2005.

- [12] David P. Black, Michael A. Riley, and Christopher K. McCord. Synergies in intra- and inter-personal interlimb rhythmic coordination. *Motor Control*, 11(4):348 – 373, 2007.
- [13] K. Bouyarmane and A. Kheddar. Using a multi-objective controller to synthesize simulated humanoid robot motion with changing contact configurations. In *2011 IEEE/RSJ International Conference on Intelligent Robots and Systems*, pages 4414–4419, Sep. 2011.
- [14] E Burdet, R Osu, DW Franklin, TE Milner, and M Kawato. The central nervous system stabilizes unstable dynamics by learning optimal impedance. *NATURE*, 414:446–449, 2001.
- [15] B. Busch, M. Toussaint, and M. Lopes. Planning ergonomic sequences of actions in human-robot interaction. In *2018 IEEE International Conference on Robotics and Automation (ICRA)*, pages 1916–1923, 2018.
- [16] Baptiste Busch, Guilherme Maeda, Yoan Mollard, Marie Demangeat, and Manuel Lopes. Postural optimization for an ergonomic human-robot interaction. In *2017 IEEE/RSJ International Conference on Intelligent Robots and Systems (IROS)*, pages 2778–2785. IEEE, 2017.
- [17] Antoine Bussy, Abderrahmane Kheddar, André Crosnier, and François Keith. Human-humanoid haptic joint object transportation case study. In *2012 IEEE/RSJ International Conference on Intelligent Robots and Systems*, pages 3633–3638. IEEE, 2012.
- [18] Judith Bütepage and Danica Kragic. Human-robot collaboration: From psychology to social robotics, 2017.
- [19] A. Colin Cameron and Pravin K. Trivedi. *Regression Analysis of Count Data*. Econometric Society Monographs. Cambridge University Press, 2 edition, 2013.
- [20] Matteo Candidi, Arianna Curioni, Francesco Donnarumma, Lucia Maria Sacheli, and Giovanni Pezzulo. Interactional leader–follower sensorimotor communication strategies during repetitive joint actions. *Journal of the Royal Society Interface*, 12(110):20150644, 2015.
- [21] Cyrielle Caussy, François Pattou, Florent Wallet, Chantal Simon, Sarah Chalopin, Charlene Telliam, Daniel Mathieu, Fabien Subtil, Emilie Frobert, Maud Alligier, Dominique Delaunay, Philippe Vanhems, Martine Laville, Merce Jourdain, and Emmanuel Disse. Prevalence of obesity among adult inpatients with covid-19 in france. *The Lancet Diabetes & Endocrinology*, 8(7):562–564, 2020.
- [22] D.B. Chaffin, G.B.J. Andersson, and B.J. Martin. *Occupational Biomechanics*. Wiley, 2006.
- [23] M. Charbonneau, V. Modugno, F. Nori, G. Oriolo, D. Pucci, and S. Ivaldi. Learning robust task priorities of qp-based whole-body torque-controllers. In *2018 IEEE-RAS 18th International Conference on Humanoid Robots (Humanoids)*.
- [24] Andrea Cherubini, Robin Passama, André Crosnier, Antoine Lasnier, and Philippe Fraisse. Collaborative manufacturing with physical human–robot interaction. *Robotics and Computer-Integrated Manufacturing*, 40:1–13, 2016.
- [25] J Edward Colgate, J Edward, Michael A Peshkin, and Witaya Wannasuphprasit. Cobots: Robots for collaboration with human operators. 1996.
- [26] E Nigel Corlett and RP Bishop. A technique for assessing postural discomfort. *Ergonomics*, 19(2):175–182, 1976.

- 
- [27] Arturo Cruz-Maya, Roxana Agrigoroaie, and Adriana Tapus. Improving user's performance by motivation: Matching robot interaction strategy with user's regulatory state. In *International Conference on Social Robotics*, pages 464–473. Springer, 2017.
- [28] Michael Damsgaard, John Rasmussen, Søren Tørholm Christensen, Egidijus Surma, and Mark De Zee. Analysis of musculoskeletal systems in the anybody modeling system. *Simulation Modelling Practice and Theory*, 14(8):1100–1111, 2006.
- [29] GC David. Ergonomic methods for assessing exposure to risk factors for work-related musculoskeletal disorders. *Occupational medicine*, 55(3):190–199, 2005.
- [30] Michiel P. de Looze, Tim Bosch, Frank Krause, Konrad S. Stadler, and Leonard W. O'Sullivan. Exoskeletons for industrial application and their potential effects on physical work load. *Ergonomics*, 59(5):671–681, 2016. PMID: 26444053.
- [31] K. Deb, A. Pratap, S. Agarwal, and T. Meyarivan. A fast and elitist multiobjective genetic algorithm: Nsga-ii. *IEEE Transactions on Evolutionary Computation*, 6(2):182–197, 2002.
- [32] Kalyanmoy Deb. Multi-objective optimisation using evolutionary algorithms: an introduction. In *Multi-objective evolutionary optimisation for product design and manufacturing*, pages 3–34. Springer, 2011.
- [33] Scott L. Delp, Frank C. Anderson, Allison S. Arnold, Peter Loan, Ayman Habib, Chand T. John, Eran Guendelman, and Darryl G. Thelen. Opensim: Open-source software to create and analyze dynamic simulations of movement. *IEEE Transactions on Biomedical Engineering*, 54(11):1940–1950, 2007.
- [34] Oriane Dermy, François Charpillet, and Serena Ivaldi. Multi-modal intention prediction with probabilistic movement primitives. In *Human Friendly Robotics*, pages 181–196. Springer, 2019.
- [35] Oriane Dermy, Maxime Chaveroche, Francis Colas, François Charpillet, and Serena Ivaldi. Prediction of human whole-body movements with ae-prompts. In *2018 IEEE-RAS 18th International Conference on Humanoid Robots (Humanoids)*, pages 572–579. IEEE, 2018.
- [36] John A. Dewey, Elisabeth Pacherie, and Guenther Knoblich. The phenomenology of controlling a moving object with another person. *Cognition*, 132(3):383 – 397, 2014.
- [37] A. Di Fava, K. Bouyarmane, K. Chappellet, E. Ruffaldi, and A. Kheddar. Multi-contact motion retargeting from human to humanoid robot. In *2016 IEEE-RAS 16th International Conference on Humanoid Robots (Humanoids)*.
- [38] Pierre Dillenbourg, Sanna Järvelä, and Frank Fischer. The evolution of research on computer-supported collaborative learning. In *Technology-enhanced learning*, pages 3–19. Springer, 2009.
- [39] Adam Doerrfeld, Natalie Sebanz, and Maggie Shiffrar. Expecting to lift a box together makes the load look lighter. *Psychological Research*, 76(4):467–475, 2012.
- [40] A. Escande, N. Mansard, and P. B. Wieber. Fast resolution of hierarchized inverse kinematics with inequality constraints. In *2010 IEEE International Conference on Robotics and Automation*.
- [41] Mircea Fagarasanu and Shrawan Kumar. Measurement instruments and data collection: a consideration of constructs and biases in ergonomics research. *International journal of industrial ergonomics*, 30(6):355–369, 2002.

- [42] Fanny Ficuciello, Amedeo Romano, Luigi Villani, and Bruno Siciliano. Cartesian impedance control of redundant manipulators for human-robot co-manipulation. In *2014 IEEE/RSJ International Conference on Intelligent Robots and Systems*, pages 2120–2125, 2014.
- [43] L. F. C. Figueredo, R. C. Aguiar, L. Chen, S. Chakrabarty, M. R. Dogar, and A. G. Cohn. Human comfortability: Integrating ergonomics and muscular-informed metrics for manipulability analysis during human-robot collaboration. *IEEE Robotics and Automation Letters*, 2021.
- [44] T Flash and N Hogan. The coordination of arm movements: an experimentally confirmed mathematical model. *Journal of Neuroscience*, 5(7):1688–1703, 1985.
- [45] G. Ganesh, A. Takagi, R. Osu, T. Yoshioka, M. Kawato, and E. Burdet. Two is better than one: Physical interactions improve motor performance in humans. *Scientific Reports*, 4(1):3824, Jan 2014.
- [46] Claudio Gaz, Marco Cognetti, Alexander Oliva, Paolo Robuffo Giordano, and Alessandro De Luca. Dynamic identification of the franka emika panda robot with retrieval of feasible parameters using penalty-based optimization. *IEEE Robotics and Automation Letters*, 4(4):4147–4154, 2019.
- [47] Matthew Gombolay, Anna Bair, Cindy Huang, and Julie Shah. Computational design of mixed-initiative human–robot teaming that considers human factors: situational awareness, workload, and workflow preferences. *The International Journal of Robotics Research*, 36(5-7):597–617, 2017.
- [48] Matthew C Gombolay, Reymundo A Gutierrez, Shanelle G Clarke, Giancarlo F Sturla, and Julie A Shah. Decision-making authority, team efficiency and human worker satisfaction in mixed human–robot teams. *Autonomous Robots*, 39(3):293–312, 2015.
- [49] Waldez Gomes and Fernando Lizarralde. Role adaptive admittance controller for human-robot co-manipulation. In *Congresso Brasileiro de Automática-CBA*, volume 1, 2019.
- [50] S. Grafakos, F. Dimeas, and N. Aspragathos. Variable admittance control in phri using emg-based arm muscles co-activation. In *2016 IEEE International Conference on Systems, Man, and Cybernetics (SMC)*, pages 001900–001905, Oct 2016.
- [51] Paul L. Gribble, Lucy I. Mullin, Nicholas Cothros, and Andrew Mattar. Role of cocontraction in arm movement accuracy. *Journal of Neurophysiology*, 89(5):2396–2405, 2003.
- [52] R. Groten, D. Feth, R. L. Klatzky, and A. Peer. The role of haptic feedback for the integration of intentions in shared task execution. *IEEE Transactions on Haptics*, 6(1):94–105, First 2013.
- [53] Claude Guérin, Jean Reignier, Jean-Christophe Richard, Pascal Beuret, Arnaud Gacouin, Thierry Boulain, Emmanuelle Mercier, Michel Badet, Alain Mercat, Olivier Baudin, Marc Clavel, Delphine Chatellier, Samir Jaber, Sylvène Rosselli, Jordi Mancebo, Michel Sirodot, Gilles Hilbert, Christian Bengler, Jack Richecoeur, Marc Gainnier, Frédérique Bayle, Gael Bourdin, Véronique Leray, Raphaelae Girard, Loredana Baboi, and Louis Ayzac. Prone positioning in severe acute respiratory distress syndrome. *New England Journal of Medicine*, 368(23):2159–2168, 2013. PMID: 23688302.
- [54] Christopher M. Harris and Daniel M. Wolpert. Signal-dependent noise determines motor planning. *Nature*, 394:780 EP –, Aug 1998.

- 
- [55] Sue Hignett and Lynn McAtamney. Rapid entire body assessment (reba). *Applied ergonomics*, 31(2):201–205, 2000.
- [56] Enrico Mingo Hoffman, Brice Clement, Chengxu Zhou, Nikos G Tsagarakis, Jean-Baptiste Mouret, and Serena Ivaldi. Whole-Body Compliant Control of iCub: first results with OpenSoT. In *ICRA 2018 - Workshop*.
- [57] Wilhelmina E. Hoogendoorn, Paulien M. Bongers, Henrica C. W. de Vet, Marjolein Douwes, Bart W. Koes, Mathilde C. Miedema, Geertje A. M. Ariëns, and Lex M. Bouter. Flexion and Rotation of the Trunk and Lifting at Work Are Risk Factors for Low Back Pain: Results of a Prospective Cohort Study. *Spine*, 25(23):3087–3092, December 2000.
- [58] Y. Hu, M. Benallegue, G. Venture, and E. Yoshida. Interact with me: An exploratory study on interaction factors for active physical human-robot interaction. *IEEE Robotics and Automation Letters*, 5(4):6764–6771, 2020.
- [59] Aitor Iriondo Pascual, Dan Högberg, Anna Syberfeldt, Francisco García Rivera, Estela Pérez Luque, and Lars Hanson. Implementation of ergonomics evaluation methods in a multi-objective optimization framework. In *6th International Digital Human Modeling Symposium, August 31-September 2, 2020, Skövde, Sweden*, pages 361–371. IOS Press, 2020.
- [60] Mark Ison and Panagiotis Artemiadis. The role of muscle synergies in myoelectric control: trends and challenges for simultaneous multifunction control. *Journal of Neural Engineering*, 11(5):051001, 2014.
- [61] Serena Ivaldi, Lars Fritzsche, Jan Babič, Freek Stulp, Michael Damsgaard, Bernhard Graitmann, Giovanni Bellusci, and Francesco Nori. Anticipatory models of human movements and dynamics: the roadmap of the andy project, 2017.
- [62] Serena Ivaldi, Pauline Maurice, **Gomes, Waldez**, Jean Theurel, Lien Wioland, Jean-Jacques Atain-Kouadio, Laurent Claudon, Hind Hani, Antoine Kimmoun, Jean-Marc Sellal, Bruno Levy, Jean Paysant, Serguei Malikov, Bruno Chenuel, and Nicla Settembre. Using exoskeletons to assist medical staff during prone positioning of mechanically ventilated covid-19 patients: A pilot study. In Jay Kalra, Nancy J. Lightner, and Redha Taiar, editors, *Advances in Human Factors and Ergonomics in Healthcare and Medical Devices*, pages 88–100, Cham, 2021. Springer International Publishing.
- [63] Serena Ivaldi, Olivier Sigaud, Bastien Berret, and Francesco Nori. From humans to humanoids: The optimal control framework. *Paladyn*, 3(2):75–91, Jun 2012.
- [64] Stephan Jagau and Matthijs van Veelen. A general evolutionary framework for the role of intuition and deliberation in cooperation. *Nature Human Behaviour*, 1(8):1–6, 2017.
- [65] Himanshu Jain and Kalyanmoy Deb. An evolutionary many-objective optimization algorithm using reference-point based nondominated sorting approach, part ii: Handling constraints and extending to an adaptive approach. *IEEE Transactions on Evolutionary Computation*, 18(4):602–622, 2014.
- [66] Nathanaël Jarrassé, Themistoklis Charalambous, and Etienne Burdet. A framework to describe, analyze and generate interactive motor behaviors. *PloS one*, 7(11):e49945, 2012.
- [67] Nathanael Jarrasse, Vittorio Sanguineti, and Etienne Burdet. Slaves no longer: review on role assignment for human–robot joint motor action. *Adaptive Behavior*, 22(1):70–82, 2014.

- [68] Shervin Javdani, Siddhartha S. Srinivasa, and J. Andrew Bagnell. Shared autonomy via hindsight optimization, 2015.
- [69] Steven G. Johnson. *The NLOpt nonlinear-optimization package*.
- [70] S. Kager, A. Hussain, A. Cherpín, A. Melendez-Calderon, A. Takagi, S. Endo, E. Burdet, S. Hirche, M. H. Ang, and D. Campolo. The effect of skill level matching in dyadic interaction on learning of a tracing task. In *2019 IEEE 16th International Conference on Rehabilitation Robotics (ICORR)*, pages 824–829, 2019.
- [71] Virpi Kalakoski, Sanna Selinheimo, Teppo Valtonen, Jarno Turunen, Sari Käpykangas, Hilikka Ylisassi, Pauliina Toivio, Heli Järnefelt, Heli Hannonen, and Teemu Paajanen. Effects of a cognitive ergonomics workplace intervention (cogerg) on cognitive strain and well-being: a cluster-randomized controlled trial. a study protocol. *BMC psychology*, 8(1):1–16, 2020.
- [72] H. Kamide, Y. Mae, K. Kawabe, S. Shigemi, M. Hirose, and T. Arai. New measurement of psychological safety for humanoid. In *2012 7th ACM/IEEE International Conference on Human-Robot Interaction (HRI)*, pages 49–56, 2012.
- [73] Mahdi Khoramshahi and Aude Billard. A dynamical system approach for detection and reaction to human guidance in physical human–robot interaction. *Autonomous Robots*, 44(8):1411–1429, 2020.
- [74] Wansoo Kim, Jinoh Lee, Luka Peternel, Nikos Tsagarakis, and Arash Ajoudani. Anticipatory robot assistance for the prevention of human static joint overloading in human–robot collaboration. *IEEE robotics and automation letters*, 3(1):68–75, 2017.
- [75] Wansoo Kim, Jinoh Lee, Luka Peternel, Nikos Tsagarakis, and Arash Ajoudani. Anticipatory robot assistance for the prevention of human static joint overloading in human–robot collaboration. *IEEE robotics and automation letters*, 2018.
- [76] Wansoo Kim, Marta Lorenzini, Pietro Balatti, Phuong DH Nguyen, Ugo Pattacini, Vadim Tikhanoff, Luka Peternel, Claudio Fantacci, Lorenzo Natale, Giorgio Metta, et al. Adaptable workstations for human-robot collaboration: A reconfigurable framework for improving worker ergonomics and productivity. *IEEE Robotics & Automation Magazine*, 26(3):14–26, 2019.
- [77] Diederik P. Kingma and Max Welling. An introduction to variational autoencoders. *Foundations and Trends® in Machine Learning*, 12(4):307–392, 2019.
- [78] Axel S. Koopman, Idsart Kingma, Gert S. Faber, Michiel P. de Looze, and Jaap H. van Dieën. Effects of a passive exoskeleton on the mechanical loading of the low back in static holding tasks. *Journal of Biomechanics*, 83:97–103, 2019.
- [79] Petar Kormushev, Sylvain Calinon, and Darwin G Caldwell. Robot motor skill coordination with em-based reinforcement learning. In *2010 IEEE/RSJ international conference on intelligent robots and systems*. IEEE.
- [80] Jorie Koster-Hale and Rebecca Saxe. Theory of mind: a neural prediction problem. *Neuron*, 79(5):836–848, 2013.
- [81] Klas Kronander and Aude Billard. Stability considerations for variable impedance control. *IEEE Transactions on Robotics*, 32(5):1298–1305, 2016.

- 
- [82] Claudia Latella, Marta Lorenzini, Maria Lazzaroni, Francesco Romano, Silvio Traversaro, M Ali Akhras, Daniele Pucci, and Francesco Nori. Towards real-time whole-body human dynamics estimation through probabilistic sensor fusion algorithms. *Autonomous Robots*, 43(6):1591–1603, 2019.
- [83] Wolfgang Laurig and Joachim Vedder. The nature and aims of ergonomics. *Encyclopaedia of Occupational Health and Safety*, WLaJ Vedder, Editor, 1998.
- [84] Steven M. LaValle. *Planning Algorithms*. Cambridge University Press, USA, 2006.
- [85] Jeongseok Lee, Michael X. Grey, Sehoon Ha, Tobias Kunz, Sumit Jain, Yuting Ye, Siddhartha S. Srinivasa, Mike Stilman, and C. Karen Liu. DART: Dynamic animation and robotics toolkit. *Journal of Open Source Software*, 2018.
- [86] Guangyan Li and Peter Buckle. Current techniques for assessing physical exposure to work-related musculoskeletal risks, with emphasis on posture-based methods. *Ergonomics*, 42(5):674–695, 1999.
- [87] Y. Li, K. P. Tee, R. Yan, W. L. Chan, and Y. Wu. A framework of human–robot coordination based on game theory and policy iteration. *IEEE Transactions on Robotics*, 32(6):1408–1418, 2016.
- [88] Yanan Li, Gerolamo Carboni, Franck Gonzalez, Domenico Campolo, and Etienne Burdet. Differential game theory for versatile physical human–robot interaction. *Nature Machine Intelligence*, 1(1):36–43, 2019.
- [89] H. Lin, M. Howard, and S. Vijayakumar. Learning null space projections. In *2015 IEEE International Conference on Robotics and Automation (ICRA)*, pages 2613–2619.
- [90] R. Lober, V. Padois, and O. Sigaud. Efficient reinforcement learning for humanoid whole-body control. In *2016 IEEE-RAS 16th International Conference on Humanoid Robots (Humanoids)*.
- [91] Francesco Longo, Letizia Nicoletti, and Antonio Padovano. Smart operators in industry 4.0: A human-centered approach to enhance operators’ capabilities and competencies within the new smart factory context. *Computers & industrial engineering*, 113:144–159, 2017.
- [92] Dylan P Losey, Craig G McDonald, Edoardo Battaglia, and Marcia K O’Malley. A review of intent detection, arbitration, and communication aspects of shared control for physical human–robot interaction. *Applied Mechanics Reviews*, 70(1), 2018.
- [93] Carlo J. De Luca. The use of surface electromyography in biomechanics. *Journal of Applied Biomechanics*, 13(2):135–163, 1997.
- [94] Jing Luo, Zhidong Lin, Yanan Li, and Chenguang Yang. A teleoperation framework for mobile robots based on shared control. *IEEE Robotics and Automation Letters*, 5(2):377–384, 2020.
- [95] C. E. Madan, A. Kucukyilmaz, T. M. Sezgin, and C. Basdogan. Recognition of haptic interaction patterns in dyadic joint object manipulation. *IEEE Transactions on Haptics*, 8(1):54–66, Jan 2015.
- [96] Antonio Gonzales Marin, Mohammad S Shourijeh, Pavel E Galibarov, Michael Damsgaard, Lars Fritsch, and Freek Stulp. Optimizing contextual ergonomics models in human-robot interaction. In *2018 IEEE/RSJ International Conference on Intelligent Robots and Systems (IROS)*, pages 1–9. IEEE, 2018.

- [97] Pauline Maurice, Vincent Padois, Yvan Measson, and Philippe Bidaud. Human-oriented design of collaborative robots. *International Journal of Industrial Ergonomics*, 57:88–102, 2017.
- [98] Pauline Maurice, Vincent Padois, Yvan Measson, and Philippe Bidaud. Assessing and improving human movements using sensitivity analysis and digital human simulation. *International Journal of Computer Integrated Manufacturing*, pages 1–13, 2019.
- [99] L. McAtamney and N. Corlett. Rula: a survey method for the investigation of work-related upper limb disorders. *Applied Ergonomics*, 1993.
- [100] Lynn McAtamney and E Nigel Corlett. Rula: a survey method for the investigation of work-related upper limb disorders. *Applied ergonomics*, 24(2):91–99, 1993.
- [101] Benjamin R Meagher and Kerry L Marsh. The costs of cooperation: Action-specific perception in the context of joint action. *Journal of experimental psychology: human perception and performance*, 40(1):429, 2014.
- [102] A. Melendez-Calderon, V. Komisar, and E. Burdet. Interpersonal strategies for disturbance attenuation during a rhythmic joint motor action. 147:348–358, 2015. Exported from <https://app.dimensions.ai> on 2019/01/26.
- [103] A. Melendez-Calderon, V. Komisar, G. Ganesh, and E. Burdet. Classification of strategies for disturbance attenuation in human-human collaborative tasks. In *2011 Annual International Conference of the IEEE Engineering in Medicine and Biology Society*, pages 2364–2367, Aug 2011.
- [104] C. Messeri, A. M. Zanchettin, P. Rocco, E. Gianotti, A. Chirico, S. Magoni, and A. Gaggioli. On the effects of leader-follower roles in dyadic human-robot synchronisation. *IEEE Transactions on Cognitive and Developmental Systems*, pages 1–1, 2020.
- [105] George Michalos, Sotiris Makris, Panagiota Tsarouchi, Toni Guasch, Dimitris Kontovrakis, and George Chryssolouris. Design considerations for safe human-robot collaborative workplaces. *Procedia CIRP*, 37:248–253, 2015.
- [106] E. Mingo Hoffman, A. Rocchi, A. Laurenzi, and N. G. Tsagarakis. Robot control for dummies: Insights and examples using opensot. In *2017 IEEE-RAS 17th International Conference on Humanoid Robotics (Humanoids)*, pages 736–741, Nov 2017.
- [107] V. Modugno, U. Chervet, G. Oriolo, and S. Ivaldi. Learning soft task priorities for safe control of humanoid robots with constrained stochastic optimization. In *2016 IEEE-RAS 16th International Conference on Humanoid Robots (Humanoids)*.
- [108] V. Modugno, G. Nava, D. Pucci, F. Nori, G. Oriolo, and S. Ivaldi. Safe trajectory optimization for whole-body motion of humanoids. In *2017 IEEE-RAS 17th International Conference on Humanoid Robotics (Humanoids)*.
- [109] Keivan Mojtahedi, Bryan Whitsell, Panagiotis Artemiadis, and Marco Santello. Communication and inference of intended movement direction during human–human physical interaction. *Frontiers in Neurorobotics*, 11:21, 2017.
- [110] Alexander Mörtl, Martin Lawitzky, Ayse Kucukyilmaz, Metin Sezgin, Cagatay Basdogan, and Sandra Hirche. The role of roles: Physical cooperation between humans and robots. *The International Journal of Robotics Research*, 31(13):1656–1674, 2012.

- 
- [111] J.-B. Mouret and S. Doncieux. SFERESv2: Evolvin' in the multi-core world. In *Proc. of Congress on Evolutionary Computation (CEC)*, 2010.
- [112] Richard M. Murray, S. Shankar Sastry, and Li Zexiang. *A Mathematical Introduction to Robotic Manipulation*. CRC Press, Inc., USA, 1st edition, 1994.
- [113] Shinnosuke Nakayama, Manuel Ruiz Marín, Maximo Camacho, and Maurizio Porfiri. Plasticity in leader–follower roles in human teams. *Scientific Reports*, 7(1):14562, 2017.
- [114] Benjamin Navarro, Andrea Cherubini, Aicha Fonte, Robin Passama, Gérard Poisson, and Philippe Fraisse. An iso10218-compliant adaptive damping controller for safe physical human-robot interaction. In *2016 IEEE International Conference on Robotics and Automation (ICRA)*, pages 3043–3048. IEEE, 2016.
- [115] Shengli Niu. Ergonomics and occupational safety and health: An ilo perspective. *Applied Ergonomics*, 41(6):744–753, 2010. Special Section: Selection of papers from IEA 2009.
- [116] Enrico Occhipinti. Ocr: a concise index for the assessment of exposure to repetitive movements of the upper limbs. *Ergonomics*, 41(9):1290–1311, 1998.
- [117] International Federation of Robotics. Report by the International Federation of Robotics. <https://ifr.org/service-robots>. Accessed: 2021-10-16.
- [118] International Federation of Robotics. Robots and the Workplace of the Future. <https://ifr.org/papers>. Accessed: 2021-10-16.
- [119] International Federation of Robotics. Robots in Daily Life, the positive impact of robots on well-being. <https://ifr.org/papers>. Accessed: 2021-10-16.
- [120] Open Design Lab, Penn State University. Open design lab scaling calculator. [http://tools.openlab.psu.edu/tools/proportionality\\_constants.htm](http://tools.openlab.psu.edu/tools/proportionality_constants.htm). Accessed: 2020-01-10.
- [121] V. Ortenzi, H. Lin, M. Azad, R. Stolkin, J. A. Kuo, and M. Mistry. Kinematics-based estimation of contact constraints using only proprioception. In *2016 IEEE-RAS 16th International Conference on Humanoid Robots (Humanoids)*.
- [122] T. Ortmaier, M. Groger, D.H. Boehm, V. Falk, and G. Hirzinger. Motion estimation in beating heart surgery. *IEEE Transactions on Biomedical Engineering*, 52(10):1729–1740, 2005.
- [123] Kazuya Otani and Karim Bouyarmane. Adaptive whole-body manipulation in human-to-humanoid multi-contact motion retargeting. In *2017 IEEE-RAS 17th International Conference on Humanoid Robotics (Humanoids)*.
- [124] Liuba Papeo, Timo Stein, and Salvador Soto-Faraco. The two-body inversion effect. *Psychological Science*, 28(3):369–379, 2017.
- [125] Alexandros Paraschos, Christian Daniel, Jan Peters, and Gerhard Neumann. Using probabilistic movement primitives in robotics. *Autonomous Robots*, 2018.
- [126] Alexandros Paraschos, Christian Daniel, Jan R Peters, and Gerhard Neumann. Probabilistic movement primitives. In C. J. C. Burges, L. Bottou, M. Welling, Z. Ghahramani, and K. Q. Weinberger, editors, *Advances in Neural Information Processing Systems 26*. Curran Associates, Inc., 2013.

- [127] L. Penco, B. Clement, V. Modugno, E. Mingo Hoffman, G. Nava, D. Pucci, N. G. Tsagarakis, J. . Mouret, and S. Ivaldi. Robust real-time whole-body motion retargeting from human to humanoid. In *2018 IEEE-RAS 18th International Conference on Humanoid Robots (Humanoids)*.
- [128] Aldo O Perotto. *Anatomical guide for the electromyographer: the limbs and trunk*. Charles C Thomas Publisher, 2011.
- [129] Luka Peternel, Cheng Fang, Nikos Tsagarakis, and Arash Ajoudani. Online human muscle force estimation for fatigue management in human-robot co-manipulation. In *2018 IEEE/RSJ International Conference on Intelligent Robots and Systems (IROS)*, pages 1340–1346. IEEE, 2018.
- [130] Luka Peternel, Olivier Sigaud, and Jan Babič. Unifying speed-accuracy trade-off and cost-benefit trade-off in human reaching movements. *Frontiers in Human Neuroscience*, 11:615, 2017.
- [131] Luka Peternel, Nikos Tsagarakis, and Arash Ajoudani. A human–robot co-manipulation approach based on human sensorimotor information. *IEEE Transactions on Neural Systems and Rehabilitation Engineering*, 25(7):811–822, 2017.
- [132] Luka Peternel, Nikos Tsagarakis, Darwin Caldwell, and Arash Ajoudani. Adaptation of robot physical behaviour to human fatigue in human-robot co-manipulation. In *2016 IEEE-RAS 16th International Conference on Humanoid Robots (Humanoids)*, pages 489–494, 2016.
- [133] Luka Peternel, Nikos Tsagarakis, Darwin Caldwell, and Arash Ajoudani. Robot adaptation to human physical fatigue in human–robot co-manipulation. *Autonomous Robots*, 42(5):1011–1021, 2018.
- [134] Jan Peters, Sethu Vijayakumar, and Stefan Schaal. Reinforcement learning for humanoid robotics. In *Third IEEE International Conference on Humanoid Robotics 2003, Germany*, 2003.
- [135] Pierre Plantard, Hubert PH Shum, Anne-Sophie Le Pierres, and Franck Multon. Validation of an ergonomic assessment method using kinect data in real workplace conditions. *Applied ergonomics*, 65:562–569, 2017.
- [136] Michael JD Powell. A direct search optimization method that models the objective and constraint functions by linear interpolation. In *Advances in optimization and numerical analysis*, pages 51–67. Springer, 1994.
- [137] Andrea Del Prete, Francesco Nori, Giorgio Metta, and Lorenzo Natale. Prioritized motion–force control of constrained fully-actuated robots: “task space inverse dynamics”. *RAS*, 63:150 – 157, 2015.
- [138] Bob Price and Craig Boutilier. Accelerating reinforcement learning through implicit imitation. *Journal of Artificial Intelligence Research*, 19, 2003.
- [139] Laura Punnett and David H Wegman. Work-related musculoskeletal disorders: the epidemiologic evidence and the debate. *Journal of electromyography and kinesiology*, 14(1):13–23, 2004.
- [140] Susanne Quadflieg and Kami Koldewyn. The neuroscience of people watching: how the human brain makes sense of other people’s encounters. *Annals of the New York Academy of Sciences*, 1396(1):166–182, 2017.
- [141] R. Rahal, G. Matarese, M. Gabiccini, A. Artoni, D. Prattichizzo, P. R. Giordano, and C. Paccchierotti. Caring about the human operator: Haptic shared control for enhanced user comfort in robotic telemanipulation. *IEEE Transactions on Haptics*, 13(1):197–203, 2020.

- 
- [142] Rahaf Rahal, Giulia Matarese, Marco Gabiccini, Alessio Artoni, Domenico Prattichizzo, Paolo Robuffo Giordano, and Claudio Pacchierotti. Haptic shared control for enhanced user comfort in robotic telemanipulation.
- [143] David G Rand. Cooperation, fast and slow: Meta-analytic evidence for a theory of social heuristics and self-interested deliberation. *Psychological science*, 27(9):1192–1206, 2016.
- [144] Harish Chaandar Ravichandar, Daniel Trombetta, and Ashwin P. Dani. Human intention-driven learning control for trajectory synchronization in human-robot collaborative tasks. *IFAC-PapersOnLine*, 51(34):1–7, 2019. 2nd IFAC Conference on Cyber-Physical and Human Systems CPHS 2018.
- [145] K. B. Reed, M. Peshkin, and M. J. Hartmann. Haptic cooperation between people, and between people and machines, 2006.
- [146] Daniel Roetenberg, Henk Luinge, and Per Slycke. Xsens mvn: Full 6dof human motion tracking using miniature inertial sensors. *Xsens Motion Technologies BV, Tech. Rep.*, 1, 2009.
- [147] Danuta Roman-Liu. Comparison of concepts in easy-to-use methods for msd risk assessment. *Applied ergonomics*, 45(3):420–427, 2014.
- [148] Jeremy Roschelle and Stephanie D Teasley. The construction of shared knowledge in collaborative problem solving. In *Computer supported collaborative learning*, pages 69–97. Springer, 1995.
- [149] JuHyeong Ryu, Mohsen M Diraneyya, Carl T Haas, and Eihab Abdel-Rahman. Analysis of the limits of automated rule-based ergonomic assessment in bricklaying. *Journal of Construction Engineering and Management*, 147(2):04020163, 2021.
- [150] Philip N. Sabes and Michael I. Jordan. Obstacle avoidance and a perturbation sensitivity model for motor planning. *Journal of Neuroscience*, 17(18):7119–7128, 1997.
- [151] Lucia Maria Sacheli, Emmanuele Tidoni, Enea Francesco Pavone, Salvatore Maria Aglioti, and Matteo Candidi. Kinematics fingerprints of leader and follower role-taking during cooperative joint actions. *Experimental Brain Research*, 226(4):473–486, May 2013.
- [152] United States. Occupational Safety and Health Administration. *Ergonomics, the Study of Work*. U.S. Department of Labor, Occupational Safety and Health Administration, 2000.
- [153] J. Salini, V. Padois, and P. Bidaud. Synthesis of complex humanoid whole-body behavior: A focus on sequencing and tasks transitions. In *2011 IEEE International Conference on Robotics and Automation*, pages 1283–1290.
- [154] Luisa Sartori, Cristina Becchio, Bruno G Bara, and Umberto Castiello. Does the intention to communicate affect action kinematics? *Consciousness and cognition*, 18(3):766–772, 2009.
- [155] Matteo Saveriano, Fares J. Abu-Dakka, Aljaz Kramberger, and Luka Peternel. Dynamic movement primitives in robotics: A tutorial survey, 2021.
- [156] S. Scataglini and G. Paul. *DHM and Posturography*. Elsevier Science, 2019.
- [157] Stefan Schaal. Is imitation learning the route to humanoid robots? *Trends in cognitive sciences*, 3(6):233–242, 1999.

- [158] Karlheinz Schaub, Gabriele Caragnano, Bernd Britzke, and Ralph Bruder. The european assembly worksheet. *Theoretical Issues in Ergonomics Science*, 14(6):616–639, 2013.
- [159] R.C. Schmidt, Paula Fitzpatrick, Robert Caron, and Joanna Mergeche. Understanding social motor coordination. *Human Movement Science*, 30(5):834 – 845, 2011.
- [160] Elke Schneider, Sarah Copsey, and Xabier Irastorza. *Occupational Safety and Health in Figures: Work-related Musculoskeletal Disorders in the EU-Facts and Figures*. Office for Official Publications of the European Communities, 2010.
- [161] Natalie Sebanz, Günther Knoblich, and Wolfgang Prinz. Representing others’ actions: just like one’s own? *Cognition*, 88(3):B11–B21, 2003.
- [162] M. Selvaggio, P. Robuffo Giordano, F. Ficuciello, and B. Siciliano. Passive task-prioritized shared-control teleoperation with haptic guidance. In *2019 International Conference on Robotics and Automation (ICRA)*, pages 430–436, 2019.
- [163] Mario Selvaggio, Marco Cognetti, Stefanos Nikolaidis, Serena Ivaldi, and Bruno Siciliano. Autonomy in physical human-robot interaction: A brief survey. *IEEE Robotics and Automation Letters*, 6(4):7989–7996, 2021.
- [164] Yaroslav D Sergeyev and Dmitri L Markin. An algorithm for solving global optimization problems with nonlinear constraints. *Journal of Global Optimization*, 7(4):407–419, 1995.
- [165] Nicla Settembre, Pauline Maurice, Jean Paysant, Jean Theurel, Laurent Claudon, Antoine Kimoun, Bruno Levy, Hind Hani, Bruno Chenuel, and Serena Ivaldi. The use of exoskeletons to help with prone positioning in the intensive care unit during covid-19. *Annals of physical and rehabilitation medicine*, 63(4):379, 2020.
- [166] Ali Shafti, Ahmad Ataka, B Urbistondo Lazpita, Ali Shiva, Helge A Wurdemann, and Kaspar Althoefer. Real-time robot-assisted ergonomics. In *2019 International Conference on Robotics and Automation (ICRA)*. IEEE, 2019.
- [167] J. Silverio, S. Calinon, L. Rozo, and D. G. Caldwell. Learning task priorities from demonstrations. *IEEE Transactions on Robotics*, 35, 2019.
- [168] Ines Sorrentino, Francisco Javier Andrade Chavez, Claudia Latella, Luca Fiorio, Silvio Traversaro, Lorenzo Rapetti, Yeshasvi Tirupachuri, Nuno Guedelha, Marco Maggiali, Simeone Dussoni, et al. A novel sensorised insole for sensing feet pressure distributions. *Sensors*, 20(3):747, 2020.
- [169] Neville Anthony Stanton, Alan Hedge, Karel Brookhuis, Eduardo Salas, and Hal W Hendrick. *Handbook of human factors and ergonomics methods*. CRC press, 2004.
- [170] N. Stefanov, A. Peer, and M. Buss. Role determination in human-human interaction. In *World Haptics 2009 - Third Joint EuroHaptics conference and Symposium on Haptic Interfaces for Virtual Environment and Teleoperator Systems*, pages 51–56, March 2009.
- [171] D Stegeman and H Hermens. Standards for surface electromyography: The european project surface emg for non-invasive assessment of muscles (seniam). 2007.
- [172] F. Stulp, J. Buchli, E. Theodorou, and S. Schaal. Reinforcement learning of full-body humanoid motor skills. In *2010 10th IEEE-RAS International Conference on Humanoid Robots*.

- 
- [173] F. Stulp and S. Schaal. Hierarchical reinforcement learning with movement primitives. In *2011 11th IEEE-RAS International Conference on Humanoid Robots*.
- [174] F. Stulp, E. A. Theodorou, and S. Schaal. Reinforcement learning with sequences of motion primitives for robust manipulation. *IEEE Transactions on Robotics*, 28(6), 2012.
- [175] Atsushi Takagi, Gowrishankar Ganesh, Toshinori Yoshioka, Mitsuo Kawato, and Etienne Burdet. Physically interacting individuals estimate the partner’s goal to enhance their movements. *Nature Human Behaviour*, 1:0054 EP –, Mar 2017. Letter.
- [176] Atsushi Takagi, Masaya Hirashima, Daichi Nozaki, and Etienne Burdet. Individuals physically interacting in a group rapidly coordinate their movement by estimating the collective goal. *eLife*, 8:e41328, feb 2019.
- [177] Atsushi Takagi, Masaya Hirashima, Daichi Nozaki, and Etienne Burdet. Individuals physically interacting in a group rapidly coordinate their movement by estimating the collective goal. *Elife*, 8:e41328, 2019.
- [178] Atsushi Takagi, Francesco Usai, Gowrishankar Ganesh, Vittorio Sanguineti, and Etienne Burdet. Haptic communication between humans is tuned by the hard or soft mechanics of interaction. *PLOS Computational Biology*, 14(3):1–17, 03 2018.
- [179] Jukka Takala and S Niu. Responses to the equity challenge in safety and health at work: improvement of working conditions in equitable bases. In *27th international congress on occupational health*, pages 23–28, 2003.
- [180] Kendall Taylor et al. Bayesian preference learning for interactive multi-objective optimisation. In *ACM, GECCO*, 2021.
- [181] **Gomes, Waldez**, Pauline Maurice, Jan Babic, Jean-Baptiste Mouret, and Serena Ivaldi. In a collaborative co-manipulation, humans have a motor behaviour similar to a leader. *Nature Human Behaviour*, In Preparation.
- [182] **Gomes, Waldez**, Pauline Maurice, Eloïse Dalin, Jean-Baptiste Mouret, and Serena Ivaldi. Multi-objective trajectory optimization to improve ergonomics in human motion. *IEEE Robotics and Automation Letters*, 2021, Accepted for publication.
- [183] **Gomes, Waldez**, Pauline Maurice, and Serena Ivaldi. Andy data - human human object co-manipulation, August 2020. Dataset available at <https://doi.org/10.5281/zenodo.3989616>.
- [184] **W. Gomes**, V. Radhakrishnan, L. Penco, V. Modugno, J. Mouret, and S. Ivaldi. Humanoid whole-body movement optimization from retargeted human motions. In *2019 IEEE-RAS 19th International Conference on Humanoid Robots (Humanoids)*, pages 178–185, 2019.
- [185] Kurt A. Thoroughman and Reza Shadmehr. Electromyographic correlates of learning an internal model of reaching movements. *Journal of Neuroscience*, 19(19):8573–8588, 1999.
- [186] Yeshasvi Tirupachuri. Enabling human-robot collaboration via holistic human perception and partner-aware control, 2020.
- [187] Yao-Lin Tsai, Parthasarathy Bana, and Heather Knight. Can service robots help best practices for covid? In *Companion of the 2021 ACM/IEEE International Conference on Human-Robot Interaction*, HRI ’21 Companion, page 615–617, New York, NY, USA, 2021. Association for Computing Machinery.

- [188] Y. Uno, M. Kawato, and R. Suzuki. Formation and control of optimal trajectory in human multi-joint arm movement. *Biological Cybernetics*, 61(2):89–101, Jun 1989.
- [189] US Bureau of Labor Statistics. *Nonfatal Occupational Injuries and Illnesses Requiring Days Away from Work, 2015*, 2016.
- [190] L. v. der Spaa, M. Gienger, T. Bates, and J. Kober. Predicting and optimizing ergonomics in physical human-robot cooperation tasks. In *2020 IEEE International Conference on Robotics and Automation (ICRA)*, pages 1799–1805, 2020.
- [191] Enrique Valero, Aparajithan Sivanathan, Frédéric Bosché, and Mohamed Abdel-Wahab. Analysis of construction trade worker body motions using a wearable and wireless motion sensor network. *Automation in Construction*, 83:48–55, 2017.
- [192] Ashesh Vasalya, Gowrishankar Ganesh, and Abderrahmane Kheddar. More than just co-workers: Presence of humanoid robot co-worker influences human performance. *PLOS ONE*, 13(11):1–19, 11 2018.
- [193] Cordula Vesper, Laura Schmitz, Lou Safra, Natalie Sebanz, and Günther Knoblich. The role of shared visual information for joint action coordination. *Cognition*, 153:118–123, 2016.
- [194] Lorenzo Vianello, Luigi Penco, **Gomes, Waldez**, Yang You, Salvatore Anzalone, Pauline Maurice, Vincent Thomas, and Serena Ivaldi. Human-humanoid interaction and cooperation: a review. *Current Robotics Reports*, 2021.
- [195] Lorenzo Vianello, **Gomes, Waldez**, Francis Colas, Pauline Maurice, Freek Stulp, and Serena Ivaldi. Latent ergonomics maps: Real-time visualization of estimated ergonomics maps. *Sensors*, In Preparation.
- [196] Yasuhiro Wada, Yuichi Kaneko, Eri Nakano, Rieko Osu, and Mitsuo Kawato. Quantitative examinations for multi joint arm trajectory planning—using a robust calculation algorithm of the minimum commanded torque change trajectory. *Neural Networks*, 14(4):381 – 393, 2001.
- [197] Jon Walbrin, Paul Downing, and Kami Koldewyn. Neural responses to visually observed social interactions. *Neuropsychologia*, 112:31 – 39, 2018.
- [198] Jon Walbrin and Kami Koldewyn. Dyadic interaction processing in the posterior temporal cortex. *NeuroImage*, 198:296 – 302, 2019.
- [199] Jingguo Wang and Yangmin Li. Hybrid impedance control of a 3-dof robotic arm used for rehabilitation treatment. In *2010 IEEE International Conference on Automation Science and Engineering*, pages 768–773, 2010.
- [200] Felix Warneken, Maria Gräfenhain, and Michael Tomasello. Collaborative partner or social tool? new evidence for young children’s understanding of joint intentions in collaborative activities. *Developmental science*, 15(1):54–61, 2012.
- [201] Daniel M Wolpert, Zoubin Ghahramani, and Michael I Jordan. An internal model for sensorimotor integration. *Science*, 269(5232):1880–1882, 1995.
- [202] D. Woods, John M. Wyma, E. Yund, T. Herron, and B. Reed. Factors influencing the latency of simple reaction time. *Frontiers in Human Neuroscience*, 9, 2015.

- 
- [203] Yujiang Xiang, Jasbir S Arora, Salam Rahmatalla, Timothy Marler, Rajankumar Bhatt, and Karim Abdel-Malek. Human lifting simulation using a multi-objective optimization approach. *Multibody System Dynamics*, 2010.
- [204] A. Yazdani and Roya Sabbagh Novin. Posture estimation and optimization in ergonomically intelligent teleoperation systems. *International Conference on Human-Robot Interaction*, 2021.
- [205] Amir Yazdani, Roya Sabbagh Novin, Andrew Merryweather, and Tucker Hermans. Dula: A differentiable ergonomics model for postural optimization in physical hri, 2021.
- [206] K. Yuan, I. Chatzinikolaïdis, and Z. Li. Bayesian optimization for whole-body control of high-degree-of-freedom robots through reduction of dimensionality. *IEEE Robotics and Automation Letters*, 4(3):2268–2275, July 2019.



## Résumé

Cette thèse vise à fournir des outils pour améliorer l'ergonomie dans les environnements de travail. Certaines activités dans l'industrie sont couramment exécutées par les travailleurs de manière non ergonomique, ce qui peut entraîner des troubles musculo-squelettiques à court ou à long terme.

Les troubles musculo-squelettiques (TMS) liés au travail constituent un problème de santé majeur dans le monde entier, qui représente également des coûts importants pour la société et les entreprises. On sait que les TMS sont causées par de multiples facteurs, tels que des mouvements répétitifs, une force excessive et des postures corporelles non ergonomiques. Il n'est pas surprenant que les environnements de travail présentant de tels facteurs puissent présenter une incidence de TMS jusqu'à 3 ou 4 fois plus élevée que dans la population générale. Notre approche consiste à évaluer le mouvement humain, à l'optimiser et à intervenir sur la tâche en fonction du mouvement optimisé.

Pour évaluer l'ergonomie de la posture du corps, nous avons développé une simulation de modèle humain numérique (DHM en anglais) capable de reproduire les mouvements du corps entier. Dans la simulation, le mouvement initial peut être amélioré de manière itérative, jusqu'à l'obtention d'un mouvement ergonomique optimal du corps entier. Nous pensons qu'un robot en interaction physique avec un humain pourrait conduire ce dernier vers des mouvements plus ergonomiques du corps entier, voire vers un mouvement ergonomiquement optimal. Pour concevoir un contrôleur de robot qui influence la posture du corps, nous étudions d'abord le comportement moteur de l'homme dans une étude de co-manipulation entre humains. Dans cette étude, nous avons observé des modèles de comportement moteur qui ont été utilisés pour concevoir un contrôleur de collaboration pour l'interaction physique homme-robot (pHRI en anglais). L'étude de co-manipulation a ensuite été exécutée par un humain collaborant avec un robot Franka Panda.

**Mots-clés:** L'évaluation de l'ergonomie, trouble musculosquelettique, optimisation des mouvements du corps complet, optimisation multi-objective, collaboration homme-robot,

## Abstract

This thesis aims to provide tools for improving ergonomics at work environments. Some work activities in industry are commonly executed by workers in a non-ergonomic fashion, which may lead to musculoskeletal disorders in the short or in the long term.

Work-related Musculoskeletal Disorders (WMSDs) are a major health issue worldwide, that also represents important costs both for society and companies. WMSDs are known to be caused by multiple factors, such as repetitive motion, excessive force, and awkward, non-ergonomic body postures. Not surprisingly, work environments with such factors may present an incidence of WMSDs of up to 3 or 4 times higher than in the overall population. Here, our approach is to evaluate the human motion with respect to ergonomics indexes, optimize the motion, and intervene on the task based on the optimized motion.

To evaluate the body posture ergonomics, we developed a Digital Human Model (DHM) simulation capable of replaying whole-body motions. In simulation, the initial movement can be iteratively improved, until an optimal ergonomic whole-body motion is obtained. We make the case that a robot in physical interaction with a human could drive the human towards more ergonomic whole-body motions, possibly to an ergonomically optimal motion. To design a robot controller that influences the body posture, we first investigate the human motor behavior in a human-human co-manipulation study. In this human dyad study, we observed motor behavior patterns that were used to design a collaboration controller for physical human-robot interaction (pHRI). In a new study, the same co-manipulation task was then executed by humans collaborating with a Franka Emika Panda robot.

**Keywords:** Ergonomics evaluation, multi-objective optimization, whole-body motion optimization, human-robot collaboration, physical human-robot collaboration.

